Morphological and molecular phylogenetic study of tidal pool dinoflagellates

(タイドプール性渦鞭毛藻類の形態学的および分子系統学的研究)

Maihemutijiang Dawuti
(Mahmutjan Dawut)

Department of Natural History Sciences
Graduate School of Science
Hokkaido University

March 2020

ABSTRACT

Dinoflagellates are an extraordinarily diverse group of bi-flagellate eukaryotic microbes that occupy a wide range of niches in aquatic environments. Most dinoflagellates inhabit freshwater ponds, lakes and marine neritic/open ocean environments. However, there are some dinoflagellate species that specifically inhabit tidal pools on rocky beaches. These species form dense blooms and show characteristic diurnal vertical migratory behavior depending on tidal movement. During day time, the motile cells actively swim, forming a bloom at low tide. Before seawater is introduced into the pools at high tide, the dinoflagellates migrate down to the bottom of the pool and attach themselves firmly to the substratum so that the cells can avoid being washed out from the tidal pools. Despite their showy presence of characteristic blooms on rocky shores, studies on tidal pool dinoflagellates are scarce. All the previous descriptions of tidal pool dinoflagellates were based on external morphology and limited molecular work has been done. Therefore, the use of more contemporary methods such as molecular phylogenetics is needed in order to confirm many of their taxonomic positions. Due to their characteristic lifestyle to prevent being washed away from the pools, it was hypothesized that the dispersal ability of these dinoflagellates is small. However, this has not been tested so far. Thus, I conducted research to obtain a better understanding of: 1) species biodiversity of bloom forming tidal pool dinoflagellates in Japan and South Africa; 2) their taxonomic positions, based on molecular phylogenetics; and 3) the genetic distances between populations (= tidal pools) within the same species from different localities.

Following the general introduction in Chapter I, in chapter II of my thesis, I described a new species of the genus *Bysmatrum*, *B. austrafrum* Dawut *et al*. sp. nov. from South Africa. Detailed

morphological observations were made by light microscopy, as well as scanning and transmission electron microscopy (SEM and TEM). This was the second report of the internal ultrastructure of any member of this genus. The phylogenetic position of this species was determined using small-subunit ribosomal DNA (SSU-rDNA) sequence data. Based on the distinct morphology of the first apical plate (1') and its isolated position in the phylogenetic tree in relation to the other five members of this genus, I concluded that this species is a new member of this genus. Moreover, I provided the first report of the SSU rDNA sequence for *Bysmatrum arenicola*.

In chapter III, I have examined 30 *Bysmatrum* strains isolated from tidal pool water samples collected from three different prefectures, Kanagawa, Chiba and Okinawa, in Japan. The morphological analysis was done using LM and SEM. In general, the external morphology was almost identical to those of *B. subsalsum*, *B. gregarium* and *B. austrafrum*, but there were some features unique to those isolates, such as the cell size, the position of the nucleus, the degree of the displacement of the cingulum, and the habitat. I refer to them as the *Bysmatrum gregarium* species complex. All 30 strains formed three separated clades, with moderate support, distinct from any previously reported species (here, designated as Group I, II and III). It was revealed that Group I contains strains from Okinawa, Kanagawa and Chiba prefecture, while Group II and III consisted of strains from Kanagawa and Chiba. It was also demonstrated that even a single tidal pool can contain three species (genotypes) at the same time. In this study, I demonstrated that the distributional pattern of *B. gregarium* species complex is quite complex and further studies with a wider range of global sampling is merited. Based on the current available data, I concluded that those isolates (Group I to III) represent cryptic species.

In chapter IV, a small photosynthetic dinoflagellate was isolated from tidal pool water

collected in South Africa, designated as strain HG246. Based on detailed inter/external morphological observations and molecular analysis, it was confirmed as a new *Symbiodinium* species. *Symbiodinium* sp. HG246 differed from the other members of *Symbiodinium* by having an extra intercalary plate on the epicone. It also formed a robust isolated clade, with moderate support, in the phylogenetic tree inferred from the LSU rDNA sequences, separating it from the morphologically similar species, *S. natans*. This was the first report of a free-living bloom forming *Symbiodinium* species, inhabiting tidal pools.

In chapter V, I proposed a new combination, *Ansanella natalensis* (Horiguchi & Piennar) Dawut *et al*. comb. nov. This species was originally described as, *Gymnodinium natalense*. Later, it was reclassified in the genus *Biecheleria*, as *B. natalensis*, based on re-observation of the original photographs, but without molecular data. Recently, a small dinoflagellate was isolated from the same tidal pool at the type locality of *G. natalense* in South Africa. The detailed cell surface information, which was not available in the first and second reports, along with the strongly supported phylogenetic tree inferred from SSU sequence data, revealed that this species should belong to the newly erected genus *Ansanella*. Furthermore, the presence of a 51-base pair fragment of the LSU domain 2 (D2) in our species, which is characteristic of the type species of *Ansanella* and absent in *Biecheleria* species, gives further strong support to our conclusion.

In chapter VI, I proposed a new combination, *Peridiniopsis hexapraecingula* (Horiguchi & Chihara) comb. nov. This species was originally described as, *Scrippsiella hexapraecingula* in 1983, but no molecular data were available until today. In this study, I was able to collect this species again from Chiba Prefecture and able to conduct molecular phylogenetic analysis as well as morphological examinations. The phylogenetic tree indicated that this species is closely related to the type species of the freshwater dinoflagellate genus *Peridiniopsis*. Based on genetic

similarity, I proposed to transfer the species to the genus *Peridiniopsis*.

In conclusion, this thesis contains the description of two new species, demonstrated the presence of three cryptic species, and proposed two new combination, unveiled the genetic structure of tidal pool dinoflagellate species. These results will contribute to further understanding of the biodiversity and phylogeny of tidal pool dinoflagellates.

ACKNOWLEDGMENTS

First and foremost, I would like to thank God Almighty for giving me the strength, knowledge, ability and opportunity to undertake this research study and to persevere and complete it adequately. Without His blessings, this achievement would not have been possible.

Rallying past all the difficulties and hardships in my PhD journey, it would have also not been possible without the unstinting support from different people. Herein, I would take this opportunity to thank all of them.

In my journey towards this degree, I have found a great teacher, a best friend, an inspiration, and a pillar of support in my guide, my supervisor, Prof. Takeo Horiguchi. Without his wise counsels, unwavering support and patience it might not possible for me to come this far. I am greatly thankful to my advisor and the reviewer of my PhD manuscript, Prof. Maria Helena Fortunato Martins, for her sound advises and encouragements. I am very grateful to Prof. Kazuhiro Kogame for critical reading through my thesis and his insightful feedback for its improvements. I am deeply thankful to Prof. Kevin Wakeman for both his helpful advices, technical teachings, encouragements throughout my study and the valuable comments on my thesis. I also appreciate the help of Prof. Stuart D. Sym (University of Witwatersrand, South Africa) and Prof. Shoichiro Suda (University of Ryukyus, Japan) for their support of sampling in the field, and patience in revising my manuscripts.

I would like to extend my warmest appreciation to the past and present members of the Algal and Protist Systematics laboratory, Department of Natural History Sciences, Hokkaido University for their support and camaraderie affords. Special thanks to my buddies and friends in

the lab, Dr. Suttikarn Sutti, Dr. Wilfred John Eria Santiañez and Mr. Davis Iritani. Keeping my sanity and focusing on what is important during one of the hardest journeys of my life couldn't be successful without their companionship and help. Here, by taking this chance, I would like to express my sincerest gratitude and thanks to those who kept praying for me, loving me, encouraging me, helping and supporting me in all aspects of my life, Ms. Gvlqemer Abliz (Yokohama National University), Ms. Imigul Yusup (Tianjin Normal University), Ms. Muharram Aziz (Xinjiang University), Dr. Muattar Saydi (Xinjiang University), Mr. Ababekri Abdurehim.

My acknowledgment would be incomplete without thanking the biggest source of my strength, my family. The blessings of my parents Mrs. Tursungul Abdurehman & Mr. Dawut'eli Heyit and the love and care from my two brothers Abdulla Dawut and Mir'adil Dawut, have all made a tremendous contribution in helping me reach this stage in my life. I thank them for putting up with me in difficult moments where I felt stumped and for goading me on to follow my dream of getting this degree. This would not have been possible without their unwavering and unselfish love and support given to me at all times.

I would like to dedicate this work to my parents whose dreams for me have resulted in this achievement and without their loving upbringing and nurturing; I would not have been where I am today and what I am today. Had it not been for my parent's unflinching insistence and support, my dreams would have remained mere dreams. I thank my mother with all my heart.

Mahmutjan Dawut

17 December, 2019

CONTENTS

CHAPTER I

GENERAL INTRODUCTION

GENERAL CHARACTERISTICS

Dinoflagellates (Gr. δίνη/díni, to whirl), division Dinophyta, class Dinophyceae, are a group of unicellular, highly diverse, flagellate protists belonging to the eukaryotic super-group Alveolata, and one of the ecologically most important groups of modern phytoplankton (Taylor *et al.* 2008, Jeong *et al.* 2010, Lee *et al.* 2014). Although, because of the ongoing taxonomic studies and revisions, and our inadequate knowledge of species diversity in many uninvestigated regions/habitats, it is quite challenging to obtain a precise estimation of the species number, the most recent literature indicated that approximately 2000 to 2500 living and 2000 fossil species of dinoflagellates are assigned to more than 400 genera (Gómez 2005, 2012, Taylor *et al.* 2008, Hoppenrath 2016). These biflagellate eukaryotic microbes are believed to have occupied important niches in both marine and freshwater environments, from cold Arctic/Antarctic waters to warm tropical waters, and from nutrient-rich coastal regions to nutrient-poor open oceans. Most dinoflagellates are free-living with half of them known to be photosynthetic, while others, such as *Symbiodinium* spp., are important endosymbiotic partners of reef-building corals and cnidarians (Baker 2003, Lee *et al.* 2016, Nitschke *et al.* 2016, Parkinson *et al.* 2016), and still some being parasites of many protist, invertebrate and vertebrate hosts (Taylor *et al.* 2008, Horiguchi 2015). Some are toxin producers (Ten-Hage *et al.* 2000, Morton *et al.* 2002, Aligizaki *et al.* 2009), and are best known for their dominant role in causing harmful algal blooms (HABs).

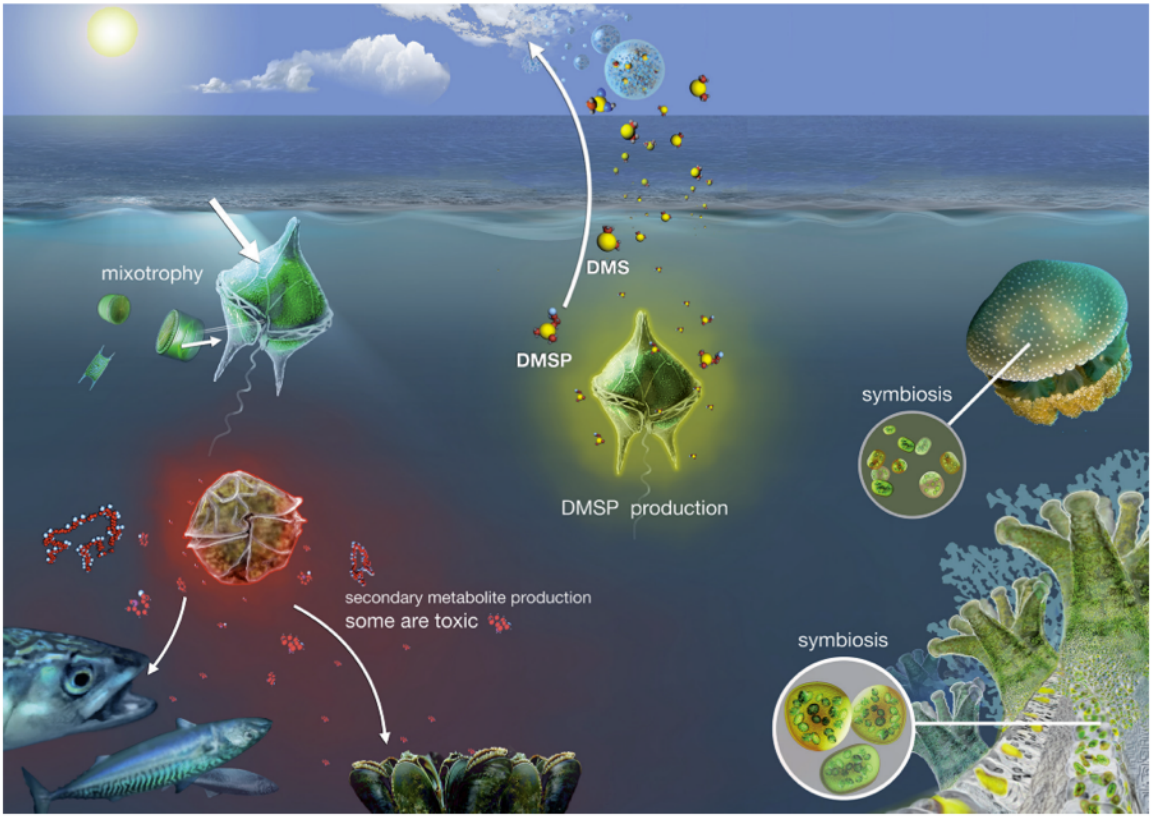

Figure 1. Some of the major ecological traits of dinoflagellates: free living planktonic cells and symbiosis with corals and other invertebrates, DMSP producers, mixotrophy, and producers of toxic/non-toxic metabolites with impacts on other marine life (from Murray *et al*. 2016).

ECOLOGICAL IMPORTANCE AND REPRODUCTION

The habitats in which dinoflagellates may be found are varied, from seawater to freshwater and from tropical to polar regions, yet the bulk of them live in the hydrosphere and their vast majority (approximately 90%) are marine planktonic or benthic forms, with greatest diversity in tropical areas. Dinoflagellates exhibit outstanding intricacy in terms of ecology (pelagic and/or benthic in both marine and freshwater habitats), life cycle (e.g. cyst formation), and, most importantly life modes (autotrophic, heterotrophic, mixotrophic) (Schnepf & Elbrächter 1992, Sherr & Sherr 2007, Taylor *et al.* 2008, Gómez 2012, Lee *et al.* 2014). Additionally, their

ecological success also results in an extraordinary physiological diversity and adaptation to specific niches (Dyhrman 2008); for example, many of these microbes are able to produce complex chemical compounds which impact their interactions with competitors and predators (Selander *et al.* 2006, Tillmann *et al.* 2008, Nagahama *et al.* 2011); may act as symbionts or parasites, use benthic or planktonic habitats (Hoppenrath *et al.* 2014, Murray *et al.* 2016, LaJeunesse *et al.* 2018); besides, dinoflagellates also produce chemicals with ecosystem-wide impacts (Figure 1), such as dimethylsulfoniopropionate (DMSP) (Kirst *et al.* 1991) which is finally transferred into biogeochemical important trace gases, and some economically important polyunsaturated fatty acids such as docosahexanoic acid (DHA) (Ratledge 2004, Guschina & Harwood 2006).

During the course of their life cycle, dinoflagellates undergo dramatic morphological changes including reproduction and interchange between motile (mastigote) and nonmotile (cyst) stages (Figure 2). In most dinoflagellates, the motile phase is dominant, but in some, they spent most of their life cycle in a coccoid phase like those living as intracellular symbionts (e.g., *Symbiodinium*). Based on their roles in the life cycle, Saldarriaga and Taylor (2017) proposed a unified terminology for all known cysts and put them in four different types: resting cyst, temporary cyst, trophic cyst and digestion cyst. The encystment of resting and temporary cysts could be caused by nutrition stress or changing of the surrounding environment such as light intensity, photoperiod, or temperature (Von Stosch 1964).

Dinoflagellates are reported to have both sexual and asexual (vegetative) reproduction (Von Stosch 1973, Walker & Steidinger 1979, Blackburn *et al.* 1989). The sexual reproduction, however, is described from a few species so far. The vegetative reproduction in dinoflagellates is

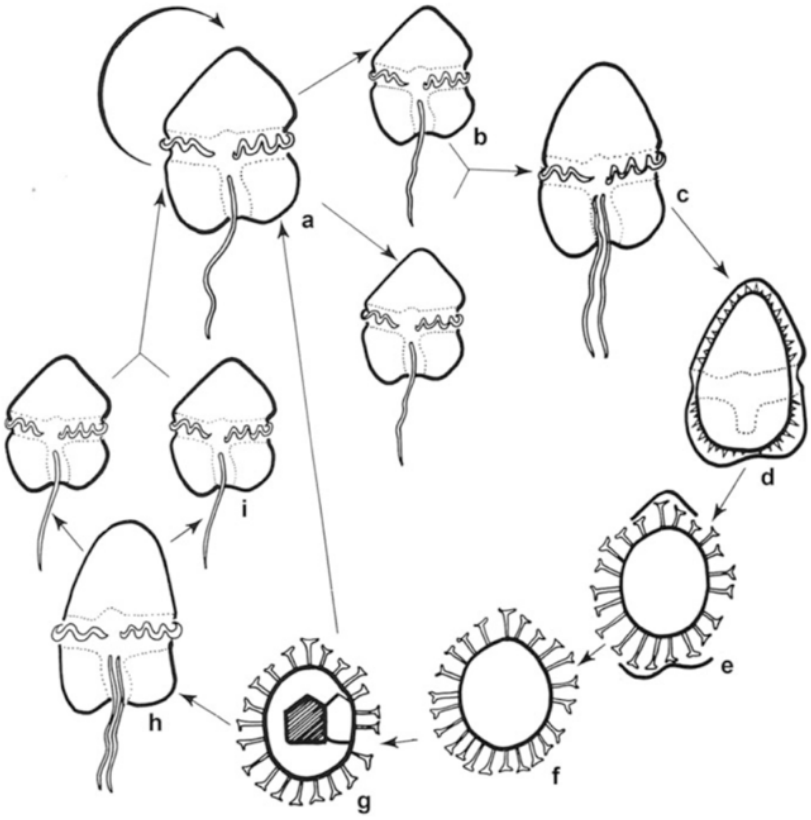

Figure 2. A diagram illustrating the common dinoflagellate life cycle (modified from Dale 1983). **(a)** Asexually reproducing motile cell (mastigote); **(b)** gametes (can be iso- or anisogametes); **(c)** planozygote; **(d)** hypnocyst (resting cyst) formation within the theca; **(e)** theca discarded (cysts may be smooth, rigid or spiny); **(f)** dormancy; **(g)** excystment through the archaeopyle; **(h)** meiocytic planozygote; **(i)** meiotic division (h and i may take place in the cyst and meiosis may involve one or two divisions). Not shown: temporary cysts that may be asexually produced from asexually reproducing motile cells (a).

of two types: desmoschisis and eleutheroschisis. Out of the three types of desmoschitic reproduction, the binary fission, which is a simple pinching and splitting of one cell onto two, is considered as the most common type. This type of reproduction commonly occurs in unarmored (naked) dinoflagellates (Blackburn *et al.* 1989). On the other hand, during the eleutheroschitic reproduction, parental cell sheds its theca (i.e. undergoes ecdysis) either before or immediately following cell division. Peridinialeans are known to have this type of reproduction (Hoppenrath 2016).

CELLULAR MORPHOLOGY AND IDENTIFICATION

Whether living as a swimming, solitary cell or a nonmotile symbiont within an invertebrate host, all living dinoflagellates have certain common (intra/extra cellular) morphological characteristics (Gómez 2012).

EXTERNAL MORPHOLOGY

Cingulum, Sulcus and Flagella

In most dinoflagellates, the motile cells possess unique furrows, i.e. cingulum and sulcus, among which the cingulum (depressed transverse furrow), one of the important criteria for morphological identification, usually encircles the whole cell. As a result, the cell seems divided into two parts, upper part (*epitheca, epicone, episome*) and lower part (*hypotheca, hypocone, hyposome*). However, the encircling pattern, relative position and displacement of the cingulum can vary, and in some taxa such as podolampids no depressed cingulum exists (Hoppenrath 2016). The longitudinal furrow, termed sulcus, is positioned perpendicular to the cingulum and runs toward the cell's posterior. The cingulum and the sulcus contain two different types of flagella, and due to the combined movement of these two flagella dinoflagellates can freely swim around. The *transverse flagellum*, typically inserted in the cingulum, generally encircles the

whole cell along with the cingulum with a special waving pattern, and the other (*longitudinal flagellum*) runs along the sulcus toward the cell posterior. This flagella arrangement is known as the *dinokont* condition. In a few dinoflagellates, however, both flagella arise from the anterior end (called *desmokont* condition) (Figure 3).

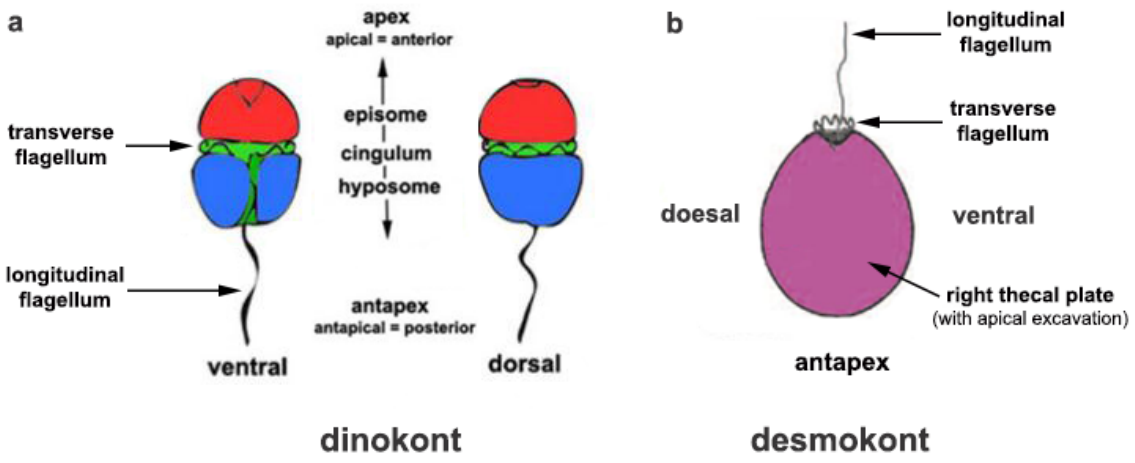

Figure 3. Overview of flagellation type of dinoflagellates. **(a)** typical dinoflagellate flagellation type, dinokont; and **(b)** desmokont.

Amphiesma (Cortex) and Tabulation

As one of the three main groups comprising the Alveolata, the other two being ciliates and apicomplexans, dinoflagellates possess vesicles beneath the outer cell membrane (= plasma membrane). These alveolos/amphiesma are shared among all three groups. The term amphiesma was originally coined and used to describe a layer separating the cytoplasm from the surrounding water. Later, Loeblich (1970) described this term more precisely using electron microscopy as a continuous membrane enclosing the cell (plasma membrane, PM), beneath which lies a series of flattened, membrane-bound vesicles (amphiesmal vesicles). This basic structure is shared by

both athecate and thecate dinoflagellates. Beneath the thecal vesicles is an unbroken layer termed the pellicle (P) (Figure 5).

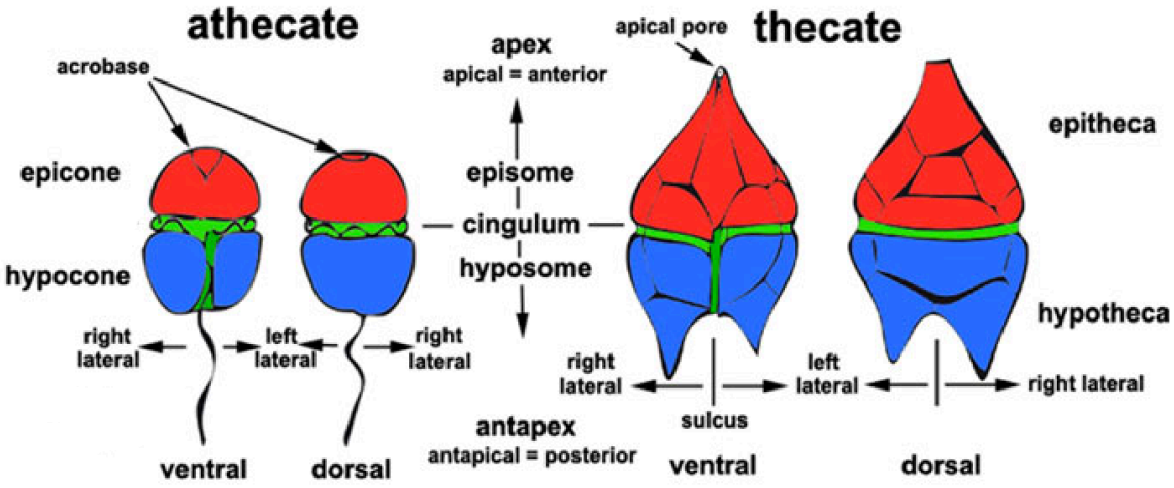

Figure 4. Schematic representation of the dinoflagellate external morphology. Red, epitheca; green, cingulum; blue, hypotheca (from Hoppenrath 2016).

It is within these vesicles (amphiesmal vesicles, AVs) that the cellulose plates (thecal plate) are formed, one per vesicle in thecate (= armoured) dinoflagellates. In athecate (= unarmored, naked) species, the vesicles are either empty or contain amorphous material (Figures 4, 5), and the vesicles themselves play a structural role (Dodge & Crawford 1971, Hoppenrath 2016).

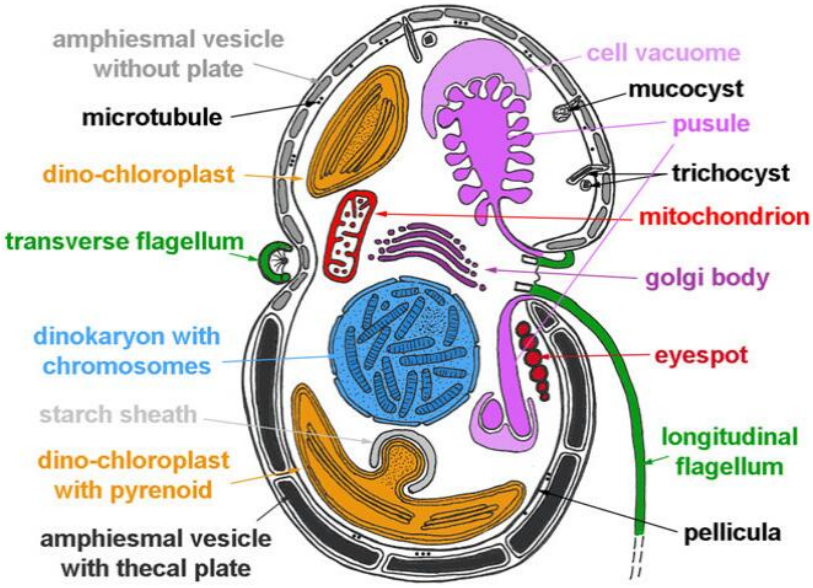

Figure 5. Schematic drawing of a generalized motile dinoflagellate cell showing ultrastructural characteristics (from Hoppenrath 2016).

These thecal plates, in different numbers, shapes and sizes, form a unique pattern by abutting one another tightly. This distinct thecal plate arrangement has been used as a major criterion in taxonomic studies for more than 100 years. Six fundamental types can be recognized (Figure 6).

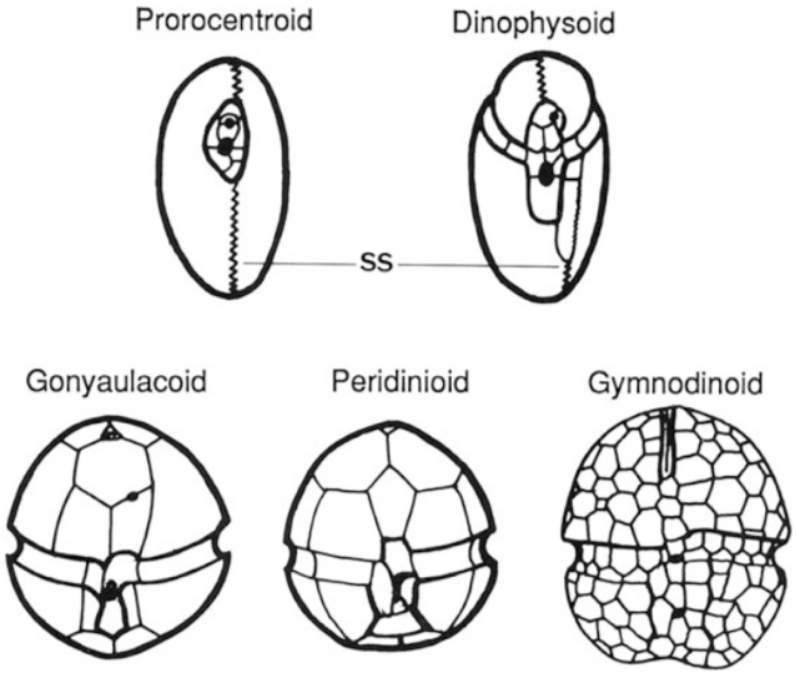

Figure 6. Basic thecal organizational types (From Fensome *et al*. 1999).

The earliest application of these plates in taxonomic research of dinoflagellates was linked back to the works of Ehrenberg (1838) and Stein (1883). To date, several tabulation systems have been proposed such as Bütschli's system, Stein's Rautenplatte and Kofoidian system. Despite its several defects, the tabulation and nomenclature system of Kofoid has subsequently gained prominence and is now widely used throughout the world (Taylor 1999, Hoppenrath 2016). This system was developed by Kofoid C. A. (1917), and persistently used until now just for the reason of being comprehensive and simpler to apply to most gonyaulacoid and peridinioid dinoflagellates (Taylor 1980).

Kofoid's system groups the plates in circular rows or series parallel to the cingulum and around the apex. On the epicone the plates are divided into the apical plates (1'–4' in the example shown) (Figure 7) surrounding the apex, the precingular plates next to the cingulum (1"–7"), and in between the two series some species possess dorsal plates, now named anterior intercalary plates (1a–3a). On the hypocone the postcingular series abuts the cingulum (1'"–5'") and partly surrounds the antapical plates (1""–2""). If plates are present between the two series, they constitute the posterior intercalary plates (uncommon in the Peridiniales, but quite common in the Gonyaulacales) (Figure 7). However, problems arise when there is a need for comparison. This major weakness becomes more evident in the determination of plate homology because numbering plates simply from left to right is no more applicable when a subdivision occurs among the plates. Likewise, deciding whether a plate is a sulcus or not will also become problematic, as its definition by a depression or marginal ridges can differ in closely related genera.

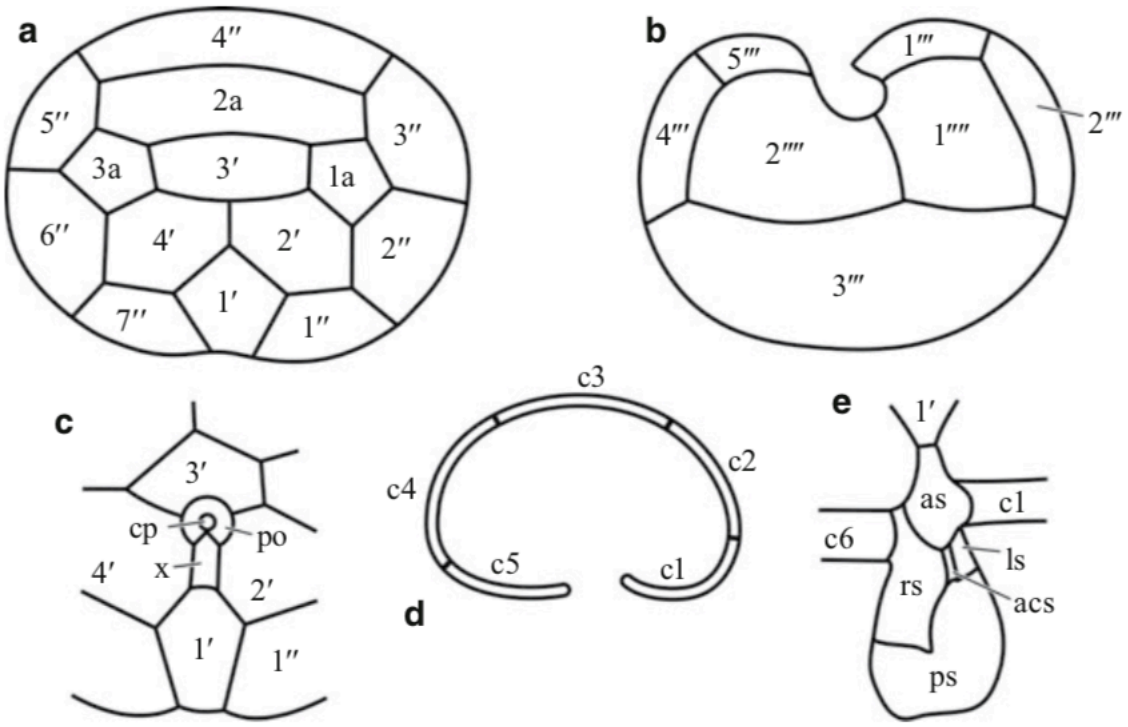

Figure 7. Illustration of the nomenclature for thecal plates in Kofoid system (using Peridinioid dinoflagellates as an example). **(a)** apical view of plates covering the epicone, **(b)** antapical view of plates covering the hypocone, **(c)** apical area, with the round pore plate (po), the small cover plate (cp) closing the pore, and the ventrally located, rectangular, so-called canal plate (x), **(d)** apical view of cross-section through a cingulum, plates marked c1–c5, **(e)** sulcal plates, respectively anterior (as), right (rs), left (ls), posterior (ps) and the small (often hidden) accessory sulcal plate (acs) (from Øjvind Moestrup *et al*. 2018).

IDENTIFICATION OF DINOFLAGELLATES

In my thesis, I am only concerned with the dinokont type of dinoflagellates and thus I will concentrate only on the dinoflagellates with dinokont morphology here. For the identification of thecate dinoflagellates, generally the thecal plate arrangement pattern is primarily used for identification at generic rank. Although there are many exceptions, traditionally, when the plate pattern is the same (similar), then these dinoflagellates are considered phylogenetically related (in many cases this statement is proven to be true). Therefore, for the thecate dinoflagellates, the

analysis of thecal plate arrangement is essential. At species level, in addition to the thecal plate arrangement, the cell morphology, cell size, position of nucleus, shape and number of chloroplasts/pyrenoids, the presence or absence of eyespots, the ornamentation of thecal plate surface, etc. are used. For identifying athecate dinoflagellates, the shape of cell contour, form of cingulum, cell size, position of nucleus, shape and number of chloroplasts/pyrenoids, the presence or absence of eyespots are used. Recently, with the advent of SEM technology, the arrangement pattern of small amphiesmal vesicles are also used as a taxonomic criterion (Figure. 6, gymnodinioid). In addition to these morphological taxonomic criteria, molecular tools are frequently used these days (see below).

INTERNAL MORPHOLOGY

Nucleus and plastids

Dinoflagellates have also several unique ultrastructural features (Figure 5). One of these is an unusual nucleus called a *dinokaryon*. This type of nucleus contains very large amounts of DNA, i.e. their genome sizes are remarkably huge and variable, ranging from 1~245 Gbp (Lin 2011, Lin *et al.* 2015). The chromosomes are fibrillary, permanently condensed (i.e., remain continuously condensed during both interphase and mitosis), and do not have typical eukaryotic histones, thus there is no nucleosome in the nuclei (Spector *et al.* 1981, Rizzo 1991). Later, it was shown that the loss of nucleosomal DNA condensation coincides with the appearance of a novel nuclear protein in dinoflagellates (Gornik *et al*. 2012).

All dinoflagellates arose from photosynthetic ancestors, and the plastids of a large majority of the photosynthetic members of the group share genetic similarities to the apicomplexan

apicoplast and the plastids of chrompodellids like *Chromera* and *Vitrella* (Janouškovec *et al*. 2017). The main type, the so-called peridinin plastid, is enveloped by three parallel membranes having no obvious connections with the nuclear envelope and containing various types of pyrenoids. Within the chloroplast, each lamella consists of thylakoids of stacks of three, without girdle lamella. This type of typical dinoflagellate plastid (peridinin type) was derived from a secondary endosymbiosis with a photosynthetic organism of red algal origin (Zhang *et al*. 1999). Interestingly, up to now, seven additional types of chloroplasts have been reported. These unusual types of plastid were obtained by capturing different groups of algae (endosymbioses) (Schnepf & Elbrächter 1999; Orr *et al.* 2012). The photosynthetic organelles in dinoflagellates derived from other protists include haptophyte-derived plastids in the family Kareniaceae (Ishida & Green 2002, Nosenko *et al.* 2006), prasinophyte-derived 'plastids' (in the genus *Lepidodinium*) (Hansen *et al.* 2007), diatom-derived plastids in the family Kryptoperidiniaceae and cryptophyte derived kleptochloroplasts (in most species of the genera *Dinophysis* and *Nusuttodinium*), (Schnepf & Elbrachter 1988, Janson 2004, Takano *et al*. 2014) etc.

Ejectile Bodies (Extrusomes)

Dinoflagellates are also known to contain several different types of extrusomes (i.e., organelles that secrete materials to the exterior), such as trichocysts, mucocysts, taeniocysts and/or nematocysts. Of these, the trichocysts are the commonest organelle possessed by many dinoflagellates. Other than that, more elaborate and complex extrusomes, nematocysts and taeniocysts, were found in polykrikoids and warnowiids (Westfall *et al*. 1983). Both are larger than trichocysts, the length of the nematocysts can reach up to 20 μm and is thought to be related to 'hunting' of prey organisms (Westfall *et al*. 1983, Gavelis *et al*. 2017).

Pusules

A special organelle of dinoflagellates is the pusule. In motile cells, there are usually two specialized vacuoles that arise from ducts opening at the flagellar bases, in addition to the generalized cell vacuolar system (vacuome). In general, the pusule consists of a central collecting chamber and surrounding pusular vesicles (or pusular tubules) (Figure 5). This organelle occupies a substantial part of the cytoplasm; however, the function of this special organelle is still unknown (Craveiro *et al*. 2015, Hoppenrath 2016).

Eyespots (Stigma)

Dinoflagellates is the only group among the protists that is known for many eyespot types (Hansen *et al*. 2007). Along with the other morphological characteristics that have been used in generic level classification of dinoflagellates, such as presence or absence of thecal plates and the number of thecal plates, the eyespot is considered to be one of the most reliable taxonomic features (Moestrup & Daugbjerg, 2007). The eyespot is usually constituted by red or orange coloured pigment globules or crystal/brick-like elements. Five different types of eyespots (type A-E) were distinguished by Moestrup & Daugbjerg (2007), all of them situated in the sulcal area close to the flagellar roots, and their positions in the cell is very constant (Figure 5). The Type A eyespot *sensu* Moestrup and Daugbjerg (2007) is the commonest type in dinoflagellates and the red globules are located within the chloroplast. The Type B is similar to Type A but there is an additional layer of crystal-like bricks between the chloroplast membrane and the microtubular root (Figure 8 II (B)). In the Type C, the red globules are distributed outside of the chloroplast, near the sulcus (Figure 8 III (C)). Type D can be found only in dinotoms (dinoflagellates with a

diatom endosymbiont) and the red globules are surrounded by a triple membrane (Figure 8IV (D)). The Type E (Figure 8VI (E)) was originally discovered by Horiguchi & Pienaar (1994b) and is confined to the order Suwessiales. Figure 8 represents the latest classification of eyespot types in dinoflagellates by Hoppenrath (2016). In addition to the five types by Moestrup & Daugbjerg (2007), Hoppenrath (2016) recognized a newly discovered eyespot type (Type VI in Figure 8) (Craveiro *et al.* 2010). Furthermore, it was demonstrated that *Amphidinium cupulatisquama* and *Cochlodinium polykrikoides* possess an unusually positioned eyespot (Tamura *et al*. 2009, Iwataki *et al*. 2008) and thus Hoppenrath (2016) subdivided the type A eyespot into three: I(A), Ia and Ib, thusmaking a total of eight different types, I (including Ia, Ib) – VI (Figure 8).

MOLECULAR TAXONOMIC WORKS

Dinoflagellates are morphologically and genetically distinct from other eukaryotes, as mentioned above. Those morphological traits, such as tabulation, have been very useful in taxonomic studies. Additionally, the application of molecular analyses in taxonomic classification not only made the work more efficient but also caused taxonomists to look back and reexamine some of those dinoflagellates that were classified based on traditional morphological approaches (Carty 2008, Moestrup *et al.* 2009a, b, Gottschling *et al.* 2017, Dawut *et al.* 2018b). The molecular markers that have been applied in phylogenetic analyses are from three different organelles in the dinoflagellates, including: (1) nuclear ribosomal genes, small subunit (SSU), internal transcribed spacer (ITS) and large subunit (LSU); (2) mitochondrial genes, such as cytochrome oxidase 1 and 3 (*cox1* and *cox3*) and cytochrome *b* (*cob*); (3) chloroplast genes, large subunit (*cp23S*)

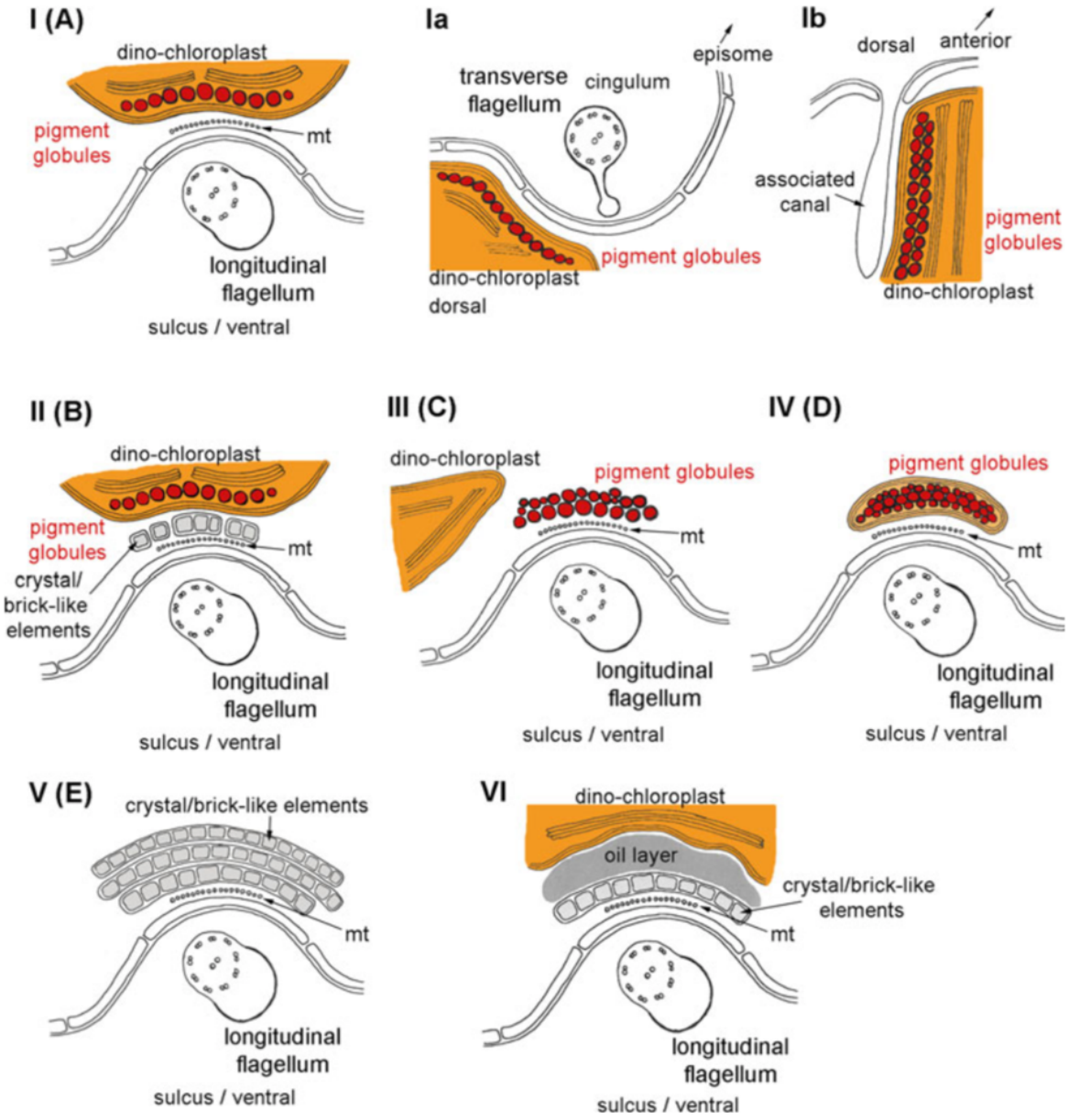

Figure 8. Schematic drawings of eight different types of eyespots in dinoflagellates, showing the transverse sections through the sulcal area, except for types Ia and Ib. Type I, located ventral in the sulcal area; found in many members of orders Peridiniales and Thoracosphaerales. Type Ia, located dorsal in the cingulum area; described from *Amphidinium cupulatisquama*. Type Ib, located apical dorsal in association with a canal; described from *Cochlodinium polykrikoides*. Type II, located ventral in the sulcal area; found in the family Borghiellaceae, but also in *Peridiniopsis borgei*. Type III, located ventral in the sulcal area; typical of the Tovelliaceae (chloroplasts may be absent). Type IV, located ventral in the sulcal area; found only in the Kryptoperidiniaceae. Type V, located ventral in the sulcal area; common in the order Suessiales; Type VI, located ventral in the sulcal area; so far found only in *Sphaerodinium* (from Hoppenrath 2016).

and coding region of the plastid-encoded photosystem II protein D1 (*psbA*) (Sampayo *et al.* 2009, Pochon *et al.* 2012, 2014). Furthermore, recent developments in the field of dinoflagellate phylogeny, as the utilization of transcriptomes, fill the gaps that have not been resolved through molecular methods (Hoppenrath *et al.* 2014, Janouškovec *et al.* 2017). As a still developing field, dinoflagellate taxonomy above genus level cannot readily be resolved by morpho-molecular methods completely.

TIDAL POOL DINOFLAGELLATES

Dinoflagellates can live in a special habitat: tidal pools (also known as Rock Pools) (Figure 9). Tidal pools are ubiquitous yet relatively understudied components of rocky shores (Metaxas & Scheibling 1993, Underwood & Skilleter 1996). Tidal pools form a widely distributed habitat where environmental conditions are subject to wider fluctuations than in the sea (Gibson 1986) and are considered dynamic ecosystems, changing with the flow of tides (Jensen and Muller-Parker 1994). Due to daily fluctuations in the environment (e.g., temperature, salinity, etc.) tidal pools experience anthropogenic pressures and extreme conditions. Studies of tidal pool communities, in general, have found species which are rarely or never recorded from open waters (Dethier 1980, Jonsson 1994, Horiguchi & Chihara 1983, 1988). Often, such tidal pool species have physiological or behavioral adaptations which can aid population persistence in individual pools (Blackwell & Gilmour 1991, Jonsson 1994).

The 'tidal pool dinoflagellates' are defined here as dinoflagellates which have adapted to the environment of tidal pools and have the ability to produce dense blooms in tidal pools (Figure 9). So far, several dinoflagellates were described from this habitat: *Bysmatrum gregarium* (Lombard

& Capon) Horiguchi & Hoppenrath (as *Peridinium gregarium* Lombard & Capon), (Lombard & Capon 1971), *Bysmatrum arenicola* Horiguchi & Pienaar (Horiguchi & Pienaar 1988b), *Scrippsiella hexapraecingula* Horiguchi & Chihara (Horiguchi & Chihara 1983), *Gymnodinium pyrenoidosum* Horiguchi & Chihara (Horiguchi & Chihara 1988), *Bysmatrum austrafrum* (Dawut *et al*. 2018a), *Ansanella natalensis* (T. Horiguchi & Pienaar) Dawut, Sym & T. Horiguchi (as *Gymnodinium natalense* Horiguchi & Pienaar) (Dawut *et al*. 2018b) and *Alexandrium hiranoi* Kita & Fukuyo (Kita & Fukuyo 1988). Among this *B. arenicola* was reported only from tidal pools with sandy bottom.

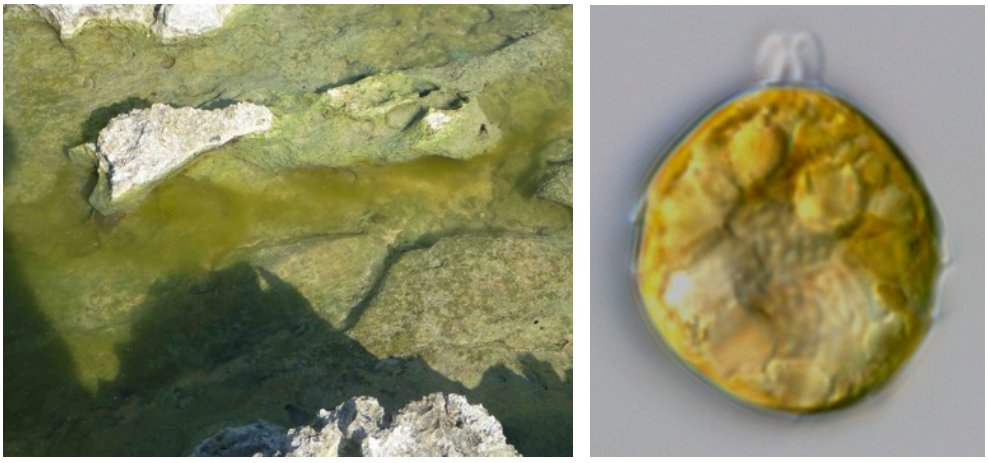

Figure 9. Photograph of a typical tidal pool with bloom taken from Odo, Southern Okinawa, and a dinoflagellate strain isolated from this tidal pool.

The bloom forming tidal pool dinoflagellates exhibit a characteristic diurnal migratory behavior depending on the tidal movement (Horiguchi & Chihara 1988). During low tide (day time), in exposed (isolated from the sea) tidal pools dinoflagellates form dense blooms and swim actively (Figures 9, 10a). However, in the evening, before the tide comes into the pool, dinoflagellates sink to the bottom and firmly attach themselves to the substratum, transforming into a non-motile stage so that cells are not washed out to the open sea during high tide. Some species produce an apical stalk from the apex of the motile cell, by which the cells firmly anchor

themselves to the substratum (Figure 9). Cell division takes place during non-motile stage at night (Figure 10c). In the next morning at low tide, the daughter cells are released from the parental thecae and repeat the same behavior (life cycle) again (Figure 10d).

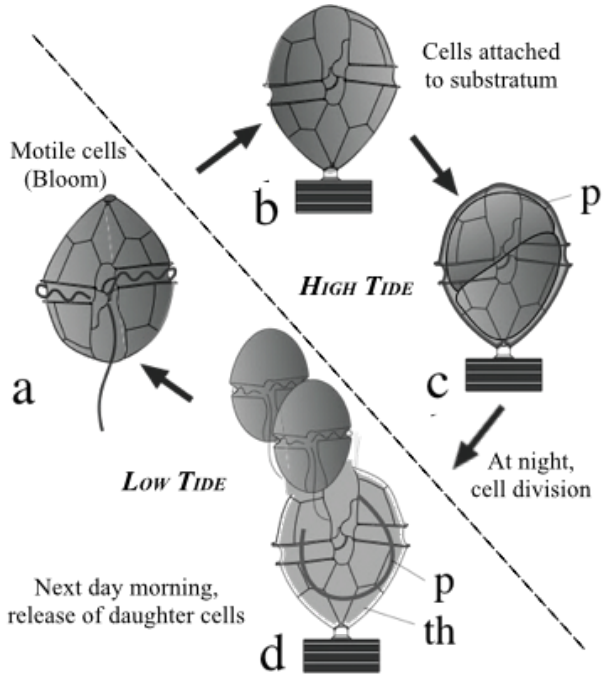

Figure 10. Line drawing of the life cycle of tidal pool bloom-forming dinoflagellates. **(a)** motile cell in bloom, at low tide; **(b)** non-motile cell, at the high tide; **(c)** dividing cell, at non-motile stage; **(d)** newly released daughter cells, at low tide. (modified from Sekida *et al*. 2001).

The existence of certain types of bloom forming dinoflagellates living in tidal pools was reported long ago (Hirano 1967). Later on, Lombard and Capon (1971) reported a species, *Peridinium gregarium*, from a tidal pool in southern California describing, for the first time in an algal group, a type of diurnal migration in which great number of individuals were held together by a mucous matrix forming a cloud-like bloom in the tidal pool. At late afternoon, the individuals would leave the matrix to return to the pool bottom. Subsequently, several bloom forming species with the same diurnal migration pattern were reported from the coasts of central and southern Japan and South Africa (Horiguchi & Chihara 1983, Horiguchi & Pienaar 1988a, 1994a, 2000, Dawut *et al*. 2018a).

Despite all above mentioned distinctive characteristics, studies on tidal pool dinoflagellates are still scarce. Moreover, all previous research on tidal pool dinoflagellates only described the external morphology. A very little molecular work has been done and their taxonomic conclusions have to be confirmed using current molecular techniques.

It was reported that dinoflagellates in tidal pools are permanent residents of this harsh habitat, and that blooms are monospecific (Shah *et al*. 2010). This means that the blooms in different tidal pools may consist of different dinoflagellate species. Yet, no extensive morpho-molecular studies concerning this type of characteristic have been done. Thus, it is necessary to answer the questions: (1) does every tidal pool contain a single species (monospecific) or multiple species? (2) is there any genetic or morphologic difference among the dinoflagellates from neighboring and distant tidal pools? (3) is the geological separation possible among the tidal pool dinoflagellates?

THE AIM OF THIS THESIS

Based on previously reported data, especially the pioneer work done by Horiguchi and his colleagues, it can be easily assumed that there are many undescribed species of tidal pool dinoflagellates. With this in mind, I conducted my research to obtain a better understanding of the following aspects:

1. to further explore the species biodiversity of bloom forming tidal pool dinoflagellates in Japan and South Africa.
2. to conduct molecular phylogenetic studies on these dinoflagellates. Most of the previous taxonomic studies on tidal pool dinoflagellates were mostly performed based only on

morphological observations. So, it is necessary to understand their phylogenetic position through molecular analyses.

3. to compare genetic distances between populations within the same species from different localities. Due to the distinct life cycle pattern of tidal pool dinoflagellates, i.e. not easily washed out to the open sea, it can be hypothesized that there should be genetic dissimilarity between the species collected from neighboring pools in the same area, distant pools in the same area, and different pools in different areas (as illustrated in Figure. 11). However, no such phylogeographic work has been done for tidal pool dinoflagellates.

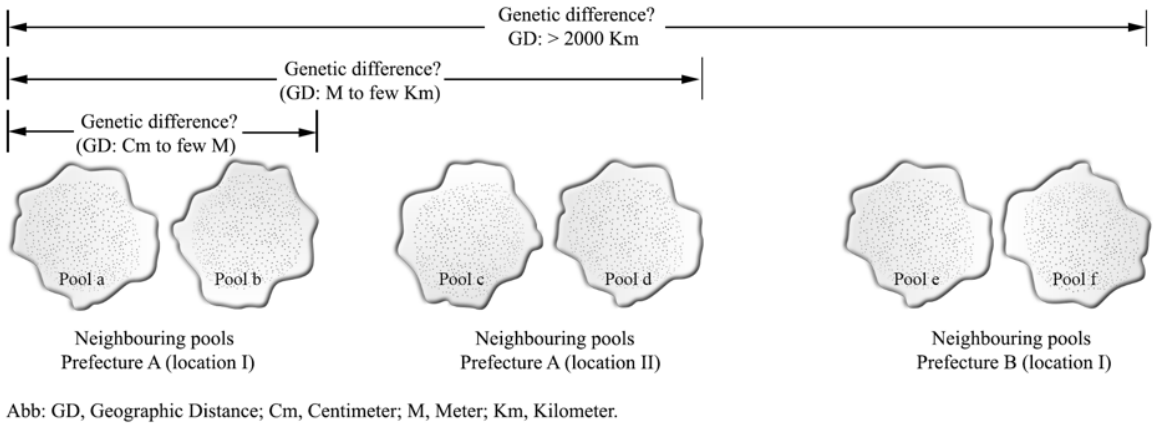

Figure 11. Schematic illustration of the relationship between geographical distribution and the genetic diversity of tidal pool dinoflagellates.

CHAPTER II

Bysmatrum austrafrum sp. nov. (Dinophyceae) a novel tidal pool dinoflagellate from South Africa

INTRODUCTION

Several dinoflagellates inhabit tidal pools where they form blooms during low tides (Horiguchi & Chihara 1983). These dinoflagellates include *Bysmatrum gregarium* (Lombard & Capon) Horiguchi & Hoppenrath (as *Peridinium gregarium* Lombard & Capon), (Lombard & Capon 1971), *Bysmatrum arenicola* Horiguchi & Pienaar (Horiguchi & Pienaar 1988b), *Scrippsiella hexapraecingula* Horiguchi & Chihara (Horiguchi & Chihara 1983), *Gymnodinium pyrenoidosum* Horiguchi & Chihara (Horiguchi & Chihara 1988), *Ansanella natalensis* (T. Horiguchi & Pienaar) Dawut, Sym & T. Horiguchi (as *Gymnodinium natalense* Horiguchi & Pienaar) (Dawut *et al*. 2018b) and *Alexandrium hiranoi* Kita & Fukuyo (Kita & Fukuyo 1988). As mentioned, the genus *Bysmatrum* includes a few tidal-pool-inhabiting, bloom-forming species.

The genus *Bysmatrum* was established based on the type species, *B. subsalsum* (Ostenfeld) Faust & Steidinger (Basionym: *Peridinium subsalsum* Ostenfeld) (Faust & Steidinger 1998). The genus was characterised by possessing the plate formula Po, X, 4′, 3a, 7″, 6c, 4s, 5‴, 2⁗, which is similar to *Scrippsiella*. However, *Bysmatrum* was distinguished from *Scrippsiella* by the fact that the 2a and 3a plates are separated by a direct contact between the 3′ and 4″ plates, a feature unique to the genus (Steidinger & Tangen 1996, Faust & Steidinger 1998, Murray *et al*. 2006). Moreover, recent studies based on molecular analyses have reported and confirmed that *Bysmatrum* occupies a clearly distinct phylogenetic position from *Scrippsiella* (Gottschling *et al*. 2012, Jeong *et al*. 2012, Limoges *et al*. 2015, Anglès *et al*. 2017).

To date, five species have been described as members of the genus *Bysmatrum*. These include *B. subsalsum* (Faust & Steidinger, 1998), *B. gregarium* (Hoppenrath *et al*. 2014), *B. arenicola* (Horiguchi & Pienaar 2000), *B. granulosum* Ten-Hage, Quod, Turquet & Couté (Ten-Hage *et al*. 2001) and *B. teres* Murray, Hoppenrath, Larsen & Patterson (Murray *et al*. 2006). Note that *Bysmatrum caponi* (Lombard & Capon) Faust & Steidinger is a synonym of *B. gregarium* (Lombart & Capon) Horiguchi & Hoppenrath (Hoppenrath *et al*. 2014). In terms of habitat, the type species *B. subsalsum* has been reported from plankton samples collected over oyster beds in Florida (Steidinger & Balech 1977); it was also reported in association with floating detritus, coral rubber and sediment at Twin Cays, Belize (Faust & Steidinger 1998). *B. arenicola* was discovered in sandy-bottomed tidal pools in South Africa. This dinoflagellate showed vertical migration within the sand layer in relation to tidal movement, and the dinoflagellate cells stayed on the sand surface during low tide, making coloured patches that never dissociate into the water column. During high tide, when the pools were submerged, the cells moved down to deeper part of sand layer (Horiguchi & Pienaar 1988b). *B. gregarium* (as *Peridinium gregarium*) was reported as a tidal pool bloom forming dinoflagellate from Palos Verdes Peninsula, California, U.S.A. (Lombart & Capon 1971). *B. granulosum* was collected from sediments and coral samples from La Reunion Island (SW Indian Ocean), and *B. teres* was collected from the first 0.5 cm of exposed sediment at low tide at Town Beach, Broome, Western Australia (Murray *et al. 2006*). Therefore, all *Bysmatrum* species are benthic, although *B. subsalsum* was also collected from plankton (Steidinger & Balech 1977, Anglès et al. 2017).

During the course of our taxonomic survey of marine benthic dinoflagellates along the coast of South Africa, we encountered several blooms in tidal pools which were subsequently established into unialgal culture. Our detailed study revealed that the organism involved was a novel species

of the genus *Bysmatrum*. Here, we describe this species based on light microscopy, scanning and transmission electron microscopy and infer its phylogenetic placement based on nuclear-encoded SSU-rDNA phylogenetic analysis.

MATERIAL AND METHODS

Water samples were collected from a tidal pool at Bordjiesrif, Cape Peninsula, South Africa (34˚18.815′S, 18˚27.737′E) on 19 January 2014 using a large pipette and transported to the Laboratory of Phycology in the Faculty of Science, Hokkaido University in small screw cap glass bottles. In the laboratory, water samples were transferred into plastic dishes containing autoclaved seawater supplemented with Daigo`s IMK medium (Nihon Pharmaceutical Co., Tokyo, Japan) for enrichment and were cultured at 20°C at an irradiance of 50 μmol photons $m^{-2}s^{-1}$ with a 16:8 light:dark regime. Swimming cells were isolated using drawn capillary Pasteur pipettes and subsequently a clonal culture (designated as HG321) was established. This culture strain has been maintained in IMK medium under the same conditions mentioned above.

Light microscopy

Light microscopic observations of motile cells were made using a Carl Zeiss Axioskop 2 microscope equipped with Nomarski interference optics (Carl Zeiss Japan, Tokyo). Photographs were taken using a Leica MC-120HD digital camera (Leica Microsystems, Germany).

Scanning electron microscopy

For scanning electron microscopy, cells were fixed in 5% glutaraldehyde (final concentration) for 40 min. The fixed cells were rinsed first with IMK medium, then with IMK medium diluted 1:1 with distilled water, and finally with distilled water. The samples were dehydrated in an ethanol series (30, 50, 70, 90, 95%) followed by two rinses in 100% ethanol for 30 min and dried in a critical point drier (Hitachi HPC-2, Tokyo, Japan). The dried cells were sputter-coated with gold for 180 s at 12 mA (Hitachi E-1045) and observed with a scanning electron microscope (S-3000N, Hitachi).

Transmission electron microscopy

Cells were concentrated by gentle centrifugation (800 r.p.m for 5 min), fixed with cold 2.5% (v/v) glutaraldehyde for 30 min on ice, rinsed with filtered sea water (FSW), and post-fixed with 1% (v/v) osmium tetroxide for 1h on ice. After one rinse in FSW and one in distilled water, the sample was dehydrated in an ethanol series of 25, 50, 70, 95, 100%, with two subsequent washes in 100% ethanol and three in 100% acetone. Finally, cells were embedded in low viscosity (LV) resin (Agar Scientific, Essex, England). After polymerization at 65°C for 16h, thin sections were cut using a diamond knife on an ultramicrotome (Leica EM UC6, Germany). Sections were picked up on formvar-coated one-slot grids and viewed with a transmission electron microscope (H-7650, Hitachi).

Phylogenetic analysis

Approximately 20 motile cells were used to extract DNA by applying the Quick Extract™ FFPE DNA extraction kit (Epicentre, Tokyo, Japan) according to the manufacture`s protocol. The

small subunit ribosomal RNA gene (SSU rDNA) was amplified using three pairs of primers (chapter IV, Table 2). The 25 µl PCR amplification process consisted of 1 initial cycle of 5 min at 94°C, 35 cycles of 30 s at 94°C (denaturation), 30 s at 50°C (annealing), 90 s at 72°C (extension). The final extension cycle was at 72°C for 7 min. The PCR products were purified and sequenced with ABI PRISM Big Dye Terminator (Perkin-Elmer, Waltham, Massachusetts, USA). The final step of sequencing was done using a DNA auto-sequencer ABI PRISM310 Genetic Analyzer (Perkin-Elmer).

The obtained sequences were aligned manually, on the basis of the published secondary structure of the SSU rRNA molecule, using alveolate taxa available at the rRNA server. The 3041 aligned sites (1688 bases augmented by the gaps from the rRNA secondary structure) were used for the analysis. *Perkinsus marinus* (Mackin, Owen & Collier) Levine (Perkinsozoa) was used as out-group for the SSU rDNA analysis. The aligned sequences were analysed by the maximum likelihood (ML) method using PAUP* version 4.0b10 (Swofford 2001) and the Bayesian method using MrBayes 3.2.1 (Huelsenbeck & Ronquist 2001, Ronquist & Huelsenbeck 2003). The programme jModel Test version 2.1.4 (Guindon & Gascuel 2003, Darriba *et al*. 2012) was used to calculate the evolutionary model that was the best fit for ML analysis of the data set. The selected model was the TIM2+I+G model. The heuristic search for the ML analysis was performed with the following options: a tree bisection reconnection branch-swapping algorithm and the Kimura 2-parameter neighbor-joining tree as a starting tree. The parameters used for the analysis were as follows: assumed nucleotide frequencies (user-specified) A=0.25389, C=0.18787, G=0.25612, T=0.30212; substitution rate matrix with A<->C=1.39472, A<->G=4.25594, A<->T=1.39472, C<->G=1, C<->T=8.84787, G<->T=1; proportion of sites assumed to be invariable=0.306814; rates for variable sites assumed to follow a gamma

distribution with shape parameter=0.582388; and number of rate categories=4. For the Bayesian analysis, GTR+I+G was selected as the best evolutionary model by MrModeltest 2.3 (Nylander *et al*. 2004). Markov-chain Monte Carlo iterations were carried out for 10,000,000 generations, when the average standard deviations of split frequencies fell below 0.01, indicating the convergence of the iterations. For comparison, we sequenced the SSU rDNA of *Bysmatrum arenicola*. The material used for this was collected from a tidal pool at Port Edward, South Africa (31˚2.777′S, 30˚13.748′E) on 28 September 2011. The DNA was extracted from material preserved in Lugol's solution, using the methods described above.

RESULTS

Bysmatrum austrafrum Dawut, Sym, Suda & Horiguchi sp. nov.

Figures 1–24.

Description: Cells photosynthetic, armoured, thecal surface reticulated, 25–45 µm long, 20–42.5 µm wide, dorsoventrally slightly flattened; epitheca conical and hypotheca trapezoidal, equal of same size; the large apical pore plate is surrounded by three segmented apical collars, apical stalk is present and canal plate is long; apical plate 1′ heptagonal, with finger-like extension at the base, broadly asymmetric, touching the anterior sulcal plate; intercalary plate 2a and 3a separated by plate 3′; cingulum descending about 1.5 times of its own width; well excavated and wide sulcus with a sulcal list formed by plate 1‴; single chloroplast with numerous, golden-brown, irregular to rod-shaped lobes radiating from a central pyrenoid traversed by some thylakoids; orange eyespot present at the sulcus; nucleus sausage-shaped, situated in the hypotheca; orange accumulation body present in variable positions.

***Holotype*:** The specimen collected on 19 January 2014, as scanning electron microscope stub (SAP: 115272) (some illustrated in Figures 5–13) deposited in the Faculty of Science Herbarium, Hokkaido University.

***Type Locality*:** Tidal pool at Bordjiesrif, Cape Peninsula, South Africa (34˚18.815′S, 18 ˚27.737′E).

***Etymology*:** *austrafrum* (*L*: South Africa) refers to the country where the species was collected.

Light and scanning electron microscopy

Cells of *Bysmatrum austrafrum* sp. nov. were photosynthetic, pentagonal to somewhat rounded in ventral view, 25–45 µm long and 20–42.5 µm wide (n = 20) (Figures 1–4, 5, 6). The epitheca was conical, while the hypotheca was trapezoidal in ventral view (Figures 1–3). The nucleus was sausage shaped and located in the hypocone (Figures 3, 4). The chloroplast was single, but with numerous, golden-brown, irregular to rod-shaped, radiating lobs from the centre of the cell; the distal end of each chloroplast lobe was densely distributed along the cell periphery (Figures 1–3). No clear pyrenoid was detected using light microscopy. The orange-coloured eyespot was small, rectangular and located near the sulcus (Figure 1). The accumulation body was an orange globule (Figure 2) of variable size and location within the cell. *Bysmatrum austrafrum* formed a dense bloom within the tidal pool. Motile cells in the bloom were entangled in a gelatinous matrix and formed a cloud-like mass (not shown). In culture, during the dark period, all the motile cells settled and attached to the substratum, becoming non-motile. An apical stalk consisting of a transparent gelatinous matrix (Figure 2) formed from the apex of motile cells and was used when the cells attached to the substratum. Cell division took place in the non-motile phase and was

stimulated by light. Motile cells were released from the non-motile parent cells, leaving behind empty thecae leaving numerous empty thecae on the bottom of the culture dish (not shown).

The thecal plate arrangement of *Bysmatrum austrafrum* was: Po, x, 4′, 3a, 7″, 6c, 4s, 5‴, 2‴′ (Figures 5–13). The thecal plate arrangement is schematically illustrated in Figures 14-16. The apical pore complex, consisting of the apical pore plate (Po) and the canal plate (X), was elongated and somewhat rounded hexagonal in shape. It had three thickened margins (collar) which were formed by the raised and overlapping apical borders of the 2′, 3′ and 4′ plates with the pore plate, but there was no raised collar at the margin which formed by connection of the canal plate (X) and the apical plate 1′ (Figures 9, 10, 14). The long axis of the apical pore complex was directed to the right side of the cell, because of the asymmetrical distribution of the epithecal plates (Figures 5, 7, 14). The size of epitheca was almost the same as that of the hypotheca in both ventral and dorsal view (Figures 1, 2, 5, 6). In apical view, the epitheca was almost circular, with a slight depression on the ventral side (Figures 7, 14). The surface of the thecal plates, with the exception of those of the sulcus and cingulum, generally was ornamented with longitudinal, reticulated ridges (Figures 5–8, 11–13).

The first apical plate (1′) was asymmetric, heptagonal, more expanded toward the right and made contact with the canal plate (x), plates 2′, 4′, 1″, 7″ and the anterior sulcal plate (Sa). The posterior extremity of plate 1′ was drawn out into a finger-like extension that made contact with the Sa plate to the left and the anterior margin of the 7″ plate to the right (Figures 5, 11, 12, 16). The other three apical plates (2′, 3′, 4′) were all hexagonal and of variable size. Plate 4′ was the largest and made contact with the Po, X, 1', 3′, 3a, 6″ and 7″ plates (Figures 5-7, 11, 14). The first intercalary plate (1a) was four-sided and contacted the 2′, 1″, 2″ and 2a plates. The 2a plate was hexagonal and plate 3a was pentagonal, separated from each other by the direct connection

between the apical plate 3′and precingular plate 4″ (Figures 6, 7, 14). In most cells, the left extremity of the 7″ plate was almost separated off by a short, incomplete, vertical (suture-like) slit (Figures 12, 16). Because this suture-like slit is incomplete, the small triangular part of the 7″ plate could not be regarded as a further precingular plate (8″).

The cingulum was well excavated, descended 1-1.5 times its own height and consisted of six plates which were only faintly or not detectably reticulated. The first cingular plate (C1) was transversely elongated like any cingular plate, and its sigmoid right edge was firmly united to the anterior sulcal plate (Sa) (Figures 5, 12, 16). The entire margins on both sides of the cingulum were lined by narrow cingular lists. The lower cingular list at the left extreme extended to partially border the right edge of postcingular plate 1‴ and on the other extreme bordered the left edge of plate 5‴ and extended to border right side of the 2‴′ plate (Figures 5–8, 12, 13, 16). The right edge of the plate 5‴ was also bordered by similar looking narrow fin (Figures 8, 13, 16). The right extreme of the upper cingular list extended to the list (Isl) on the left edge of the right sulcal plate (Sr), but actually these two lists are disconnected by a small gap (Figures 12, 16).

The anterior of the sulcus of this species was relatively narrow, expanded somewhat posteriorly, with an abrupt widening mostly brought about by antapical rather than sulcal plates (Figure 12). The sulcus itself did not reach the antapex (Figures 8, 12, 13). An elongation of the anterior sulcal plate (Sa) extended into the epitheca, making connection with the C1, 1′, 1″ and 7″ plates (Figures 5, 11, 12, 16). The irregular shaped left sulcal plate (Sl) was commonly covered to some extent by the extended cingular plate lists (i.e. the list of postcingular plate 1‴ and the internal sulcal list). The posterior sulcal plate (Sp) was irregularly ‘boomerang-shaped’, while the right sulcal plate (Sr) was more or less pentagonal in shape and slightly reticulated (Figures 12, 13, 16).

The first postcingular plate (1‴) was the smallest of the five postcingular plates, and was pentagonal, with a left sulcal list (Lsl) (Figures 5, 8, 12, 15). Both antapical plates (1⁗, 2⁗) were partially ornamented with reticulated projections and not indented. Both were roughly pentagonal, the first being elongated (Figures 8, 12, 13, 15).

Intercalary bands were present in the mature cells (Figure 6), but they were not obvious in young cells (Figure 5). They were narrow and smooth (Figures 6, 7, 13). All plates had different sizes of pores, mostly restricted to groupings around the margin of each plate (Figure 9), except those of the sulcus and cingulum (Figure 12).

Transmission electron microscopy

Cells of *Bysmatrum austrafrum* had a typical dinoflagellate organization (Figure 17). The cell contained a typical dinokaryotic nucleus with chromosomes in the hypocone (Figure 17). Chloroplast lobes were irregular to rod-shaped or elliptical in sectional view, radiating out from the centre of the cell. The thylakoids were grouped in bands of three as is typical of peridinin-containing dinoflagellates (Figures 18, 19). In most chloroplast lobes, the peripheral thylakoids formed a girdle lamella-like configuration (Figure 18). Each chloroplast lobe possessed a pyrenoid at its proximal end (Figure 17), the matrix of which was traversed by many thylakoid bands (Figures 17, 20). It is likely that all the pyrenoid matrices were connected and formed a single central pyrenoid, thus the chloroplast number was actually one. The pyrenoid complex was surrounded by numerous, small starch granules, but no apparent starch sheaths were observed (Figures 17, 20). Therefore, the presence of pyrenoid could not be confirmed using light microscopy.

The pusule consisted of a collecting chamber with surrounding spherical vesicles (Figure 21). The typical trichocysts were observed (Figure 22). The eyespot consisted of a double layer of globules located between the chloroplast envelope and the outermost thylakoids (Figure 23). This represents the Type A eyespot *sensu* Moestrup & Daugbjerg (2007). The cell covering of this species consisted of the plasma membrane and the amphiesmal vesicles. The thecal plates were completely enclosed in the individual amphiesmal vesicles (Figure 24).

Phylogenetic analysis

The phylogenetic position of the *B. austrafrum* (accession No. LC315693) was analyzed by ML and Bayesian analyses on the basis of a partial SSU rDNA sequence. The sequence of *B. arenicola* (accession No. LC315694) was also sequenced for the first time and included in the alignment. The ML phylogenetic tree is presented in Figure 25, with the bootstrap values (BT) of ML analysis and the posterior probability (PP) indices of Bayesian analysis. The topologies of the ML and the Bayesian trees were mostly congruent. *Bysmatrum arenicola* formed a clade with other *Bysmatrum* species (*B. subsalsum*, *B. gregarium*, and *B. austrafrum*) with maximal support (BT/PP = 100%/1.0). *B. austrafrum* formed a clade with moderate support with *B. subsalsum* (BT/PP = 61%/0.89). *B. arenicola* rooted at the base of the *Bysmatrum* clade.

DISCUSSION

On the basis of the cell shape (pentagonal), the finely reticulated thecal surface, the possession of an equatorially-positioned cingulum and a cingulum displaced by a distance exceeding its own width, *B. austrafrum* is similar to *B. subsalsum* and *B. gregarium*. The other three species of

Bysmatrum, *B. arenicola*, *B. granulosum*, and *B. teres*, markedly differ from *B. austrafrum* in both cell size and cell contours. The light micrographs of the re-examined holotype of *Bysmatrum gregarium* (as *Peridinium gregarium*, Horiguchi and Pienaar 1988a) made it possible for a direct comparison with the current material.

The morphological comparisons between *B. austrafrum*, *B. gregarium* and *B. subsalsum* are presented in Table 1. Cells of *B. austrafrum* had a unique size, intermediate between that of *B. subsalsum* and *B. gregarium.* The shape of apical pore complex (APC) in *B. austrafrum* (hexagonal) differed from those of *B. subsalsum* (tear-drop shaped, Faust 1996, Faust & Steidinger 1998) and *B. gregarium* (tear-drop to polygonal, Horiguchi & Pienaar 1988a, Mohanmmad-Noor *et al.* 2007, Jeong *et al*. 2012).

The shape of apical plate 1′ is another useful distinguishing characteristic of *B. austrafrum*. The face of the 1′ plate was asymmetric and pentagonal in both *B. subsalsum* and *B. gregarium* (Faust & Steidinger 1998, Horiguchi & Pienaar 1988a), while in *B. austrafrum*, it is broadly asymmetric and heptagonal, with a unique finger-like extension in contact with the 7″ plate rather than with the anterior sulcal (Sa) plate. In the former two species, the corresponding portion of the 1′ plate directly touches the Sa plate and lacks any such extension. In fact, none of the other known species of *Bysmatrum* has this finger-like extension (Figure 16).

The current work represents only the second report of the ultrastructure of any member of this genus, the first being that of *Bysmatrum arenicola* (as *Scrippsiella arenicola*; Horiguchi & Pienaar 1988b). *Bysmatrum austrafrum* and *B. arenicola* have similar chloroplast and pyrenoid types. The chloroplast lobes are rod-shaped and radiate from a central pyrenoid complex. The pyrenoid matrix is traversed by many thylakoid bands and is surrounded by many small starch granules (Horiguchi & Pienaar 1988b). Because a conspicuous starch sheath covering a common

pyrenoid matrix is absent, it is difficult to confirm the presence of pyrenoid using light microscopy. Once their ultrastructure becomes known, this pyrenoid/chloroplast configuration may prove common to all *Bysmatrum* species, and thus become a characteristic of the genus as a whole. The presence of trichocysts in *B. austrafrum* was demonstrated here for the first time in this genus, while the existence of this structure has not been specifically highlighted in *B. arenicola* (Horiguchi & Pienaar 1988b). It would be interesting to see whether other species of *Bysmatrum* possess trichocysts. The eyespot in the genus seems to be widespread and has been reported in *B. granulosum*, *B. gregarium* and *B. subsalsum*. However, their type/s, with the exception of *B. austrafrum* (Type A, *sensu* Moestrup & Daugbjerg 2007), has/have not been determined so far. The absence of an eyespot in *B. arenicola* seems to be the result of secondary loss.

The identification and classification of members of the genus *Bysmatrum* to date have been mainly based on morphological features. Inferred phylogenies from SSU rDNA sequences for the genus, now that we have added those of *B. arenicola* and *B. austrafrum* to those of *B. subsalsum* (Gottsching *et al*. 2012, Anglès *et al*. 2017) and *B. gregarium* (as *B. caponiid*, Jeong *et al*. 2012) show strong support for the genus as a valid taxon. Even more important is that a clear characteristic morphological feature, i.e. the separation of the 2a and 3a plates, provides a synapomorphy for the genus.

Bysmatrum arenicola is a sand-dwelling species that forms patch-like blooms on the surface of the sand layer within tidal pools, a behaviour quite different from that of other tiede pool, bloom-forming dinoflagellates, such as *B. gregarium* or *B. austrafrum*, which form dense blooms in the water column. In addition, cells of *B. arenicola* are quite different from those of the pentagonally-shaped *B. subsalsum* /*B. gregarium* /*B. austrafrum* and therefore, its inferred

phylogenetic position within the genus was quite intriguing. Its location on the phylogenetic tree suggests a basal taxon in *Bysmatrum* relative to species that were described as planktonic bloom formers. Such a relationship suggests and independent evolution of the diel vertical migration of planktonic members of this genus within tidal pools and the unusual vertical movement in the bottom sand. The flattened cell body in *B. arenicola* might be an adaptation to interstitial environment as many of the sand-dwelling species possess a compressed cell body (see Hoppenrath *et al.* 2014).

With regard to the phylogenetic position of the genus within the class Dinophyceae, Gottsching *et al*. (2012) demgottonstrated that *B. subsalsum* occupied an isolated and uncertain phylogenetic position outside the Thoracosphaeraceae. The current phylogenetic analyses, even after including more taxa, has done little to resolve this issue, and its position within the Dinophyceae remains ambiguous.

In conclusion, it is clear that *B. austrafrum* represents a new species of the genus based on distinct morphological features supported by molecular phylogenetic analyses. Furthermore, the genus itself represents a clearly characterized and valid taxon.

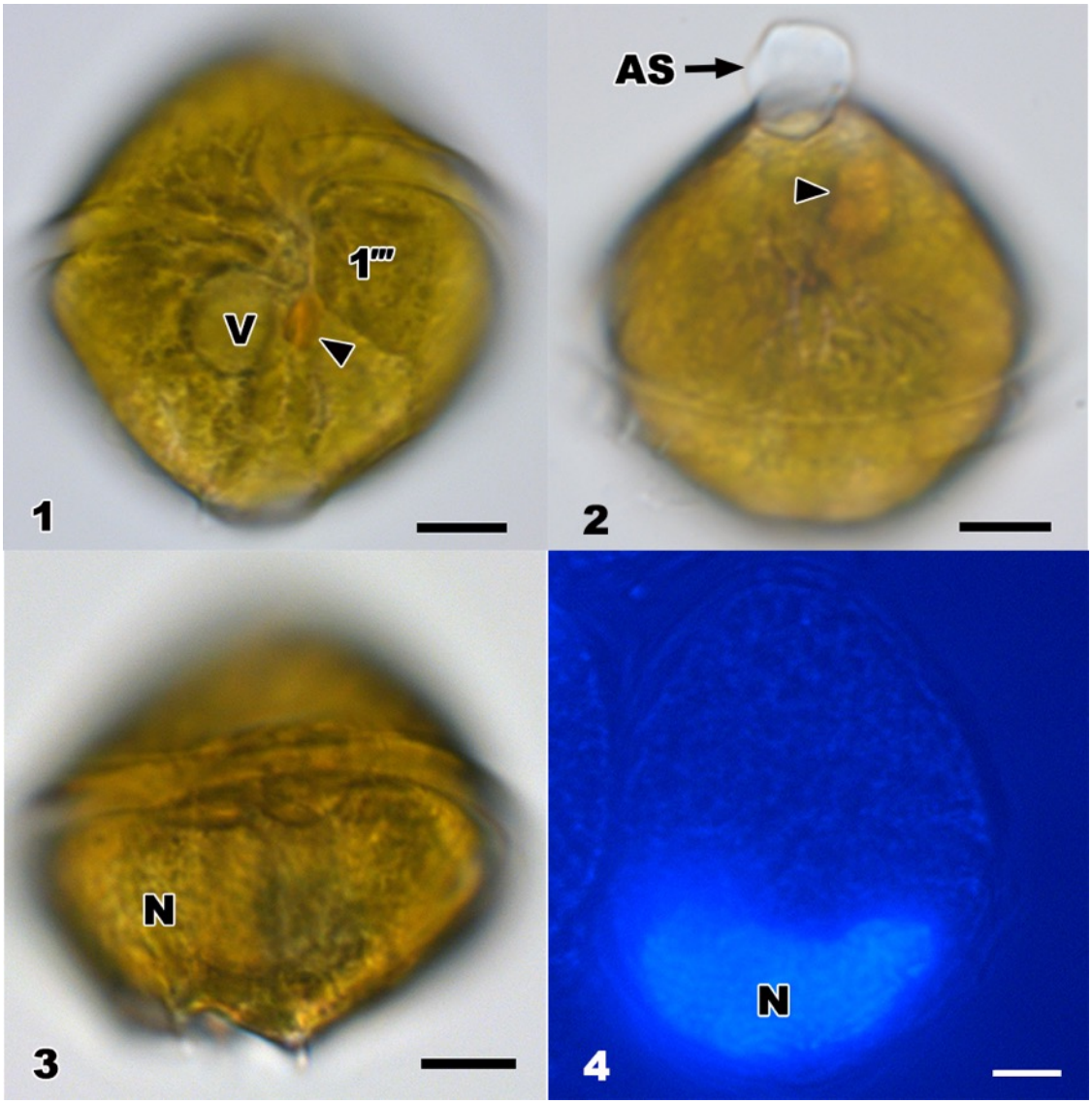

Figures 1-4. *Bysmatrum austrafrum* sp. nov. Light micrographs. Scale bars = 5 µm; **Figure. 1.** Ventral view. Arrowhead indicates the eyespot. V: vacuole. 1''': first postcingular plate; **Figure. 2.** Dorsal view, showing the apical stalk (AS). Arrowhead indicates the accumulation body; **Figure. 3.** Dorsal view. N: nucleus; **Figure. 4.** Fluorescence microscopy showing the shape of nucleus. N: nucleus.

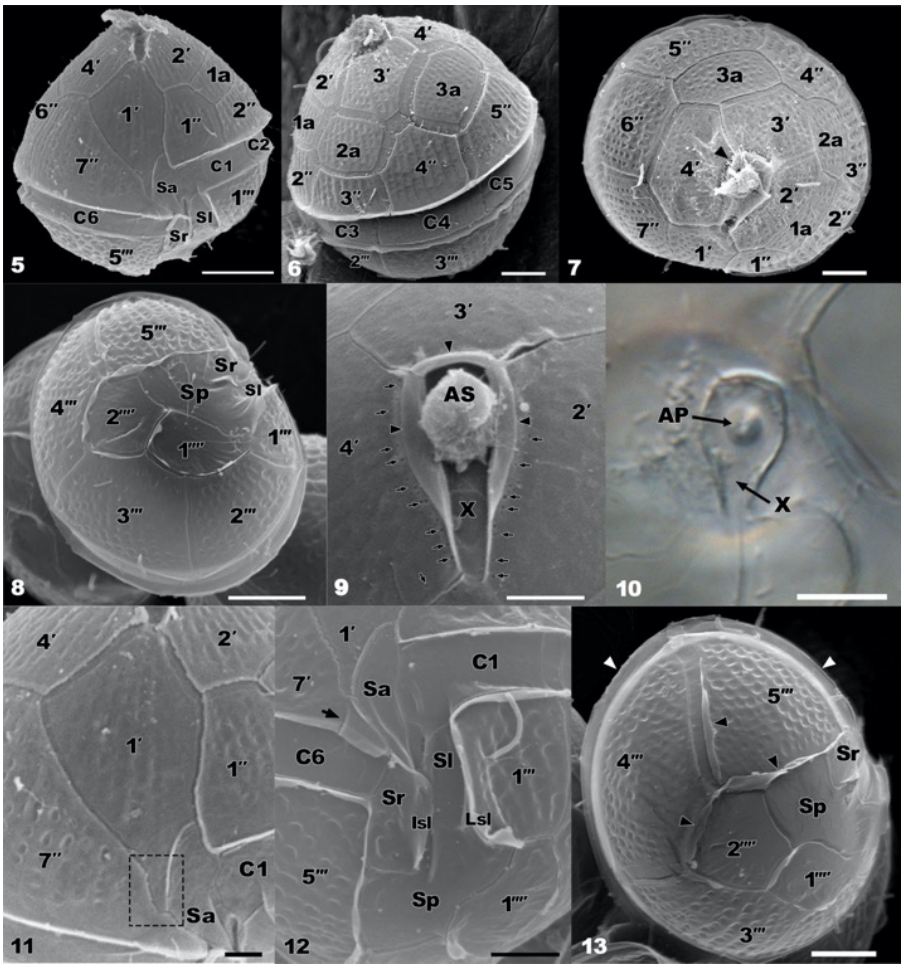

Figures 5-13. A light microscopic and scanning electron micrographs (SEM) of the surface morphology of *Bysmatrum austrafrum* sp. nov.; **Figure. 5.** Ventral view of young cell. Note lack of intercalary bands. Scale bar = 2 µm; **Figure. 6.** Dorso-anterior view of matured cell showing the developed smooth intercalary bands and hexagonal plate 2a. Scale bar = 5 µm; **Figure. 7.** Detail of the epithecal architecture including the position of the apical pore complex (arrowhead). Intercalary plates 2a and 3a are separated by plate 3′. Also note the quadrangular plate 1a and the pentagonal plate 3a. Scale bar = 3 µm; **Figure. 8.** Antapical view showing the thecal plate arrangement of the hypotheca. Note that smooth surface of the posterior plates 1⁗ and 2⁗. Scale bar = 4 µm; **Figure. 9.** The apical pore complex is a recessed chamber with a centrally located raised dome (Apical stalk: AS) surrounded by a collar formed by three plates (arrowheads). It includes the apical pore (obscured) and the canal plate (X). The apical pore complex is surrounded by pores of different sizes (small arrows). Scale bar = 3 µm; **Figure. 10.** Light microscopy of apical pore complex showing the raised collar and the hexagonal apical pore complex including apical pore (AP) and canal plate (X). Scale bar = 5 µm; **Figure. 11.** Detail of the ventral epitheca showing the asymmetric and heptagonal first apical plate (1′). Note the posterior extension to plate 1’ (squared). Scale bar = 2 µm; **Figure. 12.** Details of the sulcus. The anterior sulcal plate (Sa) is extended into the epitheca. Also note the incomplete suture-like slit in the left extension of Plate 7’ (arrow). Scale bar = 2 µm; **Figure. 13.** Antapical view showing the cingular list and lists of the postcingular plate 5‴ and 2’’’ (arrowheads). Scale bar = 3 µm.

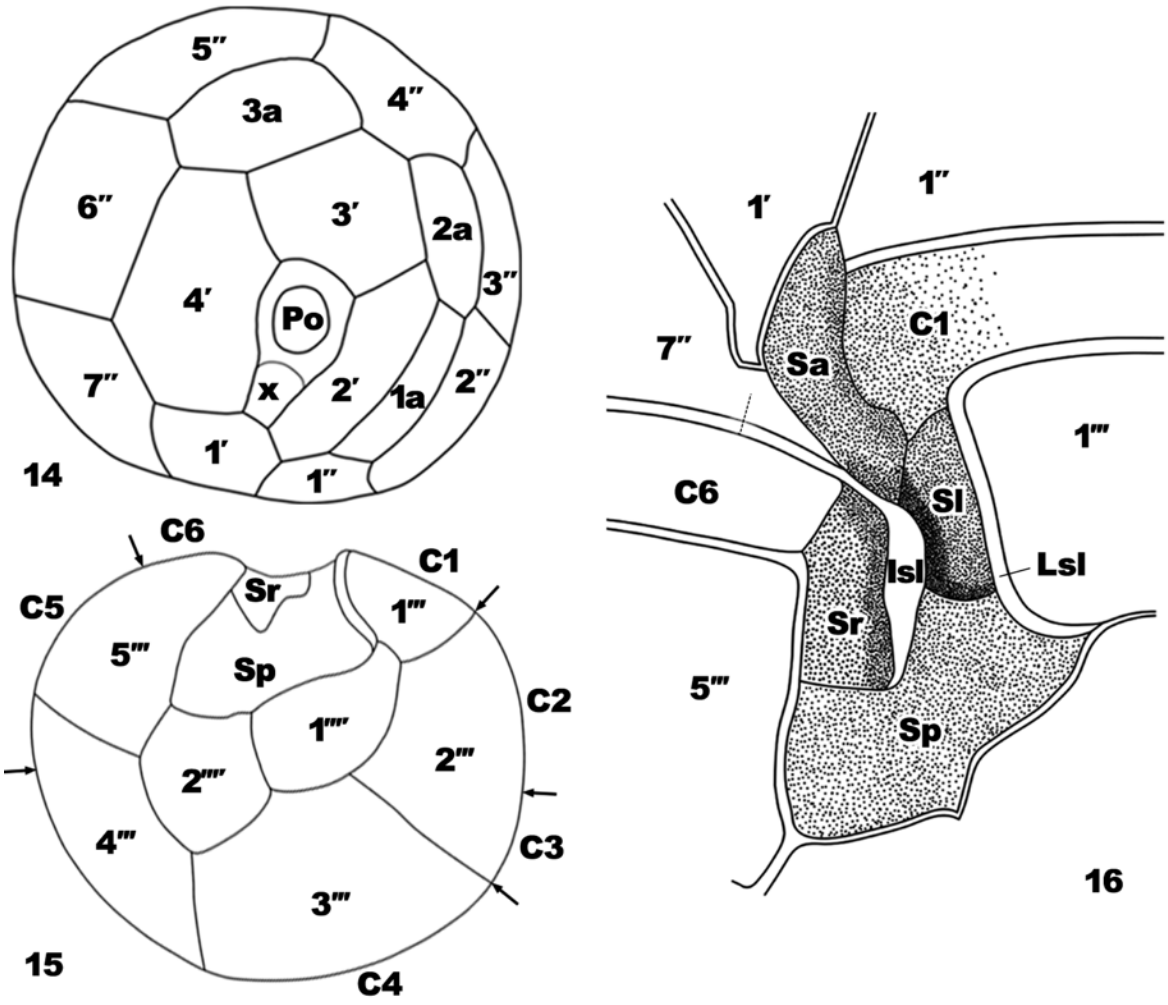

Figures 14-16. Line drawing of plate tabulation in *Bysmatrum austrafrum* sp. nov.; **Figure. 14.** Thecal arrangement of the epitheca; **Figure. 15.** Thecal arrangement of the hypotheca; **Figure. 16.** Thecal arrangement of the sulcal area. Sa: anterior sulcal plate, Sr: right sulcal plate, Sp: posterior sulcal plate, Sl: left sulcal plate, Isl: internal sulcal list, Lsl: left sulcal list.

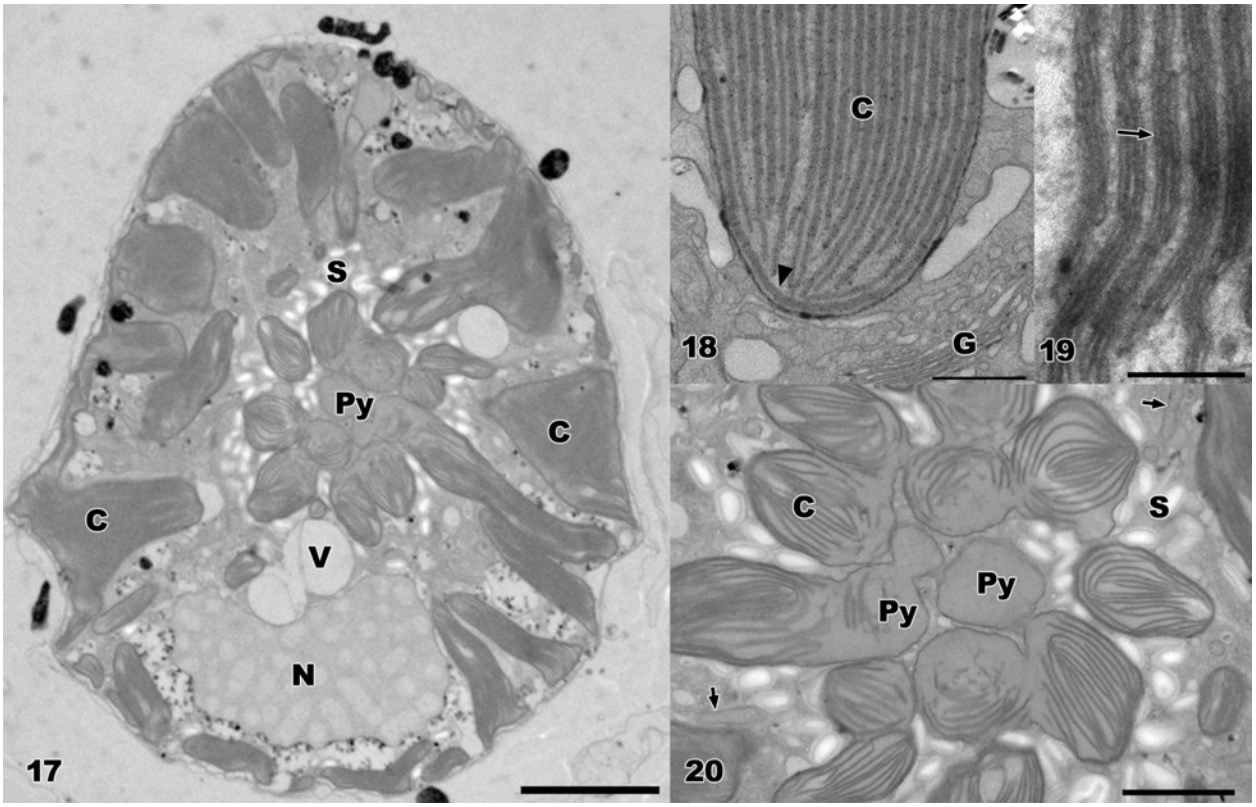

Figures 17-24. Transmission electron micrographs (TEM) of *Bysmatrum austrafrum* sp. nov.; **Figure. 17.** Longitudinal section through the cell showing general arrangement of organelles. C: chloroplast, N: nucleus, Py: pyrenoid, S: starch. V: vacuole. Scale bar = 5 μm; **Figure. 18.** Detail of the chloroplast (C). Note the girdle lamella-like thylakoids (arrow head). G: Golgi body. Scale bar = 500 nm; **Figure. 19.** Close up of thylakoids. The chloroplast profiles contain typical lamellae consisting of bands of three thylakoids (arrow), but occasionally part of the lamellae consist of only two thylakoids Scale bar = 200 nm; **Figure. 20.** Detail of the pyrenoid in the cell centre. The pyrenoid (Py) is central, surrounded by numerous small starch granules (S). Arrows indicate the regular mitochondria. Scale bar = 2 μm;

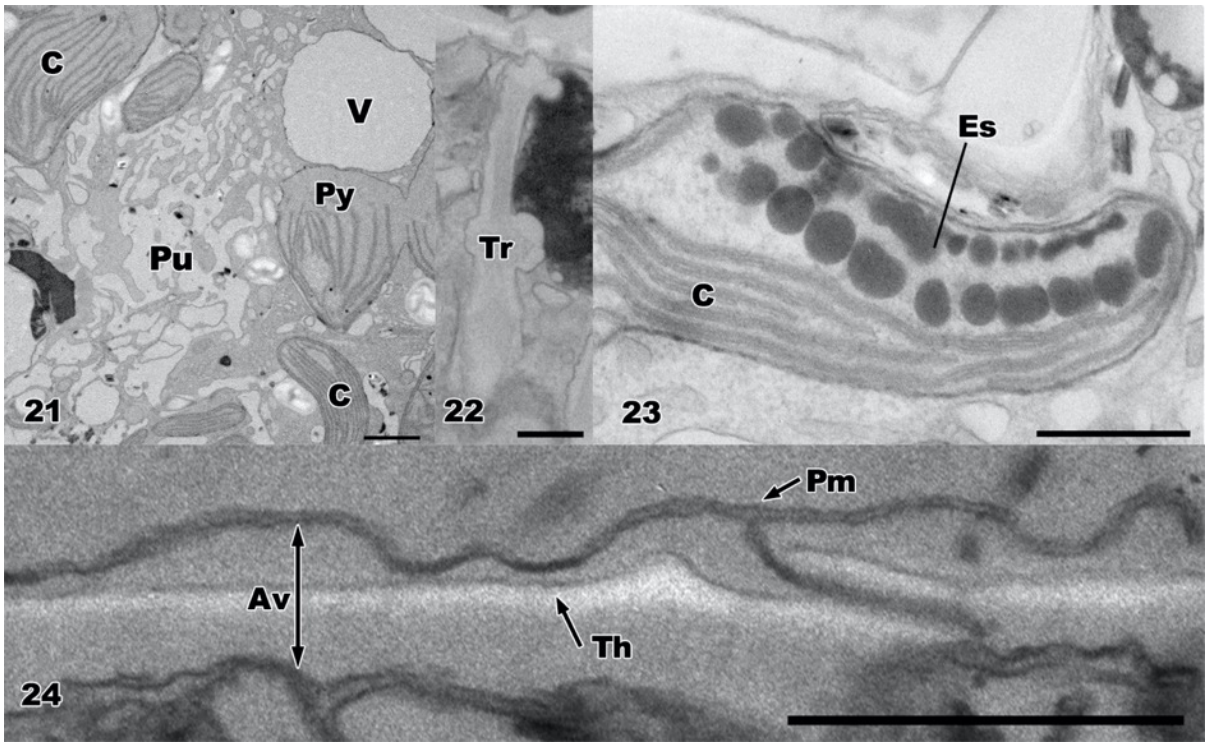

Figure 21. Detail of the Pusule (Pu). The pusule consists of central collecting chamber and surrounding vesicles (asterisks).C: chloroplast. Scale bar = 2 μm; **Figure. 22.** Trichocyst (Tr) located in the apical pore region. Scale bar = 300 nm; **Figure. 23.** Bilayered globules of the eyespot (Es) located between the plastid envelope and the outermost thylakoids within the chloroplast (C). Scale bar = 1 μm; **Figure. 24.** Detail of the amphiesma. Pm: plasma membrane, Th: thecal plate, Av: amphiesmal vesicle. Scale bar = 500 nm.

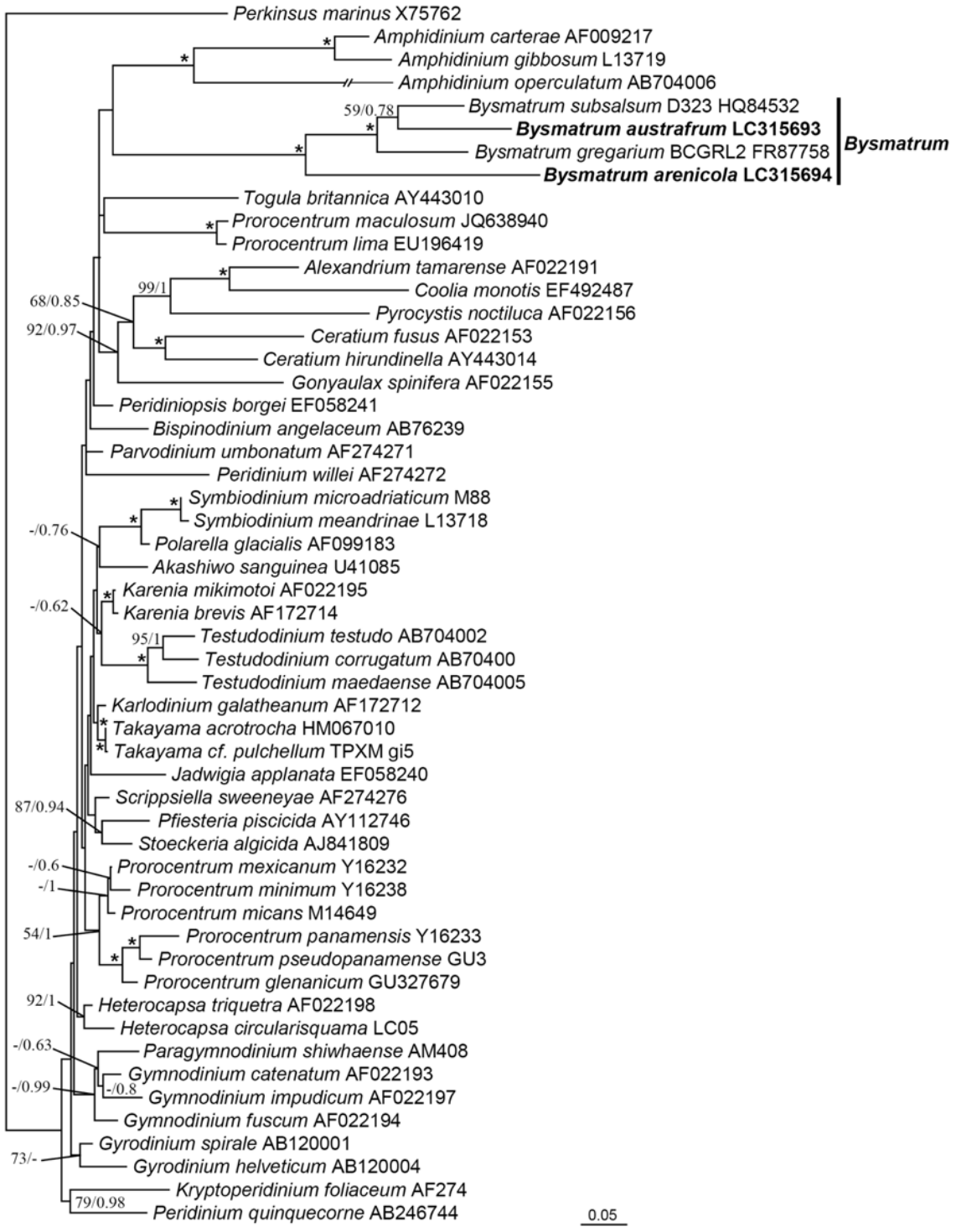

Figure 25. Topology of maximum likelihood (ML) phylogenetic tree inferred from partial small-subunit (SSU) ribosomal (r) DNA sequence alignment. Bootstrap support for ML analysis (100 pseudoreplicates) and Bayesian posterior probability (>50% and >0.8, respectively) are indicated. Nodes marked with an asterisk indicate 100% bootstrap support for ML analysis together with a Bayesian posterior probability of 1.

Table 1. Comparison of morphological features between species of the genus *Bysmatrum*.

Features	*B. gregarium*[a,b,c,d]	*B. subsalsum*[a]	*B. austrafrum* sp. nov.
Length (μm)	20.0-34.0	32.0-41.0	25.0-45.0
Width (μm)	20.0-34.0	31.0-51.0	20.0-42.5
Shape	pentagonal	pentagonal	pentagonal through round
Apical pore complex	tear-drop to polygonal	tear-drop	hexagonal
Apical stalk	yes	yes	yes
Thecal pores	*	*	yes
Cingulum descending	0.5-1 its width	1 its width	1-1.5 its width
1′ morphology	pentagonal	pentagonal	heptagonal
Intercalary bands	striated	striated	smooth
Antapical plates	indented	indented	not indented
Antapical spine	yes	N	N
Pyrenoid	*	*	yes
Nucleus	epithecal	equatorial	hypothecal
Habitat	tidal pool	epibenthic	tidal pool

[a] Faust & Steidinger (1998), [b] Jeong *et al.* (2012), [c] Horiguchi & Pienaar (1988a), [d]Mohammad-Noor *et al.* (2007)

N: feature was not observed; yes: present; *: as yet unknown;

CHAPTER III

Morpho-molecular diversity and phylogeny of *Bysmatrum gregarium* species complex (Dinophyceae) from Japan, with notes on their geographical distribution

INTRODUCTION

Dinoflagellates constitute one of the main groups of marine and freshwater protists (Gómez 2012). Their morphology is astonishingly diverse (Taylor 2008); They can be thecate or athecate. In thecate dinoflagellates, the plate pattern is referred to as tabulation. Since the unified classification, using the tabulation as the primary guide to relationship, of living and fossil dinoflagellates was proposed by Fensome *et al*. (1993), six basic types of tabulation were recognized, gymnodinoid, suessioid, peridinioid, gonyaulacoid, dinophysoid, and prorocentroid, on which major orders are based (Fensome *et al*. 1993, Taylor 1987b, c, 2004, 2008). In the Peridiniales, plate tabulation is one of the most important features for species identification. Each genus is circumscribed by a specific tabulation formula. The genus *Peridinium* was first described by Ehrenberg in 1838. Later studies indicate that this genus should be separated into several genera due to the different numbers of cingular and sulcal plates and the presence or absence of an apical pore (Loeblich 1968). Thus in 1959, Balech proposed a genus, *Scrippsiella*, by designating the *S. sweeneyae* as its type species; and a second species, *S. saladense* Balech, which he transferred from the genus *Peridinium* on the basis of six cingular plates and four sulcal plates (Balech 1974). Subsequently, a species from genus *Peridinium*, *P. subsalsum*, moved to genus *Scrippsiella*, as *S. subsalsum*, for the same reason mentioned above, by Steidinger & Balech (1977). Later, two other species, *S. arenicola* Horiguchi et Pienaar (1988a) and *S. caponii* Horiguchi et Pienaar (1988b) (= *P. gregarium* Lombard *et* Capon, 1971) were also classified into this genus. Recent studies, however, revealed some morphological characteristics that which differentiate these three species, *S. subsalsum*, *S. arenicola* and *S. caponii*, from other planktonic

scrippsielloid species by thecal reticulation and the lack of contact between intercalary plates 2a and 3a, which are separated by apical plate 3'. Hence, in 1998, Faust & Steidinger proposed a new genus, *Bysmatrum* for these three species, *B. subsalsum* (Ostenfeld) Faust et Steidinger, *B. arenicola* (Horiguchi & Pienaar) Faust et Steidinger and *B. gregarium* (= *B. caponii*, illegitimate) (Horiguchi & Pienaar) Faust et Steidinger, by designating, *B. subsalsum* as the type species.

To date, total of six species have been classified into genus *Bysmatrum*. *B. sunsalsum*, *B. arenicola*, *B. gregarium*, *B. granulosum* Ten-Hage, Quod, Turquet & Couté, *B. teres* Murray, Hoppenrath, Larsen & Patterson and *B. austrafrum* Dawut, Sym, Suda & Horiguchi (Ten-Hage *et al*. 2001, Murray *et al*. 2006, Dawut *et al*. 2018a). All the species in this genus shared a stable thecal plate arrangement (i.e., tabulation), which is as follows: Po, X, 4', 3a, 7", 6c, 4s, 5'", 2"", and the main morphological distinguishing features of the genus *Bysmatrum* are that all species possess three anterior intercalary (1a, 2a, 3a) plates, that the second and third anterior intercalary plates are not in contact with one another, that there are six cingular plates and that the posterior sulcal plate does not touch the cingulum. Moreover, all species so far described possess apical stalks, by which they attach to the substrate. Some species, can proliferate in their habitats and form bloom (Lombard & Capon 1971, Horiguchi & Pienaar 1988a, Faust & Steidinger 1998, Dawut *et al*. 2018a). In terms of habitat, all six species of *Bysmatrum* described from tropical and subtropical regions (Faust 1996, Faust and Steidinger 1998, Steidinger & Balech 1977), except *B. gregarium* was also reported from temperate areas, such as from a tidal pool near Los Angeles, CA, USA (Lombard & Capon 197) and from plankton samples collected from western Korea (Jeong *et al*. 2012). Out of six reported species so far, three of them described from tidal pools and from blooms in their habitat. *B. arenicola* was described from tidal pools with sandy substrata along the east coast of South Africa, and known to form a patch-like blooms on the

surface of tidal sand (Horiguchi & Pienaar 1988b); *B. gregarium* originally described from tidal pools in southern California, and reported to form a cloud-like mess (bloom) in the tidal pools (Lombard & Capon 1971); *B. austrafrum* was collected from a tidal pool, in South Africa, with dense bloom (Dawut *et al*. 2018a). Besides, *B. teres* was also sampled from tidal sand in Western Australia, but no reports of bloom formation (Murray *et al*. 2006). Furthermore, there are other reports about several dinoflagellates inhabit tidal pools where they form blooms during low tides (Horiguchi & Chihara 1988), as *Scrippsiella hexapraecingula* Horiguchi & Chihara (Horiguchi & Chihara 1983), *Gymnodinium pyrenoidosum* Horiguchi & Chihara (Horiguchi & Chihara 1988), *Ansanella natalensis* (Horiguchi & Pienaar) Dawut, Sym & T. Horiguchi (as *Gymnodinium natalense* Horiguchi & Pienaar; Horiguchi & Pienaar 1994) (Dawut *et al*. 2018b) and *Alexandrium hiranoi* Kita & Fukuyo (Kita & Fukuyo 1988).

As it mentioned in the previous chapter, tidal pools are one of the very unique habitats where the environmental conditions are subject to wider fluctuations than in the sea (Gibson 1986). The tidal flow is the main factor that effecting the environmental conditions (e.g., temperature, salinity, etc.) of the tidal pools, followed by the anthropogenic causes. Nevertheless, studies have revealed the existence of several microalgal species, such as *Bysmatrum* spp, which are rarely or never recorded from open waters (Dethier 1980, Jonsson 1994, Horiguchi & Chihara 1983, 1988). Often, such tidal pool species have physiological or behavioral adaptations which can aid population persistence in individual pools (Blackwell & Gilmour 1991, Jonsson 1994). However, the questions like the geological distribution and the phylogenetic relationship of the tidal pool species within the neighboring and distant tidal pools, are still remained unanswered.

To elucidate the morphological and phylogenetic relationships between the tidal pool species from different tidal pools (neighboring and distant), and to investigate the species diversity of

bloom forming microalgae, I chose *Bysmatrum gregarium*-complex as research material and collected samples from different localities in Japan.

MATERIALS AND METHODS

Sampling and culture establishment

Water samples were collected from three different prefectures in Japan, from August, 2015 to December, 2015 (Table 1), using a large pipette and transported to the Laboratory of Phycology in the Faculty of Science, Hokkaido University in small screw cap glass bottles. In the laboratory, water samples were transferred into plastic dishes containing autoclaved seawater supplemented with Daigo`s IMK medium (Nihon Pharmaceutical Co., Tokyo, Japan) for enrichment and were cultured at 20°C at an irradiance of 50 μmol photons $m^{-2}s^{-1}$ with a 16:8 light:dark regime. Swimming cells were isolated using drawn capillary Pasteur pipettes and subsequently clonal cultures were established. These culture strains have been maintained in IMK medium under the same conditions mentioned above (Table 1).

Light microscopy

Light microscopic observations of motile cells were made using a Carl Zeiss Axioskop 2 microscope equipped with Nomarski interference optics (Carl Zeiss Japan, Tokyo). An image analysis system was used to measure the length and width of motile cells from micrographs taken using a Leica MC-120HD digital camera (Leica Microsystems, Wetzlar, Germany).

Scanning electron microscopy

For scanning electron microscopy, cells were fixed in 5% glutaraldehyde (final concentration) for 40 min. The fixed cells were rinsed first with IMK medium, then with IMK medium diluted 1:1 with distilled water, and finally with distilled water. The samples were dehydrated in an ethanol series (30, 50, 70, 90, 95%) followed by two rinses in 100% ethanol for 30 min and dried in a critical point drier (Hitachi HPC-2, Tokyo, Japan). The dried cells were sputter-coated with gold for 180 s at 12 mA (Hitachi E-1045) and observed with a scanning electron microscope (S-3000N, Hitachi).

DNA extraction, polymerase chain reaction (PCR) amplification

Approximately 20 motile cells were used to extract DNA by applying the Quick Extract™ FFPE DNA extraction kit (Epicentre, Tokyo, Japan) according to the manufacture`s protocol. The small subunit ribosomal RNA gene (SSU rDNA) was amplified using three pairs of primers (Table 2, chapter III). The 25 µl PCR amplification process consisted of 1 initial cycle of 5 min at 94°C, 35 cycles of 30 s at 94°C (denaturation), 30 s at 50°C (annealing), 90 s at 72°C (extension). The final extension cycle was at 72°C for 7 min. The PCR products were purified and sequenced with ABI PRISM Big Dye Terminator (Perkin-Elmer, Waltham, Massachusetts, USA). The final step of sequencing was done using a DNA auto-sequencer ABI PRISM310 Genetic Analyzer (Perkin-Elmer).

Phylogenetic analysis

The DNA sequences determined in the present study were aligned using MAFFT v7.130b (Katoh & Standley 2013). Gblocks (Castresana 2000) was used to edit and eliminate gap positions in the

aligned sequences. The aligned sequences were analysed by the maximum likelihood (ML) method using PAUP* version 4.0b10 (Swofford 2001) and the Bayesian method using MrBayes 3.2.1 (Huelsenbeck & Ronquist 2001, Ronquist & Huelsenbeck 2003). The programme jModel Test version 2.1.4 (Guindon & Gascuel 2003, Darriba *et al*. 2012) was used to calculate the evolutionary model that was the best fit for ML analysis of the data set.

The selected model was the GTR+I+G model. The heuristic search for the ML analysis was performed with the following options: a tree bisection reconnection branch-swapping algorithm and the Kimura 2-parameter neighbour-joining tree as a starting tree. The parameters used for the analysis were as follows: assumed nucleotide frequencies (user-specified) A=0.260, C=0.200, G=0.269 and T=0.271; substitution rate matrix with A<->C: 1.23194, A<->G: 4.25828, A<->T: 1.23194, C<->G: 1.00000, C<->T: 9.37658, G<->T: 1.00000; proportion of sites assumed to be invariable=0.341; rates for variable sites assumed to follow a gamma distribution with shape parameter=0.617; and the number of rate categories=4. For the Bayesian analysis, GTR+I+G was selected as the best evolutionary model by MrModeltest 2.3 (Nylander *et al*. 2004). Markov-chain Monte Carlo iterations were carried out until 2,000,000 generations were attained, when the average standard deviations of split frequencies fell below 0.01, indicating the convergence of the iterations.

RESULTS

Based on the phylogenetic analysis, I have recognized three main clades (group I, II, and III) in the *B. gregarium*-complex. The three strains from each group were mainly examined morphologically, Maeda 7-4 (here and after as M7-4) from the group I, Nemoto 1-2 (here and

after as N1-2), from the group II and Heisaura 3-2 (here and after as H3-2) from the group III. The reason that I have selected above-mentioned representative strains randomly, because according to my preliminary survey, there were little morphological differences within each group.

Light microscopy

In general, cells of all three strains of *Bysmatrum gregarium*-complex has mostly similar morphology. Cells were photosynthetic, armored, pentagonal to somewhat rounded in ventral view; the epitheca was conical, whereas the hypotheca was trapezoidal in ventral view; an apical stuck (AS) was present with mucilaginous material produced from the apical region. Cells have single but different colored chloroplast that its lobes were radiating from the center of the cell. No clear pyrenoid was detected, from any of them, using light microscopy. A reddish eyespot was present at the sulcus area (Figures 1, 2, 3). However, they showed some minor difference in their morphology, in particularly, the cells size, color of the chloroplast, position of the nucleus etc.

Bysmatrum sp. M7-4 was 24.4–33.2 (28.4 ±3, n=20) µm long and 23–31 (25.8 ±2.9, n=20) µm wide. The nucleus was located in the hypocone, near the cingulum (Figure 1c). The chloroplast was golden in color (Figure 1). An orange-colored globule, accumulation body (Ac), was observed (Figure. 1a–c). A wide and strongly striated intercalary bands also could be detected with the light microscopy (Figure 1c). The details of the apical pore complex (APC) was observed; it was tear-drop to somewhat polygonal shaped, and consisted with pore plate (Po) and elongated canal plate (X) (Figure 1d).

Whereas, *Bysmatrum* sp. N1-2 and H3-2 possessed yellowish-brown chloroplast. The cell size of the *Bysmatrum* sp. N1-2 and *Bysmatrum* sp. H3-2 were 21.8–33.2 (26.8 ±2.9, n=20) µm long and 20.2–32.4 (24.8 ±3.5, n=20) µm wide and 24.4–34.3 (28.3 ±3.1, n=20) µm long and 22.5–31.4 (25.9 ±3, n=20) µm wide, respectively. The cell's hypotheca was indented, in both *Bysmatrum* sp. N1-2 and H3-2, in its right side (Figures 2a, c; 3a, c). The nucleus of the *Bysmatrum* sp. N1-2 and H3-2 was situated in the epitheca, near the cingulum (Figures 2a, c; 3a). An orange accumulation body, at the cell hypocone, was seen in *Bysmatrum* sp. N1-2 (Figure 2a), with light microscope, but not observed from the *Bysmatrum* sp. H3-2. A big vacuole (V) was present in both *Bysmatrum* sp. N1-2 (Figure 2b) and *Bysmatrum* sp. M7-4 (Figure 1a). Interestingly, the thecal plates of the *Bysmatrum* sp. H3-2 were clearly visible under the light microscope (Figures 1b–d).

All three strains were collected where they formed a bloom. In culture, they showed a diurnal behavior; during the dark period, all the motile cells settled and attached to the substratum, becoming nonmotile. An apical stalk consisting of a transparent gelatinous matrix (Figures 1b, 2a, 3a, b) formed from the apex of motile cells and was used when the cells attached to the substratum. Cell division took place in the nonmotile phase during night period. Upon stimulation of light, motile cells were released from the nonmotile parent cells, leaving behind empty thecae on the bottom of the culture dish (not shown). Some external morphological features of the cell can be observed using light microscope, as it shown in the Figures 1d and 2d.

Scanning electron microscopy

The thecal plate arrangement of all three strains were identical and was Po, X, 4', 3a, 7", 6C, 4S, 5"', 2"" (Figures 3-6). The surface of the thecal plates was reticulated. The cell surface of the

Bysmatrum sp. M7-4 and H3-2 was ornamented with different size of pores; especially the APC area and the edges of the thecal plates (Figures 4b, e, 6e); some pores were different from the regular pores, in which they have small dome shaped structures raised from the pores (Figure 4e). The APC was tear-drop to somewhat polygonal in shape, and consisted of Po and X plates. The Po plate was oval to circular in all three strains, but the X plate was differed in their shape; the X plates of the *Bysmatrum* sp. M7-4 and N2-1 were elongated and trapezoidal in shape, and the pate surface of the X plate of the *Bysmatrum* sp. M7-4 was ornamented with pores which were smaller that the once on the thecal plates (Figures 4e, 5e), whereas the X plate of the *Bysmatrum* sp. H3-2 was seemingly have two small plates, although the lower end of those two small plates were not completely separated (Figure 6e).

The epitheca was comprised of three latitudinal rows. First row, consisted with four plates (1'–4') which touched with and encircled the APC, known as apical plates. The apical plate 1' was broadly asymmetric, irregularly pentagonal in shape; the upper end of this plate contacted the X plate, and the lower end the sulcal anterior plate (Figures 4a, 5a, d, 6a, d). The apical plates 2', 3', and 4' were irregularly hexagonal. Second row, intercalary, constituted with three plates (1a, 2a, 3a). Among which, the 2a and 3a did not contact with each other, due to the connection of 3' and 4". The 1a of all three strain was four-sided, where the 1a of *Bysmatrum* N1-2 was more elongated than the other two (Figures 4a, 5a, c, d, 6a, d). Seven precingular plates (1"–7") were constituted the third row of the epitheca. Mostly the first precingular plate (1") was the smallest and the 7" plate the largest. The left edge of the 7" plate extended toward the cingulum (Figures 4a, c, d, 5a, c, d, 6a, c, d).

The cingulum of all three strain was well excavated and have narrow cingular lists. The plate surface of all six cingular plates (C1–C6), in *Bysmatrum* sp. M7-4, N1-2 and H3-2, was striated

by depressions running parallel to the longitudinal axis of the cell; the degree of striation, however, differed from one another; the cingular plates of the Bysmatrum H3-2 was finely striated, while the *Bysmatrum* sp. M7-4, N1-2 showed rather faintly striation in their cingular plates (Figures 4a–d, 5a–c, 6a–c, f). Plus, only the cingular plates of the *Bysmatrum* sp. M7-4 ornamented by marginal pores on both sides (Figure 4b). The sulcus area, formed by four plates, anterior sulcal plate (Sa), posterior sulcal plate (Sp), and right and left sulcal plates (Sr and Sl) (Figures 4a, b, f, 5a, b, f, 6a, b, f). The Sa was elongated and touched with the first apical plate (1'). An elongation of the Sa, in M7-4, however, extended into the epitheca (Figure. 4a, b). The right (Sr) and left (Sl) sulcal plates were irregular in shape, and the Sl was commonly covered to some extent by the internal (Isl) and left (Lsl) sulcal lists, which were actually the extended cingular plate lists (Figures 4a, 5a, 6a). The posterior sulcal plate (Sp) was irregularly 'boomerang shaped'. The sulcal plates were generally smooth and ornamented by pores (Figures 4a, b, f, 5a, b, f, 6a, b, f). A slight ornamentation in the Sr of *Bysmatrum* M7-4 (Figure 4a, b) and in the Sr and Sp of *Bysmatrum* H3-2 was observed (Figure 6a, b). But, all four sulcal plates of *Bysmatrum* sp. N1-2 were smooth and no pores were detected (Figure 5a, b).

The hypotheca was comprised total of seven plates that formed two latitudinal rows, namely, postcingular plates (five plates, 1'''–5''') and antapical plates (1'''' and 2''''). All postcingular plates were four sided, except third postcingualr plate (3'''), which was irregularly pentagonal. Among wich, the first postcingular plate (1''') was the smallest and possessed a consistent list (Figures 4a–c, f, 5a, c, f, 6a–c, f); also, the 5''' of *Bysmatrum* N1-2 was seems to have a list which was formed by the extension of the lower cingular list (Figure 5f). The antapical plates (1'''' and 2'''') were irregularly shaped and partially ornamented (Figures 4a, b, f, 5f, 6b, c, f). Intercalary bands were present, mostly in the mature cells (Figures 4a–d, f, 5a–d, f, 6a–f). However, the intercalary

bands of the *Bysmatrum* M7-4 was much wider than the other two, and the sutures were also clearly visible from the SEM micrographics (Figure 4f).

Phylogenetic analysis

The maximum likelihood (ML) and Bayesian inference (BI) analysis based on SSU rDNA sequences yielded similar phylogenetic trees. The ML tree is illustrated in Fig. 7. All the isolates from this study, divided into three clades (group I–III). The group I and II formed a clade, although its statistical support was low. The group I included strains form Chiba and Okinawa prefecture, and formed a sister clade to a *B. subsalsum* species from South China Sea. The strains from Okinawa prefecture were limited to the group I. The group II and III both included isolates from Kanagawa and Chiba prefectures. The support of each divergent lineage was high or poor, group III was highly supported (100/-) and the group I and II had no support. Two strains from Heisaura (Heisaura 8 and 3-4), Chiba prefecture formed a clade with *B. gregarium* species (BCGRL2) with a high support (100/1). Another strain from Heisaura (14) positioned at the base of the clade mentioned above with high support (98/1).

The phylogenetic tree revealed interesting geographical pattern of these dinoflagellates, for example, as mentioned above, the strains from Okinawa (Maeda and Kesaji) were only limited to the group I. However, the group I also includes the strains from Chiba (Heisaura) and Kanagawa (Arasaki and Tsurugizaki). Interestingly, a single tidal pool can contain different genotypes, i.e. the isolate Heisaura 3-1 (H3-1), H3-3 and H3-4 (Figure. 7) were collected from a bloom occurring in the same tide pool in Chiba, but H3-1 and H3-3 were nested separately within Group III and Group II, and H3-4 was formed a sister with clade *B. gregarium* from Korea, with

a strong support value (100/1) (Figure. 7). Also, the Heisaura 9-2 (H9-2) and H9'-1 was isolated from the water sample collected from the same tidal pool.

DISCUSSION

Morphological comparison between the groups and their geological distribution

In general, all three strains showed mostly similar morphology. Such as, the pentagonal cell shape from the ventral view; possession of a reddish eyespot and epical stalk; collared apical pore complex; well excavated cingulum with its list on the margin; the extension of the cingular list towards the 1''' plate. most importantly all the described strains have the same thecal tabulation: Po, X, 4', 3a, 7'', 6C, 4S, 5''', 2'''' (Figures 1–6). However, there are some morphological traits that inconsistent among each strain. A comparison of the features of the three isolates was given in the Table 2.

The *Bysmatrum* sp. N1-2 is the smallest among the three strains, 21.8–33.2 µm long and 20.2–32.4 µm; the cell size of the *Bysmatrum* sp. M7-4 and H3-2 ranged from 24.4–34.3 µm in length and 22.5–31.4 µm in width; yet, the size range was overlapped. Also, the presence of a relatively wide range of sizes in cultured cells may reflect different stages of the life cycle (e.g., gametes, planozygotes), which might also explain the production of cysts in culture (Anglès *et al*. 2017). The anterior part of the cells of the strain M7-4 and N1-2 was mostly similar; both have tear-drop to polygonal shaped APC and elongated rectangular canal plate (X). The X plate of the *Bysmatrum* sp. M7-4, however, ornamented with pores (Figure 5e). Almost all three *Bysmatrum* strains have the same shape and number of apical, intercalary and precingular plates, with the slight difference in the shape of 1a plate of the strain N1-2, which is more elongated compare to

the other two (Figures 5a, d). The central and posterior part of all three strains, in terms of thecal morphology, is the least variable. Cingular plates of all three strains were striated, although the degree of striation was differed slightly. The displacement of *Bysmatrum* sp. N1-2 and H3-2 was the same, displaced 1-1.5 times of its width, while the cingulum of the M7-4 was displaced exactly 1 times of its own width. Other than that, no thecal pores were observed from N1-2; and its sulcal plates were smooth, while the plates surface of the Sr, in strain M7-4 and H3-2, was partially ornamented (Figures 4a, b, f, 6b).

In terms of geological distribution, all the strains studied here were collected from tidal pools. Although all the isolates from different prefectures were unevenly dispersed among those three groups, but the molecular analysis showed some geological separation between the strains (Figure 7). There are two kind of geological isolation might be understood from the phylogenetic tree. First, long distanced separation, the strains from Okinawa prefecture only occurred in the group I. Second, short distanced separation. This is the separation among the strains collected from the same latitude (i.e., from the same prefecture); the strains form Tsurugizaki (Chiba) were also nested only in the group I (Figure 7). Moreover, SHAH *et al.* (2010), in their survey, have reported that blooms in different micro-environments, such as tidal pools, consisted of a single dinoflagellate species (monospecific) for each habitat.

As mentioned in the Introduction, tidal pool dinoflagellates possess unique diurnal vertical migratory behavior in tidal pools in relation to tidal movement. The unique point is that the motile cells actively swim only during low time when the tidal pools are exposed. Several hours before sea water comes into tidal pools at high timed, the motile cells immigrate toward the bottom of pools and attach themselves to substrate firmly so that the cells are not washed out from tidal pools. This type of life cycle suggests that the limited chance of dispersal and thus

limited chance of expansion of distribution range of these tidal pool dinoflagellates - the hypothesis; the tidal pool dinoflagellates might have very limited distributional ranges. However, no research works have been done to confirm this hypothesis. In my study, I was able to collect morphologically similar dinoflagellates, i.e. *Bysmatrum gregarium*-complex from Okinawa, Chiba and Kanagawa prefectures and compared genetic distances between the strains from different or similar localities. As to the expansion of distributional range problem, it was found that the group I contains the strains from Okinawa, Chiba and Kanagawa, although the strains from Okinawa were limited to the group I. The strains from Chiba and Kanagawa were both included in groups II and III, in addition to the group I. Thus, the hypothesis that the tidal pool dinoflagellates might have limited distribution was not proved and rather they might have widespread distribution. Furthermore, I have found that even a single tidal pool can contain two to four strains of different genotypes (see results). Therefore, my study revealed that the species of *Bysmatrum gregarium*-complex have basically wide distribution and therefore, there were chances of transportation of the cells outside of tidal pools by probably ocean current. Although it is hard to be washed out from tidal pools because of attached nature of nonmotile cells, the strong waves at the time of typhoon might agitate tidal pools vigorously and might wash out nonmotile cells to open seas. The presence of tidal pool dinoflagellates in the open ocean can be tested using environmental clone analyses using specific primers for tidal pool dinoflagellates, but this will be the future subject.

As to the distributional pattern of microorganisms, there is a hypothesis that ‘everything is everywhere’ and this means microorganisms tend to be cosmopolitan and distribute throughout the globe. However, recent studies revealed that even morphologically similar strains, each has different genotypes depending on geographical regions, i.e. the presence of cryptic species

(Knowlton 1993). The planktonic 'cosmopolitan' diatom, *Skeletonema costata* are now recognised to include geographically separated six semi-cryptic species (Sarno *et al*. 2005). Also, the toxic dinoflagellate *Alexandrium tamarense*-complex showed the clear geographical patterns (John *et al*. 2003). According to Hagino *et al*. (2011), the 'cosmopolitan species' *Emiliania huxleyi*, which has worldwide distribution, can be divided at least into two groups genetically and each group prefers cold water and warm water, respectively (For other examples, see Medlin *et al*. (2007). Therefore, the hypothesis everything is everywhere might not stand in most cases. It should be noted that these studies are mainly based on planktonic species and little works have been done for benthic dinoflagellates. My study showed that on contrary to my hypothesis that the benthic dinoflagellates, like tidal pool dinoflagellates possess wider distributional area than first anticipated. However, the distribution of group I–III seems to be limited to the Japanese coastal waters. But some strains share the genotype with Chinese and Korean strains. We still do not know whether the hypothesis 'everything is everywhere' is valid for these benthic dinoflagellates and more studies with wide range of samplings are necessary to conclude this problem.

Morphological comparison with similar species

The main morphological characters used to classify *Bysmatrum* to species level are cell shape and size, plate ornamentation, morphology of the APC, cingulum displacement, and nucleus position (Murray *et al*. 2006, Anglès *et al*. 2017). The comparison between the similar species of *Bysmatrum* is presented in Table 2. Those three representatives from each group, M7-4 (Group I), N1-2 (Group II) and H3-1 (Group III), on the basis of the cell shape (pentagonal), the finely reticulated thecal surface, the possession of an equatorially positioned cingulum and a cingulum

displaced by a distance exceeding its own width, mostly resembled that of the *B. subsalsum*, *B. gregarium* and *B. austrafrum*. The other three species of *Bysmatrum*, *B. arenicola*, *B. granulosum* and *B. teres*, are significantly different.

Among all three morphologically similar species, *Bysmatrum* sp. M7-4 resembles the *B. subsalsum* the most (Figures 1, 4, Table 2). *B. subsalsum* has been reported from multiple regions, Aral Sea (Ostenfeld 1908), the Caribbean (Faust & Steidinger 1998), the Gulf of Mexico (Limoges *et al*. 2015), the Mediterranean Sea (Gottschling *et al*. 2012, Anglès *et al*. 2017), Argentina (Balech 1964, as *P. subsalsum*), Japan (Horiguchi, 1983: but this might be one of those group I to III) and in the South China Sea and French Atlantic (Luo *et al*. 2018). Anglès *et al*. (2017), reported cryptic species of *B. subsalsum.* Within all the reported *B. subsalsum* species complex, the species from the South China Sea, isolate TBBYS02, is the one that morphologically and phylogenetically closely related to the M7-4. They are almost identical but there are some morphological differences. *B. subsalsum* TBBYS02 is slightly larger than the M7-4; the X plate of the M7-4 was trapezoidal and ornamented with thecal pores (Figure 4e), but there was no report about the morphology of the X plate of *B. subsalsum* TBBYS02. The antapical plates of M7-4 was not indented, whereas the *B. subsalsum* reported to have indentation in its antapex (Steidinger & Balech 1977, Faust & Steidinger 1998). One of the most notable differences is the habitat; all the reported *B. subsalsum* species are planktonic, *Bysmatrum* sp. M7-4, however, isolated from a tidal pool.

Bysmatrum sp. N1-2 and H3-2 are shared a number of morphological characteristics with the *B. gregarium* and *B. austrafrum*. But the heptagonal first apical (1') plate, the antapical plates without indentation and the hypothecal nucleus of the *B. austrafrum*, make it different from those of the *Bysmatrum* sp. N1-2 and H3-2. *B. gregarium*, also, have some morphological traits that

differ from the *Bysmatrum* sp. N1-2 and H3-2. Such as the possession of an antapical spine, shorter cingulum displacement (0.5-1 its width), and striated intercalary bands. Furthermore, there no detailed report on its canal plate (X).

Cryptic or new species?

The molecular data puts all the isolates with in the genus *Bysmatrum* with a moderate support, those isolates formed three separate groups, group I–III (Figure 7). However, both ML and BA analysis could not quite resolve the true taxonomic position of these groups within the genus. Only the group III has its bootstrap value (100/-) and long divergent from other groups. With regard to the external morphology, the selected traits showed mostly similar traits with those of *B. subsalsum*, *B. gregarium* and *B. austrafrum*. Although they show some noticable differences, it is still difficult to distinguish these strains from each other clearly. Also, the support for each clade in the molecular phylogenetic analysis is also poor. Therefore, it is necessary to apply more gene markers, as ribosomal rDNA large subunit (LSU rDNA) or/and internal transcribed spacers (ITS), and more detailed internal morphological observation, to determine the final evolutionary position of those isolates within the genus *Bysmatrum*. In conclusion, it is safe to conclude that those three groups are the cryptic species of the genus *Bysmatrum*. Yet, the detailed morphological information of all the other strains in each group is needed.

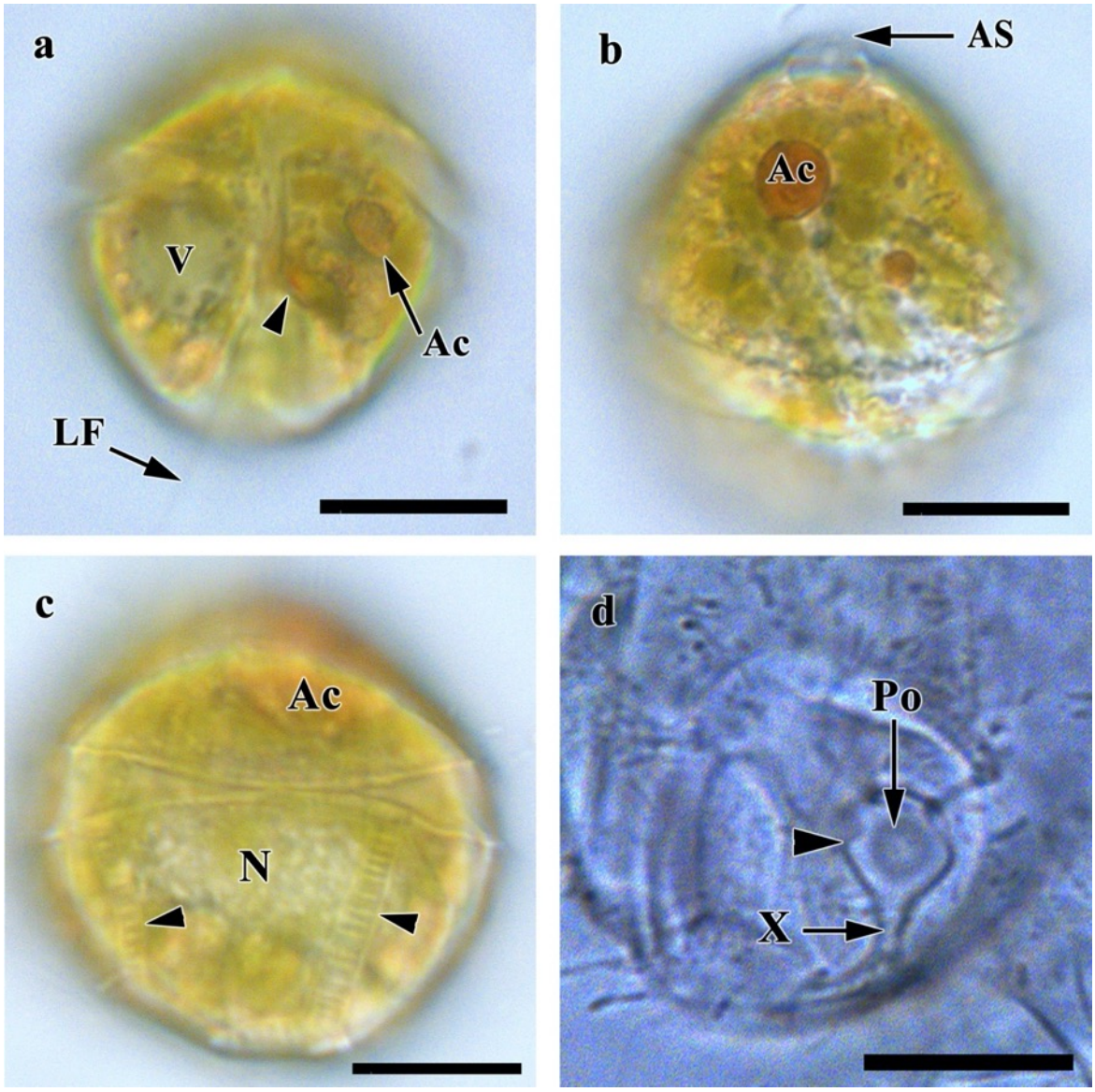

Figure 1. *Bysmatrum* sp. M7-4 light micrographs. Scale bars = 10 µm. **(a)** Ventral view. Arrowhead indicates the eyespot. V: vacuole. Ac: accumulation body. LF: longitudinal flagellum. **(b)** Dorsal view, showing the apical stalk (AS) and accumulation body (Ac). **(c)** Dorsal view, showing the hypothecal nucleus (N) and the finely striated intercalary bands (arrowheads). **(d)** Details of the apical pore complex (APC) consisted of apical pore plate (Po) and canal plate (X); arrowhead indicates the raised collars of the APC.

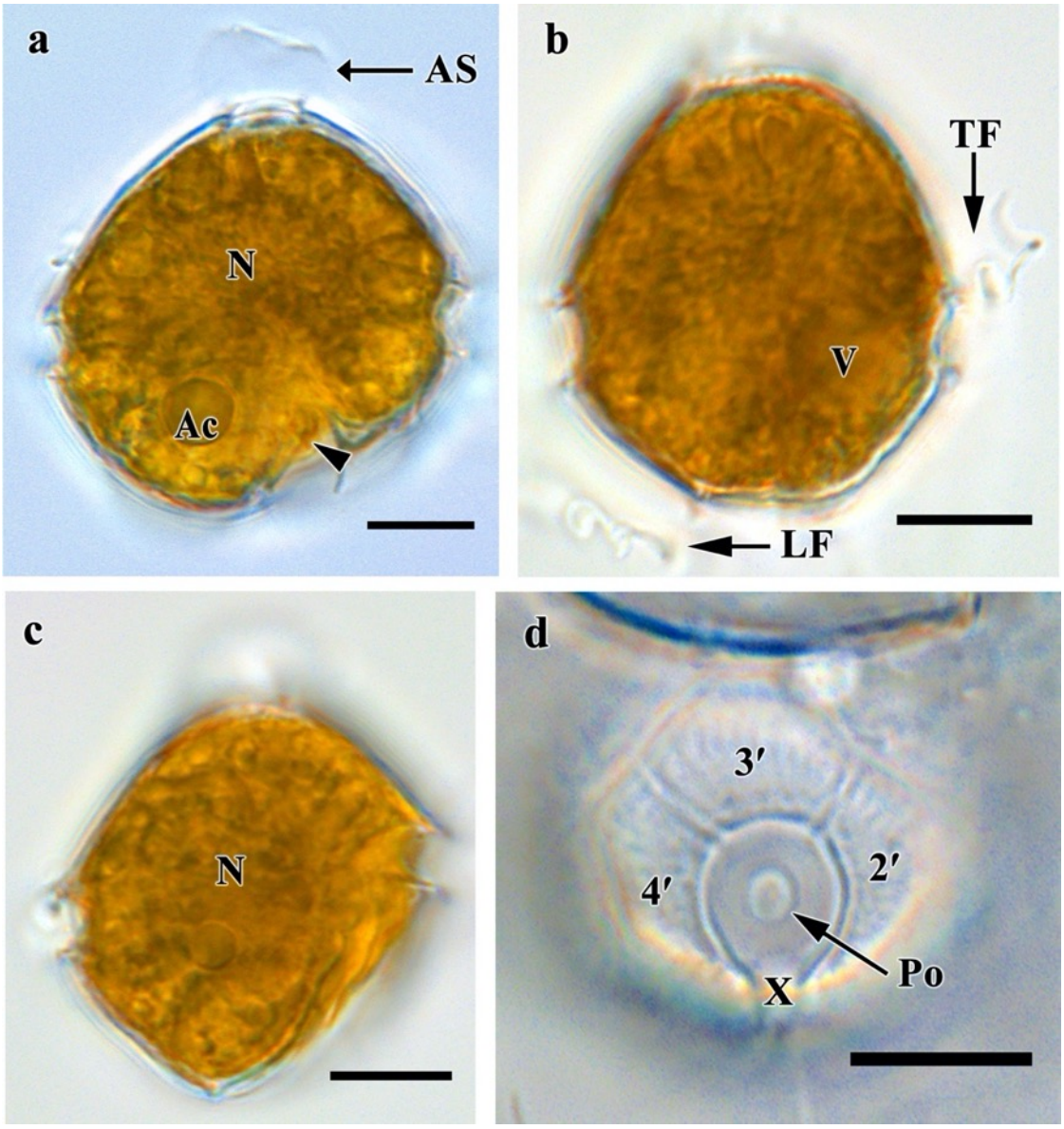

Figure 2. *Bysmatrum* sp. N1-2 light micrographs. Scale bars = 10 µm. **(a)** Ventral view. Arrowhead indicates the eyespot. N: nucleus. Ac: accumulation body. AS: apical stalk. **(b)** Dorsal view, showing the vacuole (V), longitudinal (LF) and transverse (TF) flagellum. **(c)** Right lateral view, showing the equatorial (cell centre) nucleus (N). **(d)** Details of the apical pore complex (APC) consisted of apical pore plate (Po) and canal plate (X).

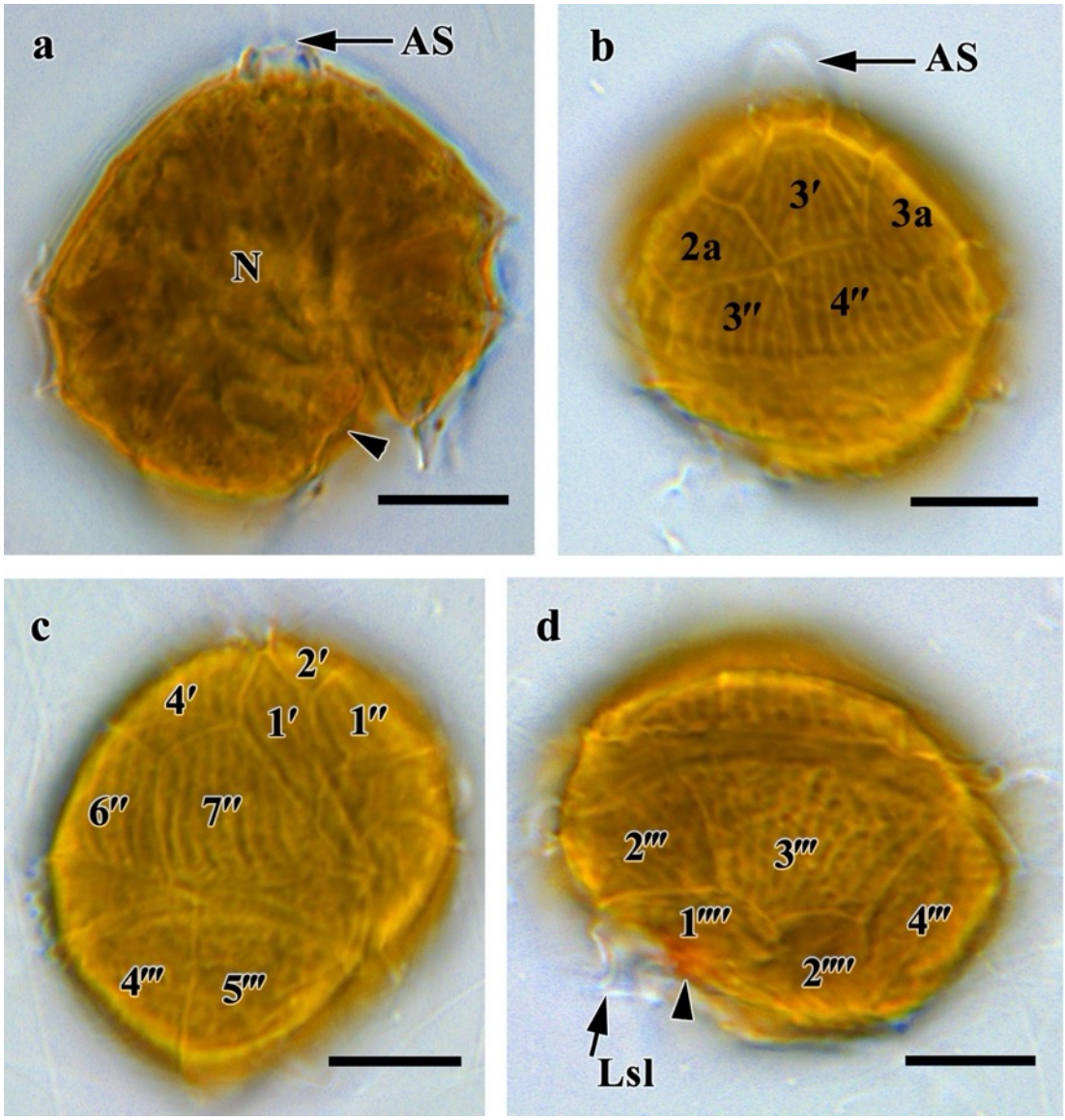

Figure 3. *Bysmatrum* sp. H3-2 light micrographs. Scale bars = 10 µm. **(a)** Ventral view. Arrowhead indicates the eyespot. N: nucleus. AS: apical stalk. **(b)** Dorsal view, showing the apical stalk (AS) and the separation between the 2a and 3a intercalary plates. **(c)** Right lateral view, showing the broadly asymmetric first apical plate (1') and other ornamented plates that visible under the light microscopy. **(d)** Antapical view, showing the striated postcingualr (2'"–4'") and antapical (1"" and 2"") plates; Lsl: left sulcal list.

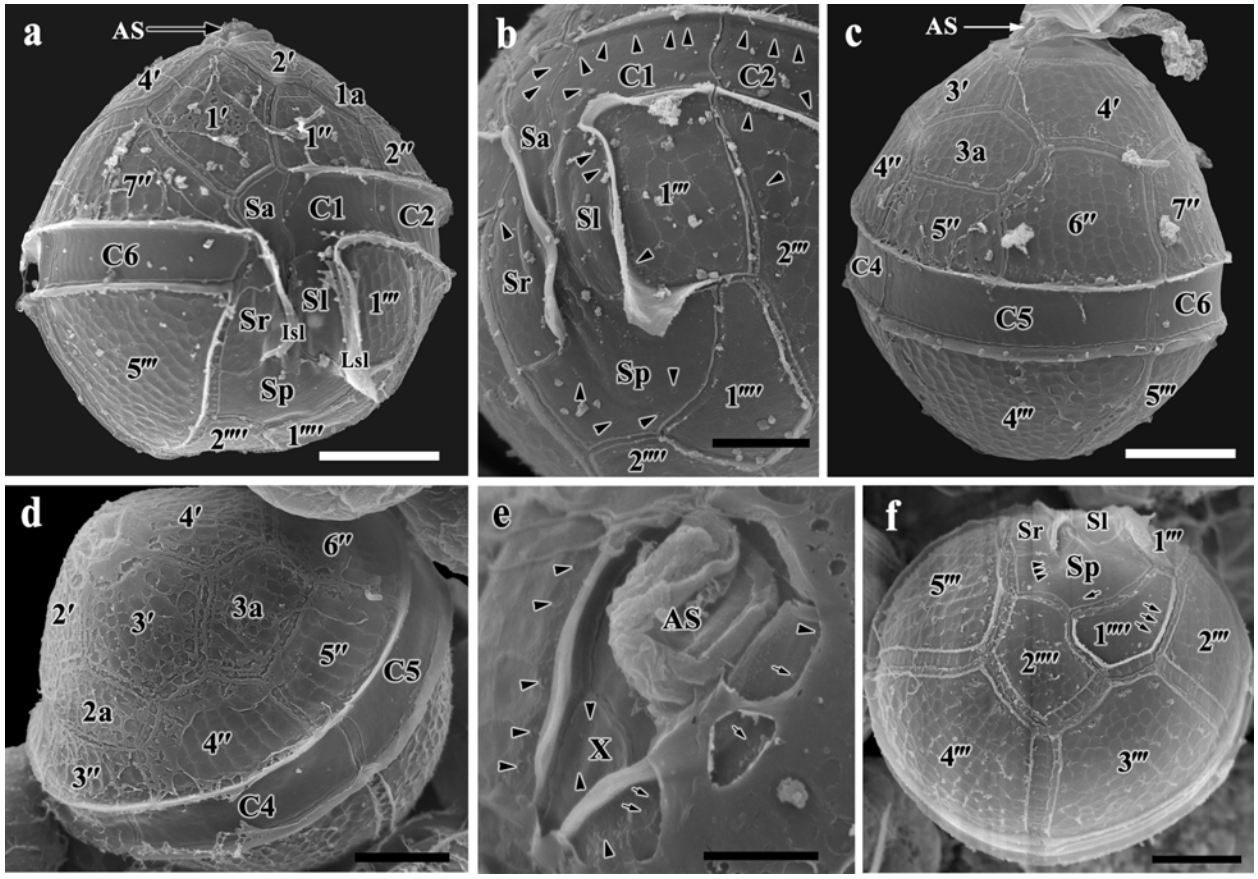

Figure 4. Scanning electron micrographs (SEM) of the surface morphology of *Bysmatrum* sp. M7-4; **(a)** Ventral view of the motile cell. The first apical plate (1') was asymmetric, and the anterior sulcal plate (Sa) was slightly extended in to apitheca. Scale bar = 6 μm; **(b)**. the details of the sulcal area. Arrowheads indicates the pores that spread randomly on the surface of the sulcal and cingular plates. Scale bar = 4 μm; **(c)** Dorsal view of the cell. Showing the faintly striated cingular plates. Scale bar = 6 μm; **(d)** apical view showing the thecal plate arrangement of the epitheca and the separation between 2a and 3a. Scale bar = 6 μm; **(e)** The apical pore complex (APC) is a recessed chamber with a centrally located raised dome (Apical stalk: AS) surrounded by a collar; and the shape of the canal plate (X); arrowheads and small arrows showed the two different pores. Scale bar = 2 μm; **(f)** thecal plate arrangement of the hypotheca; arrowheads and small arrows showed the two different pores. Scale bar = 6 μm.

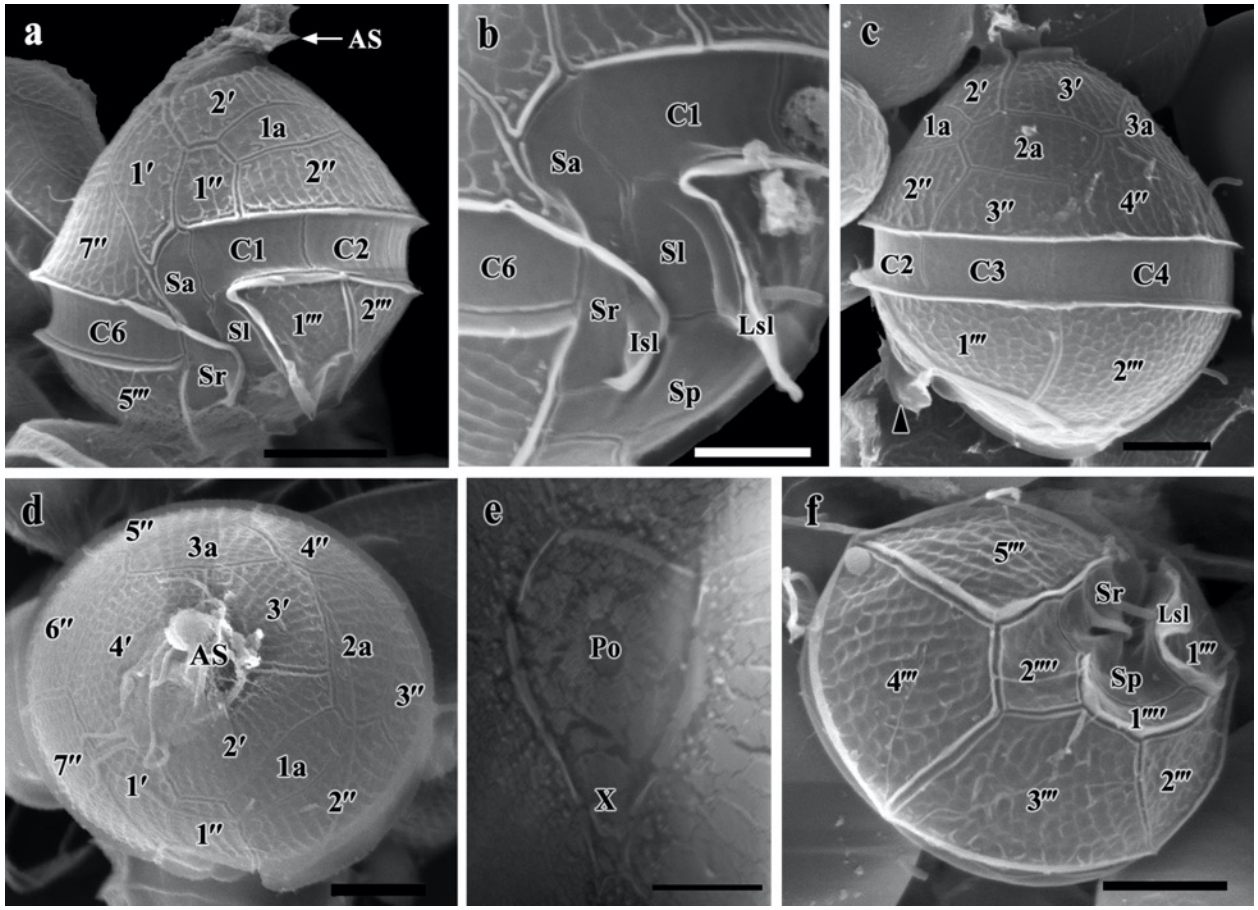

Figure 5. Scanning electron micrographs (SEM) of the surface morphology of *Bysmatrum* sp. N1-2; **(a)** Ventral view of the motile cell. The first apical plate (1') was asymmetric. Scale bar = 6 μm; **(b)**. the details of the sulcal area. Scale bar = 4 μm; **(c)** Dorsal view of the cell. Showing the faintly striated cingular plates, and the indentation of the antapical plates. Scale bar = 6 μm; **(d)** apical view showing the thecal plate arrangement of the epitheca and the separation between 2a and 3a. The first intercalary plate (1a) was four-sided, and elongated. Scale bar = 6 μm; **(e)** Details of the apical pore complex (APC); apical pore plates (Po) was round to ellipsoidal, canal plate (X) was elongated, quadrangular in shape. Scale bar = 2 μm; **(f)** thecal plate arrangement of the hypotheca; Scale bar = 6 μm.

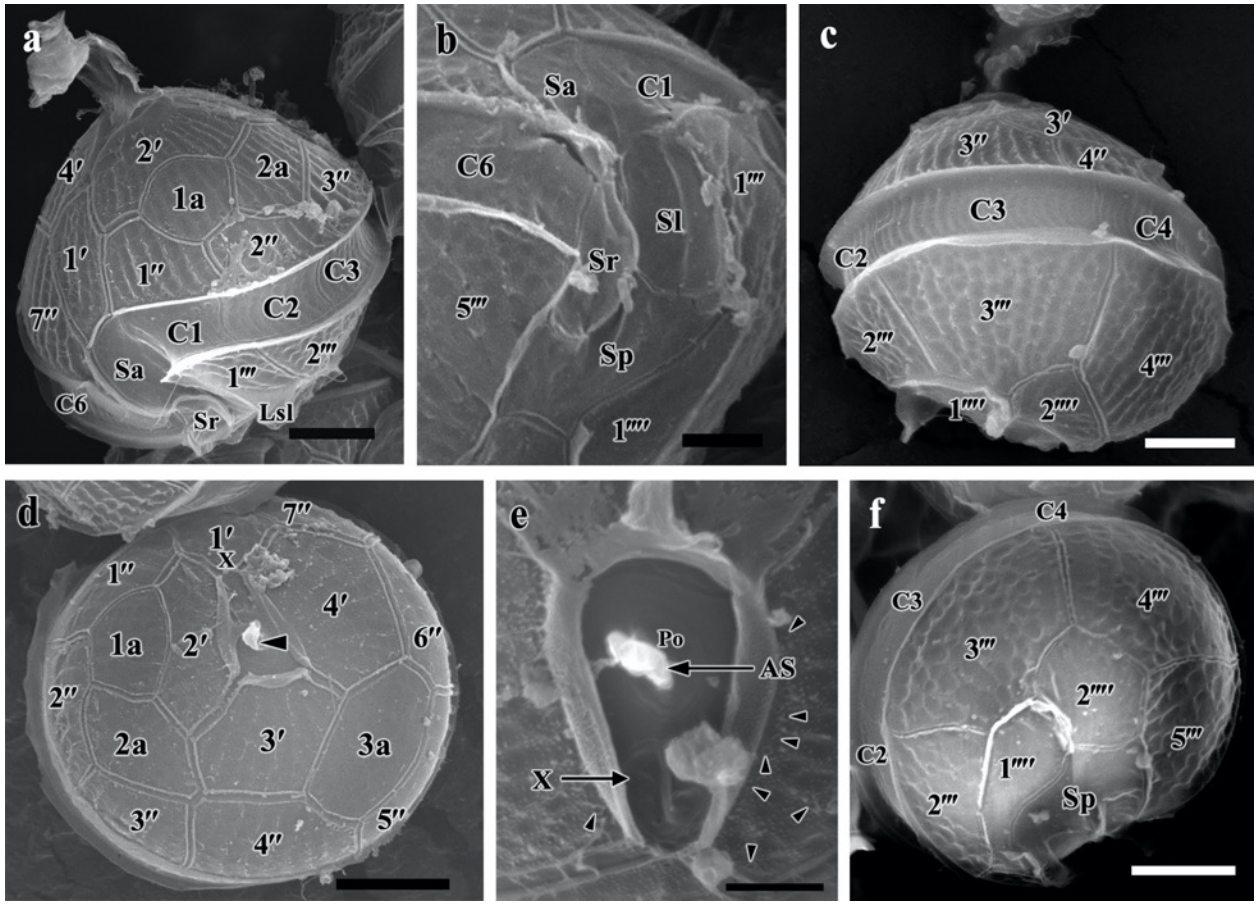

Figure 6. Scanning electron micrographs (SEM) of the surface morphology of *Bysmatrum* sp. H3-2; **(a)** Ventral view of the motile cell. The first apical plate (1') was asymmetric and pentagonal. Scale bar = 6 μm; **(b)**. the details of the sulcal area. Scale bar = 4 μm; **(c)** Dorsal view of the cell. Cingular plates finely striated; antapical plates indented. Scale bar = 6 μm; **(d)** apical view showing the thecal plate arrangement of the epitheca and the separation between 2a and 3a. The first intercalary plate (1a) was four-sided, and somewhat trapezoidal in shape. Scale bar = 6 μm; **(e)** Details of the apical pore complex (APC); APC surrounded with thecal pores; apical pore plate (Po) was round; canal plate (X) seems to have two separate plates. Scale bar = 2 μm; **(f)** thecal plate arrangement of the hypotheca; Scale bar = 6 μm.

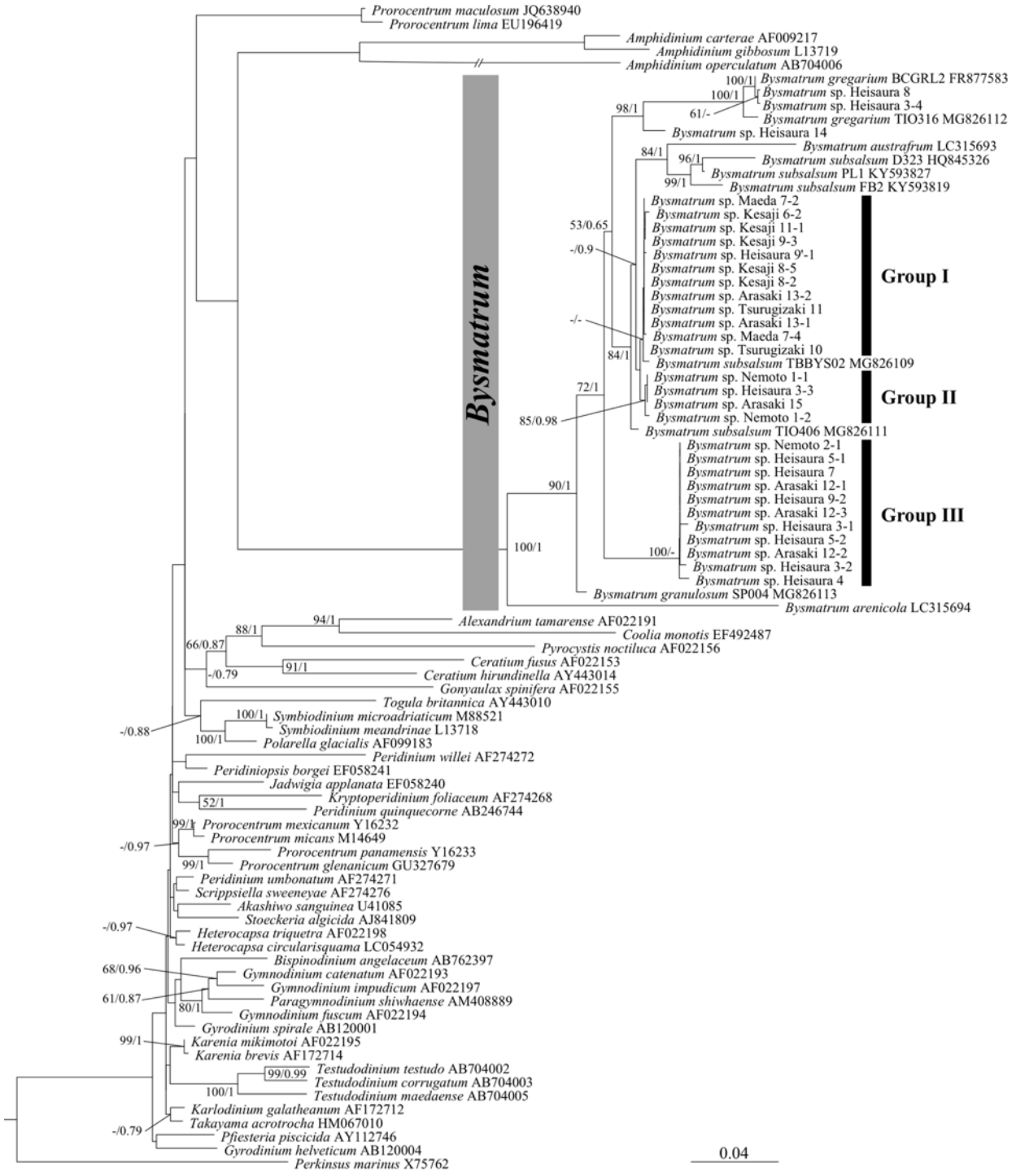

Figure 7. Topology of maximum likelihood (ML) phylogenetic tree inferred from partial small-subunit (SSU) ribosomal (r) DNA sequence alignment. Bootstrap support for ML analysis (100 pseudoreplicates) and Bayesian posterior probability (>50% and >0.8, respectively) are indicated.

Table 1. Sampling locations, time and conditions.

No.	Location	Prefecture	T (°C)	Time	Remarks
N1	Nemoto	千葉 Chiba	27	31th Aug, 2015	Small, shallow pool
N2			28		Large, little deep (remarkable bloom)
H3	Heisaura		28		Medium, shallow
H4			28		Medium, shallow
H5			30		Medium, shallow
H6			29.5		Medium, shallow
H7			30		Small, shallow
H8			30.5		Large, little deep
H9			29		Medium, little deep; collected from same pool, H9 with large pipette; H9' with plankton net.
H9'			29		
T10	Tsurugizaki	神奈川 Kanagawa	26	1st Sep, 2015	Medium, shallow
T11			25		Large, little deep
A12	Arasaki		28		Large, little deep
A13			29		Medium, little deep
A14			27		Large, deep. These three samples are collected in same pool with plankton net, but in different place.
A15			27		
A16			27		
O4	Kesaji	沖縄 Okinawa	23	12th Dec, 2015	Small, shallow
O5			23		Small, shallow
O6			25		Small, shallow
O8			25		Large, shallow
O9	Hanashiro		25		Medium, little deep
O11			25		Medium, little deep
O13			26		Small, little deep
O15	Odo		28	13th Dec, 2015	Small, little deep
O18			28		Medium, shallow (remarkable bloom)
M3	Maeda		27	July, 2016	Medium, shallow
M6			27		
M7			27		

Note:

1. Size:

Small: diameter 0.5m ~ 1.0m; Medium: diameter 1.0m ~ 2.0m; Large: diameter > 2.0m;

2. Depth:

Shallow: depth ≤20cm; Little deep: depth 20cm~50cm; Deep: depth≥50cm

Table 1. Comparison of morphological features between the species of the genus *Bysmatrum*.

Features	*B. sp.* M7-4	*B. sp.* N1-2	*B. sp.* H3-2	*B. gregarium*[a,c,d]	*B. subsalsum*[a,b,f]	*B. austrafrum*[e]
Length (µm)	24.4–33.2	21.8–33.2	24.4–34.3	20.0-34.0	32.0-41.0	25.0-45.0
Width (µm)	23.0–31.0	20.2–32.4	22.5–31.4	20.0-34.0	31.0-51.0	20.0-42.5
Shape (from ventral)	pentagonal	pentagonal	pentagonal	pentagonal	pentagonal	pentagonal through round
Apical pore complex	tear-drop to polygonal	tear-drop to polygonal	trapezoidal	polygonal	tear-drop	trapezoidal
Apical stalk	yes	yes	yes	yes	yes	yes
Thecal pores	yes	N	yes	*	*/yes	yes
Cingulum descending	1 its width	1-1.5 its width	1-1.5 its width	0.5-1 its width	1 its width	1-1.5 its width
1′ morphology	penta	penta	penta	penta	penta	hepta
1a morphology	quadra	quadra (elongated)	quadra	quadra	quadra/penta	quadra
2a morphology	hexa	hexa	hexa	hexa	hexa/penta	hexa
3a morphology	penta	penta	penta	penta	penta	penta
Intercalary bands	wide/finely striated	nerrow/smooth	nerrow/smooth	striated	striated	smooth
Antapical plates	not indented	indented	indented	indented	indented	not indented
Antapical spine	N	N	N	yes	N	N
Pyrenoid	*	*	*	N	N	yes
Nucleus	hypothecal	epithecal	epithecal	epithecal	epithecal	hypothecal
Accumulation bodies	orange	orange	N	orange	N	orange
Habitat	tidal pool	tidal pool	tidal pool	tidal pool	epibenthic	tidal pool
Distribution	Okinawa, Japan	Kanagawa, Japan	Chiba, Japan	South California, USA	Okinawa, Japan; Belize; Florida	Cape Peninsula, South Africa

[a] Faust & Steidinger (1998), [b] Murray et al (2006), [c] Horiguchi & Pienaar (1988b), [d] Mohammad-Noor et al (2007), [e]Dawut et al (2018), [f]Luo et al (2018)

N: feature was not observed; yes: present; *: we do not know yet;

CHAPTER IV

Morphology and phylogeny of a new free-living, tidal pool, bloom-forming dinoflagellate *Symbiodinium* sp. HG246 (Dinophyceae) from South Africa

INTRODUCTION

The dinoflagellates are flagellated protists which are known for the extraordinary complexity in their morphology and the significant ecological role in both marine and fresh water environments (Stoecker 1999, Hansen 2011, Guiry 2012). They also display remarkably intricate life mode (Murray *et al*., 2016). Roughly half of the extant dinoflagellate species are photosynthetic and the rests are either heterotrophic or mixotrophic. Even some of them act as symbiontic partners with various animals, such as the species that belonging to the genus *Symbiodinium*.

The yellow (golden-brown) colored symbiotic microalgae are commonly known as zooxanthellae. The vast majority of zooxanthellae are actually the members of the genus *Symbiodinium*. This genus represents the unicellular dinoflagellate symbionts associated with various marine protists and invertebrates (Yamashita & Koike 2013). This genus, *Symbiodinium*, was first formally described as a new genus by Freudenthal (1962) using a gymnodinioid-like dinoflagellate species, *Symbiodinium microadriaticum*, as the type species. For a long time, *Symbiodinium* was considered to be a monospecific genus, but now it is clear that it contains a large cryptic diversity (Saldarriaga & Taylor 2017). Most of *Symbiodinium* spp. are symbiotic with various species such as corals, sponges, sea anemones, jellyfish, nudibranchs, clams, ciliates, and foraminifera (LaJeunesse 2002, Rodriguez-Lanetty *et al*. 2003, Lewis & Coffroth 2004, Fay *et al*. 2009, Pochon & Gates 2010, Hill *et al*. 2011). As mutualistic symbionts, *Symbiodinium* occur at high densities within these various hosts and provide them with metabolic energy via photosynthesis (Hill 1996, Weisz *et al*. 2010), and fueling important ecological processes such as coral calcification and sponge bioerosion. They are, thus, widely recognized as the fundamental

part to the existence of tropical and subtropical coral reef ecosystems worldwide (LaJeunesse *et al*. 2018).

Due to their symbiotic nature as well as technical difficulties in culturing, *Symbiodinium* spp. made initial attempts at describing their diversity and ecology challenging (Schoenberg & Trench 1980, Trench & Blank 1987). The utilization of multiple gene markers, however, has significantly changed the perceptions of diversity, and disclosed many biogeographical, ecological, and evolutionary relationships among *Symbiodinium* spp. and their hosts (Baker 2003, Coffroth & Santos 2005, LaJeunesse 2005, Sampayo *et al*. 2009). By far, a number of high-resolution markers have been employed to delineate the species diversity in this genus. Historically, the pioneering work of Rowan & Powers (1992) divided the species in the *Symbiodinium* into three phylogenetic groups referred to as clades A-C using nuclear small subunit ribosomal (SSU or 18S) gene sequences (SSU rDNA). Later, the application of the more variable nuclear large subunit ribosomal (LSU or 28S) gene sequences (LSU rDNA) led to the classification of *Symbiodinium* into nine different groups, clade A to I (Santos *et al*. 2002, Pawlowski *et al*. 2001, Pochon & Gates 2010). Among which, some clades, such as clade D, F, and G have been further divided into sub-clades D1-D2, F2-F5, and G1-G2, respectively, using LSU rDNA and the chloroplast large subunit ribosomal DNA (cp23S) domain V (Hill *et al*. 2011, Pochon *at al*. 2004, Pochon *et al*. 2006); there are, hence, nine formally recognized clades (A-I) and eight sub-clades (D1-D2, F2-F5, and G1-G2). Some of these clades are composed of more than 100 sequence types based on higher resolution markers, such as ITS2 rDNA (Franklin *et al*. 2012).

As being one of the most diverse group, every year, scores of publications report on some aspects of *Symbiodinium* diversity, and most of which are without any morphological description.

By far, only 22 species, from different clades, have been formally classified and named (Table 1). However, LaJeunesse *et al*. (2018) based on the assessment of genetic, morphological, physiological, ecological, and biogeographic evidence, proposed that the evolutionary divergent "Clades" should be treated as genera in the family Symbiodiniaceae; and provided generic names for all six new genera (former = Clades) except clade H, I, and some sub-clades of clade F and G. Only six new generic names have proposed, and the previous genus name, included all eight clades, *Symbiodinium*, is kept for clade A. The free-living species, *S. natans*, was suggested as the type species for this redefined genus rather than the previous type species *S. microadriaticum* (LaJeunesse *et al*. 2018).

The symbioses are obligatory for many hosts. The survival of host animals, sometimes, completely dependent on the symbiotic partner. Only 20% of coral species can vertically transmit the *Symbiodinium* to their progeny (Harrison 2011); the rest, thus, should acquire new *Symbiodinium de novo* from the environment. This suggests that i) an environmental pool of *Symbiodinium* is crucial for the establishment of the new symbiotic relationship (Harrison 2011); ii) *Symbiodinium* can live freely outside the host temporarily or permanently. The reports on free-living *Symbiodinium* can be date back to early 1980s (Loeblich & Sherley 1979, Chang 1983), but it did not receive much attention until the first molecular identification of free-living *Symbiodinium* in 1999 (Carlos *et al*. 1999). Subsequently, significant numbers of investigations have been reported on their occurrence in the water column, sediments, tidal pools, and on macroalgal surfaces (Gou *et al*. 2003, Thornhill *et al*. 2006, Koike *et al*. 2007, Hirose *et al*. 2008, Littman *et al*. 2008, Manning & Gates 2008, Porto *et al*. 2008; Adams *et al*. 2009; Hansen & Daugbjerg 2009, Pochon *et al*. 2010, Reimer *et al*. 2010, Venera-Ponton *et al*. 2010 Takabayashi *et al*. 2012, Zhou *et al*. 2012, Huang *et al*. 2013, Yamashita & Koike 2013, Jeong *et al*. 2014).

Although a number of free-living *Symbiodinium* species have been reported from various habitats, such as sand, tidal pools, macroalgal surfaces, and the water column, only two species were formally classified based on morphological and molecular analysis, and named. Of which, *S. natanse* was described from the water column in nearshore waters of Tenerife in the northeast Atlantic Ocean. Based on the detailed morphological observation and molecular analysis, *S. natans* was classified as a new member on the genus *Symbiodinium*, and a new sub-clade in the clade A (Hansen & Daugbjerg, 2009). Jeong *at el*. (2013) also reported a free-living species that of the genus *Effrenium* (= clade E). Although this particular species was acquired from a plankton sample, but there are reports that indicating the occurrence of the same strains from rather benthic habitat, including corals and macro-algal surfaces, from various localities (Chang 1983, Jeong *et al*. 2012, 2014, Yamashita & Koike, 2013). Nonetheless, there is no detailed morpho-molecular investigation have been reported for the tidal pool, free-living *Symbiodinium*. In the expedition of the east coast of Cape Province, South Africa in 2012, the blooms of dinoflagellates were noted in tidal pools of rocky shores. The causative organism of these blooms was found to be a member of the genus *Symbiodinium*. In this chapter, I am reporting a new species of the genus *Symbiodinium* (=clade A) based on the detailed inter/external morphological observation as well as molecular analysis. This is the first report of a tidal pool bloom-forming *Symbiodinium*.

MATERIALS AND METHODS

Sampling and culture establishment

The clonal culture used in this study was established from a water sample collected using a large pipette from a tidal pool at the Heads in Knysna Lagoon, Western Cape, South Africa (34.55' 20" S, 23.03' 37" E) on 11th December 2012. Single cells were isolated by micropipette into a sterile medium. A successful clonal culture (strain HG246) was established and formed the subject material of the current study. The established culture was maintained in Daigo's IMK medium (Nihon Pharmaceutical Co., Tokyo, Japan) at 20°C under an irradiance of 50 µmol photons $m^{-2}s^{-1}$ with a 16:8 light: dark regime.

Light microscopy

Light microscopic observations of motile cells were made using a Carl Zeiss Axioskop 2 microscope equipped with Nomarski interference optics (Carl Zeiss Japan, Tokyo). An image analysis system was used to measure the length and width of motile cells from micrographs taken using a Leica MC-120HD digital camera (Leica Microsystems, Wetzlar, Germany). The shapes and number of chloroplasts were characterized using autofluorescence (Carl Zeiss Axioskop 2 with a filter set No. 15).

Scanning electron microscopy

For scanning electron microscopy, a 100 µL aliquot of a dense culture of motile cells was fixed with 2% osmium tetroxide (OsO_4) for 40-60 min. Fixed cells were then placed on a SEM plate

glass (Φ 8.5 mm) pre-coated with poly-l-lysine. The cells were allowed to settle on the surface of a glass plate for 10 min. The attached cells were rinsed twice with distilled water for 30 min each. The samples were then dehydrated in an ethanol series (30, 50, 70, 90, 95%, 10 min at each step) followed by two rinses in 100% ethanol for 30 min each and dried using an automated critical point drier (Leica EM CPD300, Vienna, Austria). The dried cells were sputter-coated with gold for 150 s at 10 mA (Hitachi E-1045) and observed using a scanning electron microscope (S-3000N, Hitachi).

Transmission electron microscopy

Cells were concentrated by gentle centrifugation (40 ×g for 10 min) and the pellet was fixed with cold 2.5% glutaraldehyde made up in culture medium for 30 min on ice, followed by a rinse with FSW, and post-fixed with 1% OsO_4 for 1h on ice. After a rinse in FSW followed by one in distilled water, the samples were dehydrated in an ethanol series of 25, 50, 70, 95, 100%, followed by two changes in 100% ethanol (10 min at each step), and embedded in low viscosity (LV) resin (Agar Scientific, Essex, England). After polymerization at 65℃ for 16 h, thin sections were cut using a diamond knife on an ultramicrotome (Leica EM UC6). Sections were picked up on Formvar-coated one-slot grids and viewed with a transmission electron microscope (H-7650, Hitachi).

DNA extraction, polymerase chain reaction (PCR) amplification

The DNA of approximately 15-20 motile cells was extracted using the Quick Extract™ FFPE DNA extraction kit (Epicentre, Tokyo, Japan) according to the manufacturer's protocol. The large subunit ribosomal RNA gene (LSU rDNA) was amplified using primers listed in Table S1.

The amplification was conducted in 25 µL reaction mix with the condition of: initialization (1 cycle, 6 min at 94℃; denaturation (35 cycles, 30 s at 94℃), annealing (30 s at 52℃); extension (90 s at 72℃); and final extension (at 72℃ for 6 min). The PCR products were purified and sequenced with ABI PRISM Big Dye Terminator (Perkin-Elmer, Waltham, Massachusetts, USA). The final step of sequencing was achieved using a DNA auto-sequencer ABI PRISM310 Genetic Analyzer (Perkin-Elmer).

Phylogenetic analysis

The LSU rDNA sequence determined in the present study was aligned with broadly sampled *Symbiodinium* sequences from GenBank/ European Molecular Biology Laboratory (EMBL)/ DNA Data Bank of Japan (DDBJ), using MAFFT v7.130b (Katoh & Standley 2013). Gblocks (Castresana 2000) was used to edit and eliminate gap positions in the aligned sequences. The aligned sequences were analysed by the maximum likelihood (ML) method using PAUP* version 4.0b10 (Swofford 2001) and the Bayesian method using MrBayes 3.2.1 (Huelsenbeck & Ronquist 2001, Ronquist & Huelsenbeck 2003). The programme jModel Test version 2.1.4 (Guindon & Gascuel 2003, Darriba *et al*. 2012) was used to calculate the evolutionary model that was the best fit for ML analysis of the data set.

The selected model was the GTR+I+G model. The heuristic search for the ML analysis was performed with the following options: a tree bisection reconnection branch-swapping algorithm and the Kimura 2-parameter neighbour-joining tree as a starting tree. The parameters used for the analysis were as follows: assumed nucleotide frequencies (user-specified) A=0.242423 C=0.198084 G=0.292317 and T=0.267176; substitution rate matrix with A<->C=0.749019, A<->G=3.06082, A<->T=0.750661, C<->G=0.361753, C<->T=6.1928, G<->T=1; proportion of

sites assumed to be invariable=0.376655; rates for variable sites assumed to follow a gamma distribution with shape parameter=1.00348; and the number of rate categories=4. For the Bayesian analysis, GTR+I+G was selected as the best evolutionary model by MrModeltest 2.3 (Nylander *et al*. 2004). Markov-chain Monte Carlo iterations were carried out until 500,000 generations were attained, when the average standard deviations of split frequencies fell below 0.01, indicating the convergence of the iterations.

RESULTS

Symbiodinium sp. HG246 Dawut, Sym, Suda et T. Horiguchi (Figs 1–4)

Description: Motile cells more or less mushroom-shaped, 7.2–11.6 μm long, 5.7–9.1 μm wide; episome is slightly larger than the hyposome; cingulum wide and displaced by half the cingular width; armored, thecal surface smooth, plate formula: x, EAV, 4', 6a, 8", ~7s, ~20c, 6'", 2""; elongated amphiesmal vesicle (EAV) with 15–18 tiny knobs located at the apex; cingulum consists of two rows of pentagonal plates. Chloroplast single, radiating from distinct pyrenoid situated near the cell center or in hyposome. Nucleus located in episome. Type E eyespot, consisting of numerous brick-containing vesicles, located near the sulcus. Peduncle emerging from between the longitudinal and transverse flagella.

Holotype: A SEM stub of the culture used in this study has been deposited as SAP xxxxxxxx at the Faculty of Science Herbarium, Hokkaido University.

Type Locality: Tidal pool at the Heads of Knysna Lagoon, Western Cape, South Africa (34.55' 20" S, 23.03' 37" E).

Light microscopy

The motile cells of *Symbiodinium* sp. HG246 were somewhat mushroom-shaped, with an episome slightly larger than the hyposome. In lateral view, the hyposome was dorso-ventrally flattened (Fig. 1a). Cells were 7.2–11.6 µm long (9.4 ± 1.1 µm, n=30) and 5.7–9.1 µm wide (7.5 ± 1.0 µm, n=30) (Figures 1a, b, d). The chloroplast was single and golden-brown. A distinct pyrenoid surrounded by a starch sheath is located in the cell center or the hyposome (Figures 1b, d, f); only one or two stalked chloroplast lobe/s extend/s from the central pyrenoid. The remainder of the many small lobes were spherical, ovoid or irregularly-shaped small chloroplast and interconnected, forming a chloroplast network near the cell surface. A reddish eyespot was visible at the light microscope level, near the sulcus area (Figure 1a). At day time, the majority of the cells were motile, with a very characteristic "spinning" movement. The cell division took place at night, and with the initiation of the lighting, in the morning, the daughter cells were release from the non-motile parental cells.

Non-motile cells were almost spherical, measured ~10 µm in diameter and were often packed with storage products (Figures 1e, f). Duple (Figure 1f) and quadruple (not shown) division stages in this state were observed, usually on the bottom of the culture flask.

Scanning electron microscopy

The SEM images revealed the shape and arrangement of the thecal plates of *Symbiodinium* sp. HG246 (Figure 2). At the cell's apex, the elongated amphiesmal vesicle (EAV) possessed 15–18 aligned tiny knobs and was bordered, ventrally, by a small hexagonal x plate and further surrounded by 4 apical plates (1'–4') (Figures 2a, b, e, 3a, b). The first apical plate (1') was asymmetric and the largest, whereas the 2' was quadrangular and the 3' and 4' were pentagonal

(Figures 2a, b, e, 3a, b). The six intercalary plates vary in size and shape, from pentagonal (2a & 6a) or hexagonal (1a & 5a) to heptagonal (3a). The 4a intercalary was the smallest and rhomboid (Figures 2d, e; 3a, b). All the eight precingular plates were pentagonal, except 1", which was either quadrangular or pentagonal and 4", which was the smallest and invariably quadrangular (Figures 2a, b, d, e, 3a, b). The cingulum was displaced at the region of the sulcus groove by ~0.5 of its height and comprised two wide rows of ~20 pentagonal cingular plates (Figures 2a, c, d, f, 3a). Approximately seven sulcal plates were observed including two S? plates and a large posterior sulcal plate (Sp) (Figures 2a, f, 3a). The hyposome consisted of six postcingular plates and two antapical plates. Four postcingular plates, 1‴, 2‴, 4‴, 5‴ & 6‴, were quadrangular in shape, and only 3‴ was pentagonal (Figures 2d, f, g, 3a, c). Both antapical plates, 1"" and 2"", made contact with the posterior sulcal plate (Sp); 1"" was pentagonal, while 2"" was hexagonal (Figures 2g, 3a, c).

Transmission electron microscopy

The cells of *Symbiodinium* sp. HG246 contained a typical dinokaryotic nucleus (N), with many chromosomes, in the episome (Figures 4a, f, g). Numerous chloroplast profiles (Ch) are located along the cell periphery. In the chloroplast profiles, a thylakoid-free area was observed (Figures 4a, c, e, f). The pyrenoid was single, distinct, stalked and mostly central (if not then in the hyposome), beneath the nucleus. It was surrounded by a thick starch sheath and connected to the chloroplast by one or two stalks (Figures 4a, c, f). No thylakoids penetrated the pyrenoid matrix. Mitochondrial profiles and lipid globules were scattered throughout the cell (Figures 4a–f). At the sulcus, there was a large and conspicuous eyespot, which comprised approximately six to eight layers of crystalline structures arranged in a C-shape; each layer consisted of many,

rectangular, brick-like crystalline structures, each of which in turn was enclosed by a single membrane (Figures 4a, b). A vacuole with fine fibers, which are assumed to be flagellar hairs, was commonly observed (Figure 4d). A number of peripheral, bottle-shaped apparati, considered to be mucocysts, were present, close to the inner amphiesmal membrane, each of which contained a fibrous substance of low electron-density interspersed by spots of denser material (Figure 4e). Thecal plates inside the amphiesmal vesicles have been observed in the motile cells (Figure 4b). No pusule was observed. The non-motile cell is surrounded by a continuous cell wall layer (Figures 4f, g) and can divide up to two times within the parental theca (Figure 4g).

Phylogenetic analysis

Figure 5 elucidates the phylogeny deduced from ML and Bayesian analyses (BA) base on a partial LSU rDNA (787 bases), including other 44 *Symbiodinium* sequences and three outgroup taxa (i.e., *Pelagodinium beii*, *Gymnodinium simplex* and *Polarella glacialis*). The *Symbiodinium* species was divided into 9 clades, corresponding to Clade A to I. *Symbiodinium* sp. HG246 was recovered, with moderate support (56/0.68), in the part of Clade A that has been redefined as the genus *Symbiodinium*, separated from the temperate clade A.

DISCUSSION

Species of the genus *Symbiodinium sensu lato*, as mutualistic endosymbionts, are known for their bio-geological significance, and extensively researched because of their importance to the survival and growth of reef-building corals (Scleractinia) and other invertebrates (reviewed by Baker 2003, Coffroth & Santos 2005, Pochon *et al*. 2006). The majority of studies have largely

focused on understanding the symbiosis between *Symbiodinium* and reef corals, and most of the species classifications were done using only molecular analysis. Recently, however, a few reports have been made on the existence and importance of the free-living *Symbiodinium* species from different habitats (Hirose *et al*. 2008, Takabayashi *et al*. 2012, Granados-Cifuentes *et al*. 2015). Although isolates of several free-living representatives have been established in culture from different habitats, only two, *S. natanse* Gert Hansen *et* Daugbjerg (2009) (Clade A) and *S. voratum* Jeong, Lee, Kang, LaJeunesse (2014) (Clade E), have been comprehensively described with morphological and molecular characterization. Although the culture of *S. voratum* was established from a plankton sample, there have been reports of it occurring as a member of the benthos, also involving substrata such as corals and macro-algae, from various localities (Chang 1983, Jeong *et al*. 2012, 2014, Yamashita & Koike 2013).

The *Symbiodinium* species described in this study, *Symbiodinium* sp. HG246, is the smallest (7.2–11.6 μm long, 5.7–9.1 μm wide) among all the species with a morphological description, i.e. *S. natans*, *S. microadriaticum* LaJeunesse (2017), *S. tridacnidorum* Lee, Jeong, Kang, & LaJeunesse (2015), *S. necroappetens* LaJeunesse, Lee, Knowlton & Jeong (2015), all from clade A (Table 3). Except for a minor difference in the cell size, *Symbiodinium* sp. HG246 mostly resembles the free-living species *S. natans*. The most noteworthy morphological characteristics that differentiate *Symbiodinium* sp. HG246 from the other species of this genus is the amphiesmal plate, number, shape and arrangement. All five described members of the genus *Symbiodinium* possess a different number of knobs on the EAV, with the highest number of knobs (15–18; Figure 2a, b, e) being found in *Symbiodinium* sp. HG246. *Symbiodinium* sp. HG246 and *S. tridacnidorum* have the same number of intercalary plates (1a–6a), but the 4a plate in *Symbiodinium* sp. HG246 is smaller and rhomboid (Figure 2a, b, d, e, 3a, b), while it is

pentagonal in *S. tridacnidorum*. Another variation in external morphology among all five species is to be found in the cingulum and the sulcus. Two of the three symbiotic species, *S. tridacnidorum* and *S. necroappetens*, have a similar number of sulcal plates (9–11) and their two S? plates are separated by a small accessory sulcal plate. The third, *S. microadriaticum*, has 9–13 plates and its two S? plates are in contact. *Symbiodinium* sp. HG246 only has ~7 sulcal plates and the small accessory plates are mostly found on the left side of the sulcus area (Figure 2f & 3a) and, as in *S. natans* and *S. microadriaticum*, the two S? plates are in contact. The number of cingular plates in all species range from 20–25, with the exception of *S. tridacnidorum* (17–19); and the two free-living species, *Symbiodinium* sp. HG246 and *S. natans*, have the same number of cingular plates (20). In addition, the degree of the displacement of the cingulum varies among the *Symbiodinium* species, where the cingulum of the *S. natans* was displaced more than all the other members of this genus. Apart from the cingular and sulcal plates, the hyposomal plates are considered the most stable and conservative (Balech 1980). This observation remains true here as the hyposome of all described species is the same (6''', 2'''') except for *S. tridacnidorum* (7''', 3'''').

In terms of internal morphology, the characteristics shared by the members of the family Symbiodinaceae include the possession of a single pyrenoid that is devoid of thylakoid invasion, a peripherally-arranged, single chloroplast network, the possession of a type E eyespot near the sulcus area, cytoplasm with numerous lipid droplets and starch granules (Hansen & Daugbjerg 2009, Lee *et al*. 2015, LaJeunesse 2017, LaJeunesse *et al*. 2015, 2018). *Symbiodinium* sp. HG246, however, additionally showed some unique internal traits that can justify it as a new species, such as the lack of a pusule and the possession of mucocysts. Pusules have not been mentioned in any of the Clade A members, except *S. natans*; mucocysts, on the other hand, have not been reported from any other *Symbiodinium* species.

One of the most noteworthy features that separate *Symbiodinium* sp. HG246 from the others is its habitat. Although numerous reports exist of free-living forms in various environments (habitats) (Gou *et al*. 2003, Coffroth *et al*. 2006, Thornhill *et al*. 2006, Koike *et al*. 2007, Hirose *et al*. 2008, Littman *et al*. 2008, Manning & Gates 2008, Porto *et al*. 2008, Adams *et al*. 2009, Hansen & Daugbjerg 2009, Pochon *et al*. 2010, Reimer *et al*. 2010, Venera-Ponton *et al*. 2010, Takabayashi *et al*. 2012, Zhou *et al*. 2012 Huang *et al*. 2013, Yamashita & Koike 2013, Jeong *et al*. 2014), none have been from tidal pools where they formed blooms; *Symbiodinium* sp. HG246 is the first free-living, bloom-forming *Symbiodinium* species collected from a tidal pool and maintained in culture, with molecular and morphological characterization.

Furthermore, the position of *Symbiodinium* sp. HG246 in the phylogenetic tree recovered from molecular analysis strongly supports its recognition as a new species. *Symbiodinium* sp. HG246 formed a sister clade with the free-living *S. natans* (Figure 5), as a basal clade to the other four described species, *S. natans*, *S. microadriaticum*, *S. tridacnidorum*, *S. necroappetens*. Likewise, the pairwise distance analysis showed a large genetic difference, 12.6%, between the two free-living species, *Symbiodinium* sp. HG246 and *S. natans*. In conclusion, it is clear that *Symbiodinium* sp. HG246 represents a new species of the genus *Symbiodinium* based on the distinct morphological features supported by molecular phylogenetic analysis

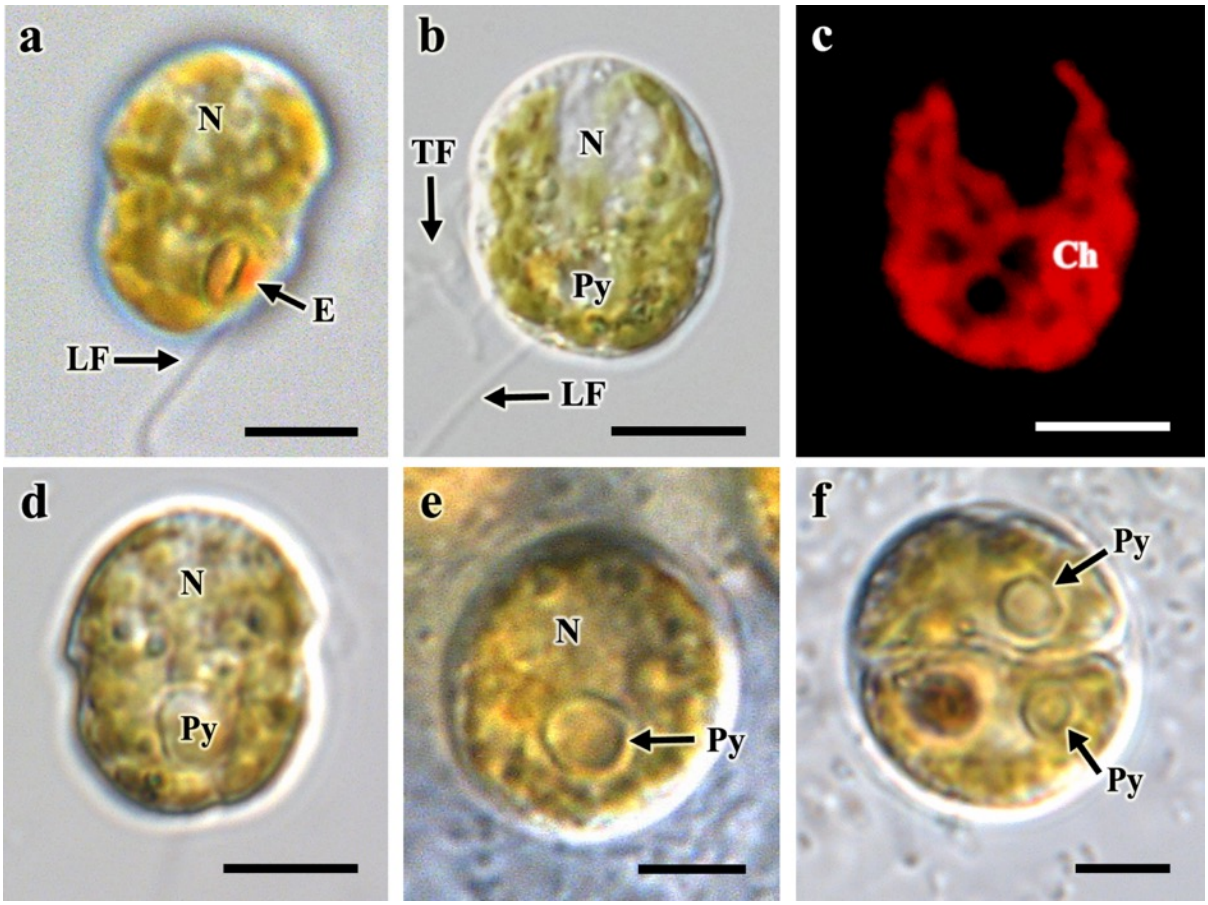

Figure 1. Light micrography of the motile (a–d) and non-motile cell (e–f) of the *Symbiodinium* sp. HG246. **(a)** Right lateral view of the motile cell showing the nucleus (N) in the episome, eyespot (E) and longitudinal flagellum (LF). **(b)** Ventral view of the motile cell; TF, transverse flagellum; Py, pyrenoid. **(c)** Autofluorescence micrograph of the motile cell indicating the peripherally arranged chloroplast (Ch) lobes. **(d)** Dorsal view of the motile cell, showing the slightly larger episome and the starch-enveloped pyrenoid (Py). **(e)** Spherical non-motile cell. **(f)** Division in non-motile cell. Scale bar = 5 µm.

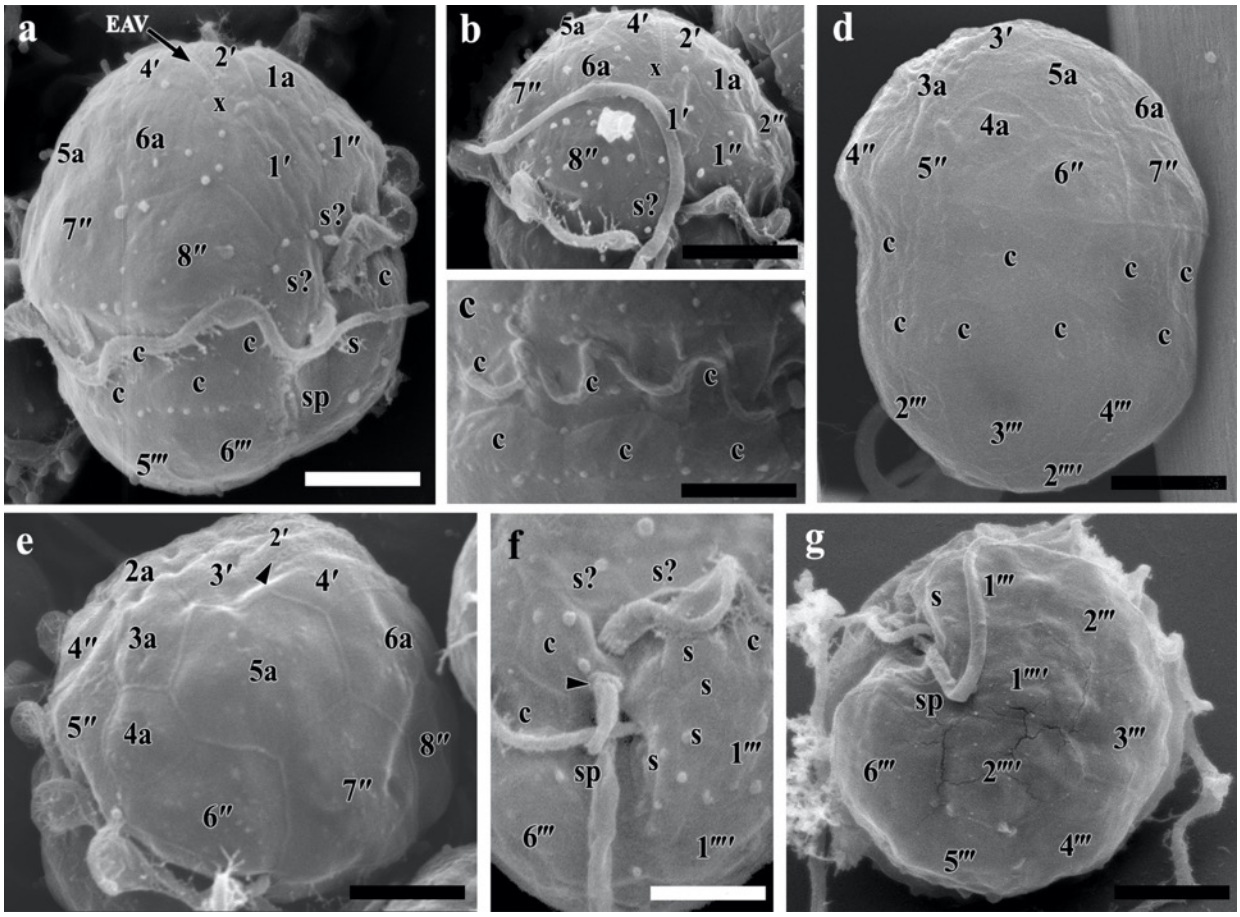

Figure 2. Scanning electron micrographs (SEM) of the motile cell of the *Symbiodinium* sp. HG246. **(a)** ventral view of the cell; black arrow shows the elongated amphiesmal vesicle (EAV) **(b)** Lateral ventral view of the episome, showing the asymmetric first apical plate (1') and x plate. **(c)** Cingulum consisting of two rows of pentagonal plates. **(d)** Dorsal view of the cell, indicating the position and shape of the extra intercalary plate (4a). **(e)** Apical view; arrowhead shows elongated amphiesmal vesicle (EAV) with linearly arranged knobs within. **(f)** Sulcus area of the cell, showing the multiple sulcal plates and the peduncle (arrowhead). **(g)** Antapical view. Scale bar = 3 μm.

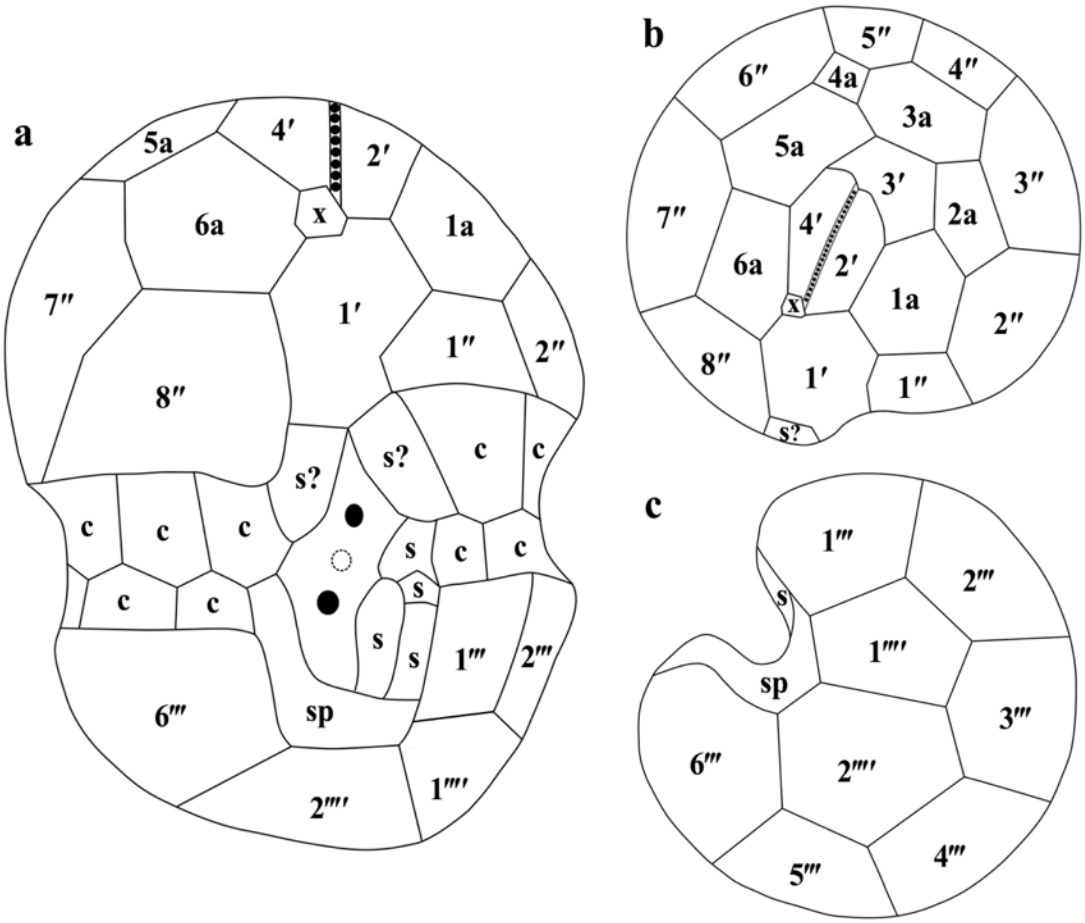

Figure 3. Line drawing of plate tabulation in *Symbiodinium* sp. HG246 based on a compilation of SEM micrographs. **(a)** Ventral view. **(b)** Apical view. **(c)** Antapical view.

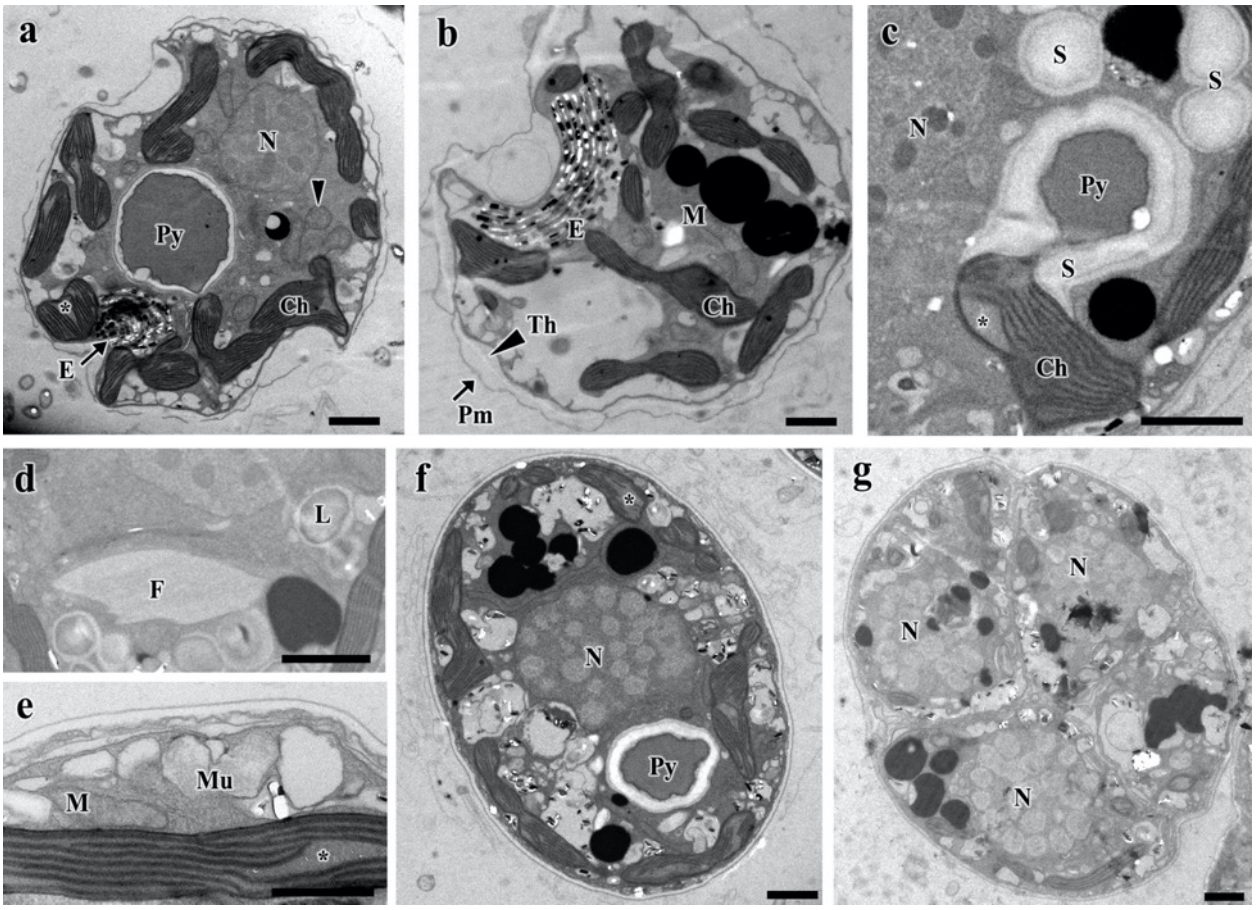

Figure 4. Transmission electron micrographs (TEM) of the motile (a–e) and non-motile (f–g) cell of the *Symbiodinium* sp. HG246. **(a)** Longitudinal section of the motile cell. N, nucleus; Ch, chloroplast; Py, pyrenoid; E, eyespot; relatively large mitochondrial profile (arrowhead); the thylakoid-free area of the chloroplast(asterisk). **(b)** Transverse section. Notice C-shaped, type E eyespot consisting of brick-like cisternae, and thecal plates inside the amphiesmal vesicle (arrowhead); Ch, chloroplast; E, eyespot; M, mitochondrial profile; Th, thecal plate; Pm, plasma membrane. **(c)** Details of the stalked pyrenoid (Py); the thylakoid-free area (asterisk) in the chloroplast (Ch) profile; starch granules (S). N, nucleus. **(d)** Flagellar hair vesicle (F). L, lipid droplets. **(e)** One of peripherally located mucocysts (Mu). M, mitochondrial profile; *, thylakoid-free area of chloroplast **(f)** Longitudinal section of the non-motile cell. N, nucleus; Py, pyrenoid; *, thylakoid-free area of chloroplast **(g)** Transverse section of the non-motile cell that has undergone two divisions. N, nucleus. Scale bar = 1 μm, (e) = 2 μm.

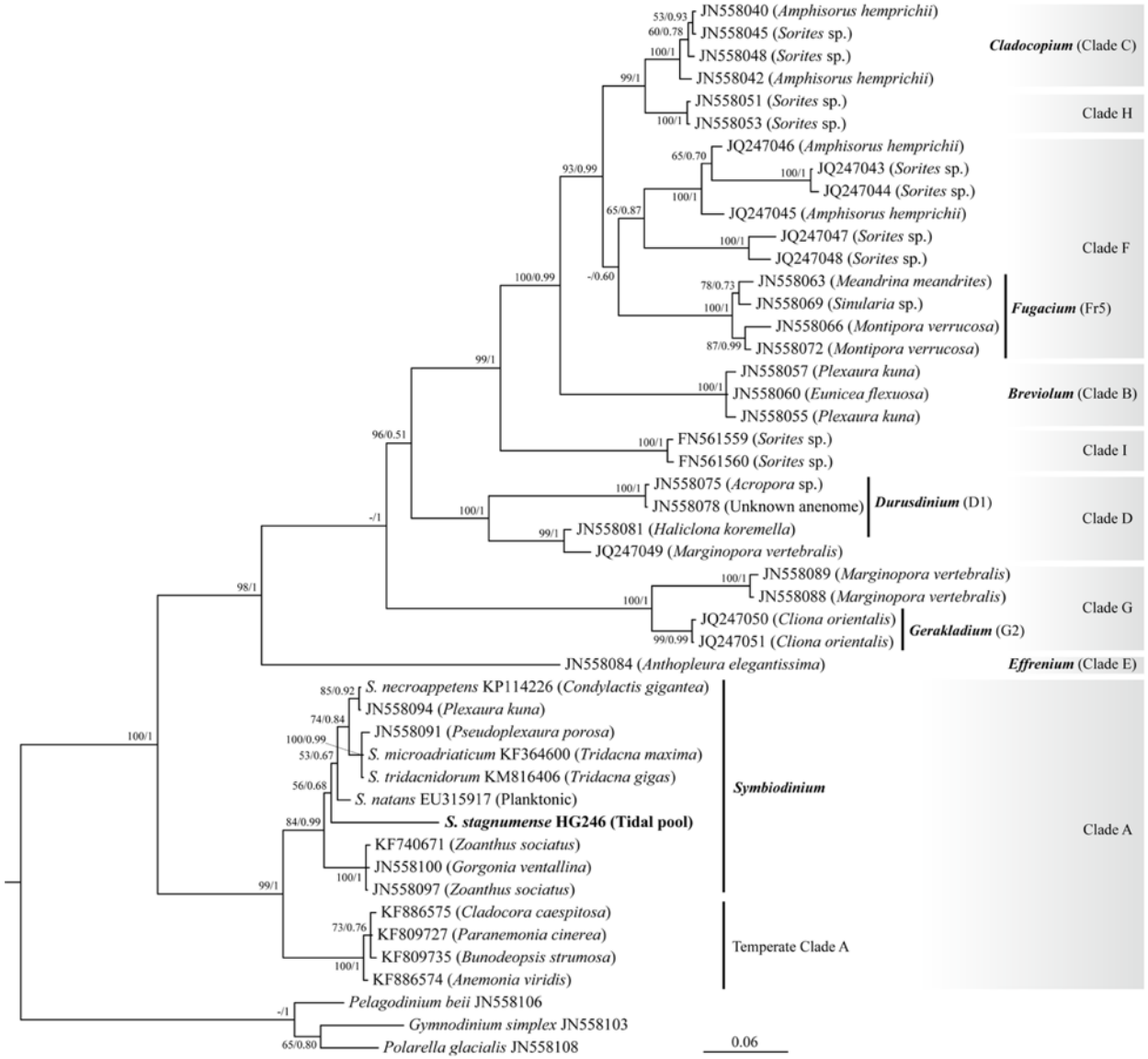

Figure 5. Topology of the Bayesian phylogenetic tree inferred from partial large-subunit (LSU) ribosomal (r) DNA sequence (D1–D3) alignment. Bootstrap support for ML analysis (100 pseudoreplicates) and Bayesian posterior probability (>50% and >0.8, respectively) are indicated at each node.

Table 1. Formally classified and named species of the family Symbiodinaceae.

Species	Host/Habitant and locality	Clade	Proposed Genus name	Reference
S. linucheae	*Linuche unguiculate* Exuma Keys, Bahamas	A	*Symbiodinium*	Trench & Thinh, 1995
S. microadriaticum	*Cassiopei* sp.	A		Freudenthal, 1962
S. natans	**Free-living** (water colum) Callao Salvaje, Tenerife	A		Hansen & Daugbjerg, 2009
S. necroappetens	*Orbicella* sp. Discovery Bay, Jamaica	A		LaJeunesse et al., 2015
S. pilosum	*Zoanthus sociatus* Discovery Bay, Jamaica	A		Trench & Blank, 1987
S. tridacnidorum	*Hippopus hippopus* Great Barrier Reef, Australia	A		Lee et al., 2015
S. aenigmaticum	*Porites astreoides* Florida Keys, USA,	B	*Breviolum*	Parkinson et al., 2015
S. antillogorgium	*Antillogorgia bipinnata* Florida Keys, USA	B		Parkinson et al., 2015
S. endomadracis	*Madracis* spp. Curacçao	B		Parkinson et al., 2015
S. minutum	*Aiptasia* sp. Florida, USA	B		LaJeunesse & Parkinson, 2012
S. pseudominutum	*Oculina diffusa* Bermuda	B		Parkinson et al., 2015
S. psygmophilum	*Oculina diffusa* Bermuda	B		LaJeunesse & Parkinson, 2012
S. goreaui	*Ragactis lucida* Discovery Bay, Jamaica	C	*Cladocopium*	Trench & Blank, 1987
S. thermophilum	*Porites lobata* Saadiyat reef, Abu Dhabi, UAE	C		Hume et al., 2015
S. boreum	*Oulastrea crispata* Penghu Island, Taiwan	D	*Durusdinium*	LaJeunesse et al., 2014
S. eurythalpos	*Oulastrea crispata* Penghu Island, Taiwan	D		LaJeunesse et al., 2014
S. glynnii	*Pocillopora* sp. Nikko Bay, Palau	D		Wham et al., 2017
S. trenchii	*Scleractinia* sp. Okinawa, Japan	D		LaJeunesse et al., 2014
S. voratum	**Free-living** (planktonic) Jeju Island, Korea	E	*Effrenium*	Jeong et al., 2013
S. kawagutii	*Montipora verrucose* Kaneohe Bay, Oahu, Hawaii	F/Fr5	*Fugacium*	Trench & Blank, 1987
S. endoclionum	*Cliona orientalis* Orpheus Island, Australia	G	*Gerakladium*	Ramsby et al., 2017
S. spongiolum	*Cliona varians* Florida Keys, USA	G		Ramsby et al., 2017

Table 2. Oligonucleotide primers used for amplification and sequencing of SSU, ITS and LSU rDNA.

Region and primer	Synthesis	Sequence (5'–3')	Reference
Small subunit rDNA			
SR1	Forward	TACCTGGTTGATCCTGCCAG	
SR5TAK	Reverse	ACTACGAGCTTTTTAACYGC	
SR4	Forward	AGGGCAAGTCTGGTGCCAG	Takano & Horiguchi (2005)
SR9	Reverse	AACTAAGAACGGCCATGCAC	
SR8TAK	Forward	GGATTGACAGATTGAKAGCT	
SR12-b	Reverse	CGGAAACCTTGTTACGACTTCTCC	
Internal transcribed spaces (ITS)			
r18Sf	Forward	GAAAGTTTCATGAACCTTAT	Yamashita and Koike, 2013
Sym28Sr	Reverse	CTTGTRTGACTTCATGCTA	
Large subunit rDNA			
D1R	Forward	ACCCGCTGAATTTAAGCATA	Yamada *et al*. 2013
25R1	Reverse	CTTGGTCCGTGTTTCAAGAC	
305F-27	Forward	CGATAGCAAACAAGTACCATGAG	Dawut *et al*. 2018
852R-70	Reverse	CGAACGATTTGCACGTCAG	
D3A	Forward	GACCCGTCTTGAAACACGGA	Yamada *et al*. 2013
28-1483R	Reverse	GCTACTACCACCAAGATCTGC	

Table 3. Morphological comparison of the described species within genus *Symbiodinium* (Clade A) species

	HG246	*S. natans*	*S. microadriaticum*	*S. tridacnidorum*	*S. necroappetens*
Cell length (motile, μm)	7.2–11.6 (9.4)	9.5–11.5 (10)	8.0–13.8 (9.8)	9.4–12.9 (10.9)	9.1–12.5 (10.8)
Cell width (motile, μm)	5.7–9.1 (7.5)	7.4–9.0 (8)	6.3–11.9 (8.1)	7.5–10.6 (8.8)	7.5–10.5 (8.8)
Chloroplast(s)	Single/Golden-brown	Many/Brownish	Single/Yellowish	Single/Brownish	? /Brownish*
Position of nucleus	Episome	Episome	Episome*	Episome*	Episome*
Position of pyrenoid	Central	Central	Central	Central	Central*
Number of knobs on EAV	15–18	12	6–8	7–9	7–12
Number of apical plates	4	4	4	5	4
Number of intercalary plates	6	5	5	6	5
Number of precingular plates	8	8	8	8	8
Number of sulcal plates	~7	?	9–13	9–11	9–11
Number of cingular plates	~20	20	22–24	17–19	21
Cingulum displaced by cell length	0.15–0.24 (0.17)	0.23	0.06–0.24 (0.14)	0.06–0.20 (0.12)	0.06–0.24 (0.14)
Cingulum displaced by cell width	0.18–0.61 (0.35)	1.0	0.18–0.72 (0.41)	0.23–0.70 (0.40)	0.18–0.72 (0.41)
Peduncle	Present	Present	Present	Present	Present
Number of postcingular plates	6	6	6	7	6
Number of antapical plates	2	2	2	3 (rarely 2)	2
Type of eyespot	E	E	E	E	E
Pusule	N	Y	?	?	?
Extrusome	Mucocysts	?	?	?	?
Plate formula	x, EAV, 4', 6a, 8", ~7s, ~20c, 6"', 2""	x, EAV, 4', 5a, 8", ?s, ?c, 6"', 2""	x, EAV, 4', 5a, 8", 9–13s, 22–24c, 6"', 2""	x, EAV, 5', 6a, 8", 9–11s, 17–19c, 7"', 3""	x, EAV, 4', 5a, 8", 9–11s, 21c, 6"', 2""
Habitat	Free-living Tidal pool	Free-living Planktonic	Symbiotic Jellyfish	Symbiotic Giant clam	Symbiotic Stony corals
Reference	(1)	(2)	(3) (4)	(4)	(5)

EAV, elongated amphiesmal vesicle; *, seen from the figures; ?, not mentioned; N, not observed; Y, observed.

(1) This study; (2) Hansen & Daugbjerg, 2009; (3) Trench & Blank, 1987; (4) Lee et al. 2015; (5) LaJeunesse et al. 2015.

CHAPTER V

Re-investigation of *Gymnodinium natalense* (Dinophyceae), a tidal pool dinoflagellate from South Africa and the proposal of a new combination *Ansanella natalensis*

INTRODUCTION

The small dinoflagellate *Gymnodinium natalense* was originally discovered in samples from a tidal pool at Amanzimtoti, KwaZulu-Natal Province (at the time of original description, Natal Province), South Africa by Horiguchi and Pienaar (1994a). It was described as a new member of the genus *Gymnodinium*, based on its medially- located cingulum and unarmoured nature. The species was characterised by a combination of features, some unique, such as a lack of trichocysts, the possession of bottle-shaped mucocysts and a special type of eyespot, the latter at that time considered completely novel for dinoflagellates (Horiguchi & Pienaar 1994b). Subsequently, this type of eyespot was reported in other dinoflagellates belonging to the family Suessiaceae (Moestrup & Daugbjerg 2007, Moestrup *et al*. 2009a). In their series of taxonomic works on woloszynskioid dinoflagellates, Moestrup *et al.* (2009a) regarded the type of eyespot as an important taxonomic character in discriminating phylogenetic lineages. They found that a clade consisting of *Symbiodinium* spp., *Protodinium simplex* Lohmann, *Biecheleria* spp. and *Polarella glacialis* Montresor, Procaccini & Stoecker is characterised by the possession of a Type E eyespot (*sensu* Moestrup & Daugbjerg 2007). The eyespot found in *G. natalense* also belongs to this type. Based on the common possession of this type of eyespot and of a similar straight apical furrow apparatus, Moestrup *et al*. (2009a) transferred *G. natalense* to the genus *Biecheleria* and proposed a new combination *Biecheleria natalensis* (Horiguchi & Pienaar) Moestrup. However, at that stage, no molecular data were available and its phylogenetic position needed confirmation by this means.

The genus *Ansanella* was recently established by Jeong *et al*. (2014), based on the type species, *A. granifera* H. J. Jeong, S. H. Jang, Moestrup & N. S. Kang. Although morphologically most reminiscent of species belonging to the genera *Biecheleria* and *Biecheleriopsis*, *A. granifera* is distinguishable by having grana-like thylakoids, a different shape to its cingular margin, and by lacking a nuclear fibrous connective (Jeong *et al*. 2014). Furthermore, the independent placement of *A. granifera* from these genera within the family Suessiaceae in their phylogenetic tree also supported its recognition as an autonomous genus. Despite the fact that *A. granifera* was shown to be phylogenetically distinct from the clade containing the Type E eyespot, it too possesses this eyespot type. Also, it was demonstrated that, although *Biecheleria* species possess a 51-base pair deletion in their D2 region of LSU rDNA, no such deletion was detected in *A. granifera* (Jeong *et al*. 2014)

During the course of a cooperative research programme between Japan and South Africa, an opportunity presented itself to collect and establish culture strains of a small dinoflagellate resembling *G. natalense* from a tidal pool at the type locality of this species (Horiguchi & Pienaar 1994a). Based on its morphology and ultrastructural characters, it was concluded that this newly isolated dinoflagellate was indeed *G. natalense*. This material afforded the opportunity to determine its phylogenetic affinity based on the small subunit ribosomal RNA gene (SSU rDNA) but also provided some additional morphological data. We also generated partial LSU rDNA sequences to confirm whether the 51 bp deletion exists in *G. natalense* or not. These new data led to the conclusion that *G. natalense* should be relegated to the genus *Ansanella* rather than to *Biecheleria*.

MATERIALS AND METHODS

Sampling and culture conditions

Water samples were collected from a tidal pool at Amanzimtoti, KwaZulu-Natal, South Africa (30°3.823′ S, 30°52.91′ E) on 27th September 2011 using a large pipette and single cells were isolated by micropipette into sterile medium during the expedition. Successful monocultures (CW-19 and CX-13) were established and formed the subject material of the current study. These two cultures were maintained in Daigo's IMK medium (Nihon Pharmaceutical Co., Tokyo, Japan) and maintained at 20°C at an irradiance of 50 µmol photons $m^{-2}s^{-1}$ with a 16:8 light: dark regime.

Light microscopy

Light microscopic observations of motile cells were made using a Carl Zeiss Axioskop 2 microscope equipped with Nomarski interference optics (Carl Zeiss Japan, Tokyo). An image analysis system was used to measure the length and width of motile cells from micrographs taken using a Leica MC-120HD digital camera (Leica Microsystems, Wetzlar, Germany). The shape and number of chloroplasts were characterised using autofluorescence (Carl Zeiss Axioskop 2 with a filter set No. 15) and the nucleus was visualized using 1 µg/mL of 4', 6-diamidino-2-phenylindole (DAPI) made up in distilled water (with filter set No. 49).

Scanning electron microscopy

For scanning electron microscopy, a 100 µL aliquot of a dense culture of motile cells was placed on a SEM plate glass (Φ 8.5 mm) pre-coated with poly-l-lysine and fixed with the vapour of 4%

osmium tetroxide (OsO_4) for 3–5 min. The cells were allowed to settle on the surface of glass plate for a further 10 min. The attached cells were rinsed twice with distilled water for 30 min each. The samples were then dehydrated in an ethanol series (30, 50, 70, 90, 95%, 10 min at each step) followed by two rinses in 100% ethanol for 30 min each and dried using a critical point drier (Hitachi HPC-2, Tokyo, Japan). The dried cells were sputter-coated with gold for 150 s at 10 mA (Hitachi E-1045) and observed using a scanning electron microscope (S-3000N, Hitachi).

Transmission electron microscopy

Cells were concentrated by gentle centrifugation (40 ×g for 10 min) and the pellet was fixed with cold 2.5% glutaraldehyde for 30 min on ice, followed by a rinse with filtered sea water (FSW), and post-fixed with 1% OsO_4 for 1h on ice. After a rinse in FSW followed by one in distilled water, the samples were dehydrated in an ethanol series of 25%, 50%, 70%, 95%, 100%, followed by two changes in 100% ethanol (10 min at each step), and embedded in low viscosity (LV) resin (Agar Scientific, Essex, England). After polymerization at 65℃ for 16 h, thin sections were cut using a diamond knife on an ultramicrotome (Leica EM UC6). Sections were picked up on Formvar-coated one-slot grids and viewed with a transmission electron microscope (H-7650, Hitachi).

DNA extraction, polymerase chain reaction (PCR) amplification, sequencing and data analysis

Approximately 20 motile cells were used to extract DNA by applying the Quick Extract™ FFPE DNA extraction kit (Epicentre, Tokyo, Japan) according to the manufacturer's protocol. The

small subunit ribosomal RNA gene (SSU rDNA) and the large subunit ribosomal RNA gene (LSU rDNA) were amplified using primers listed in the supporting information (Table S1). The 25 μL PCR amplification process (for both SSU/LSU rDNA) consisted of 1 initial cycle of 5/6 min at 94°C, 35 cycles of 30 s at 94°C (denaturation), 30 s at 50/52°C (annealing) and 90 s at 72°C (extension). The final extension cycle was at 72°C for 7/6 min. The PCR products were purified and sequenced with ABI PRISM Big Dye Terminator (Perkin-Elmer, Waltham, Massachusetts, USA). The final step of sequencing was achieved using a DNA auto-sequencer ABI PRISM310 Genetic Analyzer (Perkin-Elmer).

A total of 3,041 aligned sites (1,767 (CX-13) and 1,734 (CW-19) bases augmented by gaps from the rRNA secondary structure) were used for the analyses. The aligned sequences were analysed by the maximum likelihood (ML) method using PAUP* version 4.0b10 (Swofford 2001) and the Bayesian method using MrBayes 3.2.1 (Huelsenbeck & Ronquist 2001; Ronquist & Huelsenbeck 2003). The programme jModel Test version 2.1.4 (Guindon & Gascuel 2003; Darriba *et al*. 2012) was used to calculate the evolutionary model that was the best fit for ML analysis of the data set. The selected model was the GTR+I+G model. The heuristic search for the ML analysis was performed with the following options: a tree bisection reconnection branch-swapping algorithm and the Kimura 2-parameter neighbour-joining tree as a starting tree. The parameters used for the analysis were as follows: assumed nucleotide frequencies (user-specified) A=0.264915 C=0.189305 G=0.255024 and T=0.290759; substitution rate matrix with A<->C=1.38958, A<->G=4.61756, A<->T=1.38958, C<->G=1, C<->T=7.75988, G<->T=1; proportion of sites assumed to be invariable=0.518215; rates for variable sites assumed to follow a gamma distribution with shape parameter=0.616636; and the number of rate categories=4. For the Bayesian analysis, GTR+I+G was selected as the best evolutionary model by MrModeltest

2.3 (Nylander *et al*. 2004). Markov-chain Monte Carlo iterations were carried out until 4,500,000 generations were attained, when the average standard deviations of split frequencies fell below 0.01, indicating the convergence of the iterations. A total of 1,400 (CW-19) and 1,397 (CX-13) bases of LSU rDNA were amplified. The sequence comparison in the D2 region was done using the MUSCLE program in MEGA 7.0 (Kumar *et al*. 2016). In addition to strains CW-19 and CX-13, we included the sequence of strain CX-7 (1,797 base pairs) in our alignment (accession number LC054923, registered as *Biecheleria natalensis*), isolated at the same time as the other two strains and used this material for photosynthetic pigment analysis (Yamada *et al*. 2015).

RESULTS

Light and scanning electron microscopy

The morphology of strains CW-19 (Figure 1a, b) and CX-13 (Figure 1c, d) were almost the same. Cells were pentagonal to somewhat oval in shape in ventral view with an indentation in the hyposome (Figure 1a–d). The cells were 9.7–14.2 µm (ave. 12.3 ± 1.2 µm, n = 30) in length, and 8.3–12.2 µm (ave. 9.9 ± 1.1 µm, n = 30) in width; the episome was conical and slightly larger than the trapezoidal hyposome (Figure 1a–d). The nucleus was oval and located in the anterior to central part of the cell (Figure 1a–e). The yellowish-brown chloroplast was peripheral (Figure 1a–d, f), and contained one to three rounded pyrenoids in either the episome or the hyposome (Fig. 1b–d, f). The orange eyespot, located in the sulcus, was rectangular and folded longitudinally in the middle, resulting in an elongated C-shape (Figure 1b–d). A non-motile stage was observed occasionally, but no resting cysts were present.

The cell surface was smooth and covered with small, longitudinally arranged, polygonal amphiesmal vesicles (AVs) (Figures 2, 3). These AVs were quadrangular / pentagonal / hexagonal / heptagonal in shape (mostly hexagonal), and arranged in 11–13 horizontal rows (mostly 12 rows) in total, i.e. 5–6 rows in the episome (mostly 5), 3 rows in the cingulum, and 3–4 rows in the hyposome (mostly 4) (Figures 2, 3). A narrow furrow, the elongated apical vesicle (EAV), was present at the apex of the episome, surrounded by 6–7 small AVs (Figures 2a, d, e, 3d, e). The EAV was ornamented by ~25 small knobs (Figures 2e, 3d, e). The medially-located cingulum was displaced by a distance almost its own width. The AVs in the uppermost (closest to episome) row of the cingulum were almost pentagonal in shape, and almost all of the AVs in the middle and lowest rows were hexagonal (Figures 2b, c, 3a, c). The sulcus was relatively narrow and widened towards the antapex (Figures 2b, 3a, b). The hyposome was comprised of approximately 45–50 AVs, mostly hexagonal in shape (Figures 2b, c, e, 3a, c, f), and no peduncle was observed.

Transmission electron microscopy

The dinoflagellate possessed a typical dinokaryotic nucleus with many chromosomes and no nuclear connector was seen (Figure 4a). Relatively large mitochondrial profiles were observed, generally in the peripheral parts of the cells (Figure 4a, b). The chloroplast was single, peripherally arranged and contained pyrenoids (Figures 4a, b, 5a). Each lamella consisted of three stacked thylakoids (Figure. 5b). The pyrenoids were spherical, partially surrounded by hemispherical starch sheaths, and embedded inside the chloroplast matrix (Figures 4a, b, 5a). The pyrenoid matrix was penetrated by single thylakoids of variable length (Figure. 5a). At the sulcus, there was a large and conspicuous eyespot, which, in transverse section, comprised

approximately six to seven layers of crystalline structures arranged in a C-shape; each layer consisted of many, rectangular, brick-like crystalline structures, each of which in turn was enclosed by a single membrane (Figure. 5c, d). A number of peripheral, bottle-shaped apparati, considered to be mucocysts, were present, close to the inner amphiesmal membrane, and contained a fibrous substance of low electron-density interspersed by spots of denser material (Figure. 5e). The cell coverings of the motile cell consist of, from outside to inside, the plasma membrane (PM), amphiesmal vesicle (AV) and a pellicle layer (P) in each AV (Figure. 5e). No trichocysts were observed.

Phylogenetic analysis

Both SSU rDNA (Accession numbers LC361448 and LC361449) and LSU rDNA (Accession numbers LC373202 and LC373203) sequences of *Ansanella natalensis* were registered with GenBank. All three strains of the current material (CW-19, CX-7 and CX-13) had the same sequence. These three strains formed a robust sister relationship (98% ML/1.0 BI) with the two sequences of *Ansanella granifera* strains (Figure. 6). When properly aligned, the SSU rDNA sequence of *A. natalensis* differed from that of *A. granifera* by 7-base pairs (0.4%), excluding ambiguous positions. The clade containing members of the genus *Biecheleria* was isolated from the clade containing the current material and *A. granifera* (Figure. 6). With regard to the LSU rDNA domain 2 (D2) sequence, *Ansanella* differed from *Biecheleria* by having an additional 51-base pair fragment (Figure. 7).

DISCUSSION

The strains examined in this study were obtained from the same tidal pool, from a locality where *G. natalense* was originally collected (Horiguchi & Pienaar 1994a). Morphologically, the material here had almost the same characters with that of *G. natalense*. The only notable differences were the number of pyrenoids and the cell size. The current material displayed a variable number (1–3) of pyrenoids (Figures 4a, b, 5a), rather than the singleton mentioned in the original description of *G. natalense* (Horiguchi & Pienaar 1994a). Nevertheless, the type of pyrenoid, which is embedded in the chloroplast, with its matrix penetrated by many single thylakoids, was identical. Cells of the original material were larger than the current strains (14.4–18.0 µm vs. 9.7–14.2 µm long and 9.9–12.6 µm vs. 8.3–12.2 µm wide). Horiguchi and Pienaar (1994a) worked on wild material from the tidal pool, shortly after sampling, while current observations were made on strains artificially cultured for more than six years, and which we expect to have some impact in this regard. The rest of the morphological and ultrastructural features of strains CW-19 and CX-13 are congruent with those in the original description of Horiguchi and Pienaar (1994a). Therefore, we concluded that the strains CW-19 and CX-13 (and CX-7) are indeed conspecific with *G. natalense*.

When *G. natalense* was described, no molecular data was available; and its placement into the genus *Gymnodinium* was justified using the traditional definition of the genus, i.e. its unarmoured nature and the position and form of the cingulum. Later, Moestrup *et al*. (2009a) transferred *G. natalense* into their new genus *Biecheleria*. This taxonomic treatment was based on the possession of the same type of eyespot (Type E) and the possession of a similar type of

apical furrow apparatus (EAV). It should be pointed out that this taxonomic change was made without any support following the analysis of molecular data.

Our molecular tree clearly indicated that strains of *G. natalense* were closely related to *A. granifera*, the only member of a recently-established genus (Jeong *et al*. 2014) than to members of the genus *Biecheleria*. In fact, *G. natalense* shared several characteristics with *A. granifera*, including the similar number of latitudinal rows, the shape and position of the EAV, the possession of a type E eyespot, the presence of a pyrenoid matrix embedded in the chloroplast, the absence of a peduncle and of any nuclear chambers, the lack of a nuclear fibrous connective and of resting cyst-like cells (Table 1). Although the presence of resting cysts was not mentioned in the description of *A. granifera* (Jeong *et al*. 2014), the material was collected from sea sediments and this plausibly could have included resting cyst stages. Therefore, the lack of such a stage as a generic character should be only cautiously invoked. Furthermore, *A. granifera* and the strain CX-7 share the same major photosynthetic pigments (e.g. chlorophyll *a*, chlorophyll c_2, diadinoxanthin, peridinin, etc.) (Jeong *et al*. 2014, Yamada *et al*. 2015), albeit this photosynthetic pigment composition is one shared by many dinoflagellates (Yamada *et al*. 2015).

Although our molecular tree indicated a distant relationship between species of *Ansanella* and *Biecheleria*, it is quite difficult to distinguish these genera morphologically (Table 1). Jeong *et al*. (2014) used the presence of grana-like thylakoids as a generic feature for the genus *Ansanella*. However, such thylakoids have not been detected in *G. natalense*. Therefore, the only, as yet useful, features to distinguish these two genera are the absence of a peduncle and the lack of resting cysts in *Ansanella*. These distinguishing morphological features are supported by a distinct molecular difference between these two genera, namely the deletion of a 51-base pair fragment in the D2 domain of the LSU rDNA of *Biecheleria*, which is not present in *Ansanella*

(Figure. 7). The other similar genus, *Biecheleriopsis*, can be more-readily distinguished from *Ansanella* by the presence of a straight lower margin to the cingulum, by the possession of a nuclear fibrous connective and by the presence of a resting cyst stage (Table 1) (Moestrup *et al*. 2009b; Jeong *et al*. 2014; Takahashi *et al*. 2014).

The phylogenetic affinity of *G. natalense* with *A. granifera* and their shared morphological traits strongly support the reassignment of *G. natalense* to the genus *Ansanella*. However, *G. natalense* and *A. granifera* can be distinguished morphologically. Cells of *G. natalense* have no grana-like thylakoids, each have only one chloroplast (Figure. 4a, b) rather than the five to eight reported for *A. granifera* (Jeong *et al*. 2014) and have mucocysts that are absent in *A. granifera*. In addition, the habitats of these two species are markedly different, with *A. granifera* recovered from estuarine waters (Jeong *et al*. 2014), and *G. natalense* from a tidal pool. Therefore, these two species are clearly different from each other. In conclusion, it is appropriate to propose the transfer of *Gymnodinium natalense* to the genus *Ansanella*, making a new combination, *A. natalensis* (Horiguchi & Pienaar) Dawut, Sym & Horiguchi comb. nov.

Ansanella natalensis (Horiguchi & Pienaar) Dawut, Sym & Horiguchi comb. nov.

Figures 1–5

Basionym: *Gymnodinium natalense* Horiguchi & Pienaar (1994a, p. 22, Figures 1–13).

Synonym: *Biecheleria natalensis* (Horiguchi & Pienaar) Moestrup (2009a, p. 213)

In this study, new information concerning the surface morphology was revealed and resulted in the following emendation to its description.

Emended description:

Cells photosynthetic, unarmored, pentagonal to somewhat oval, 9.7–14.2 μm long, 8.3–12.2 μm wide; episome conical, slightly larger than trapezoidal hyposome; cell surface covered with longitudinally arranged polygonal amphiesmal vesicles; 5–6 rows in the episome, 3 rows in the cingulum, 3–4 rows in the hyposome; cingulum median, wide, distinct, displaced by a distance roughly equivalent to its own width; sulcus narrow; nucleus oval, located in episome or middle of the cell; single yellowish-brown chloroplast peripherally arranged; one to three pyrenoids present, embedded in the chloroplast, partially surrounded by a starch sheath, and with a matrix penetrated by thylakoids; with an E-type eyespot in the sulcal region, rectangular in ventral view and C-shaped in apical view; mucocysts present. No peduncle and trichocysts present.

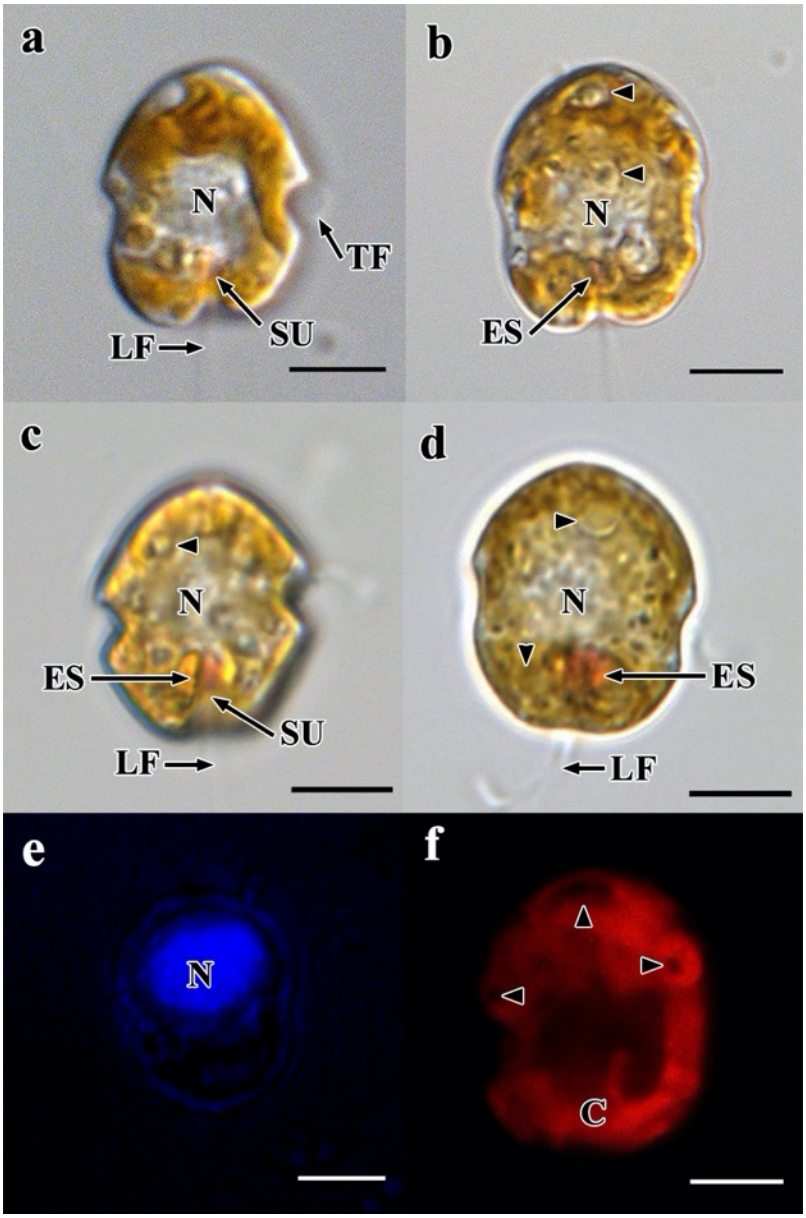

Figure 1. Light micrographs of *Ansanella natalensis* comb. nov., CW-19 (a, b, e, f) and CX-13 (c, d). **(a)** Ventral view of the cell, showing nucleus (N), sulcus (SU), longitudinal flagellum (LF) and transverse flagellum (TF). **(b)** Ventral view, showing the conical episome and wide cingulum. The pyrenoids (arrowheads) are visible and embedded in the chloroplast. Nucleus (N). The orange eyespot (ES) is situated in the sulcal area. **(c)** Ventral view showing the equatorially-positioned nucleus (N), eyespot (ES), sulcus (SU), longitudinal flagellum (LF) and pyrenoid (arrowhead). **(d)** Ventral view of the cell, showing longitudinal flagellum (LF), nucleus (N), pyrenoids (arrowheads) and C-shaped eyespot (ES). **(e)** and **(f)** Fluorescent micrographs of the same cell, showing (e) the nucleus (N) located in the episome near the cingulum; and **(f)** the peripherally-arranged chloroplast (C) and pyrenoids (arrowheads) embedded within the chloroplast. Scale bars: 5 µm.

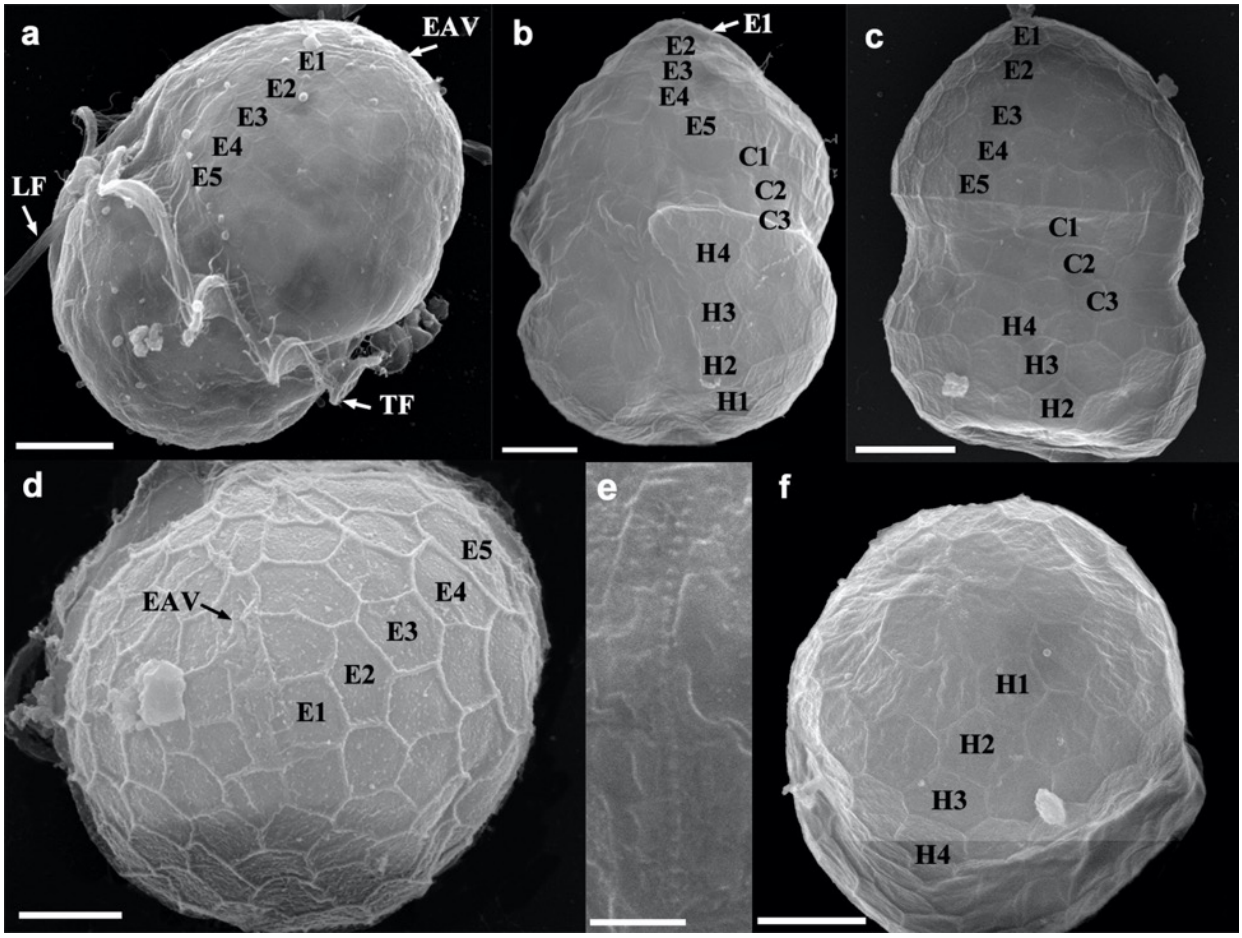

Figure 2. Scanning electron micrographs of *Ansanella natalensis* comb. nov., CW-19. **(a)** Left lateral view showing both longitudinal (LF) and transverse flagella (TF) and five rows (E1–E5) of amphiesmal vesicles (AVs) in the conical episome. **(b)** Ventral view of the cell, showing the detailed arrangement of the amphiesmal AVs. **(c)** Dorsal view of the cell, showing the wide cingulum and three rows (C1–C3) of AVs in the cingulum. **(d)** Apical view showing the position of the elongated apical vesicle (EAV) and the conical episome. **(e)** Elongated apical vesicle (EAV), showing the linearly arranged knobs. **(f)** Antapex of the cell, showing the four rows (H1–H4) of AVs in the hyposome. Scale bars: e, 1 μm; a–d, & f, 3 μm.

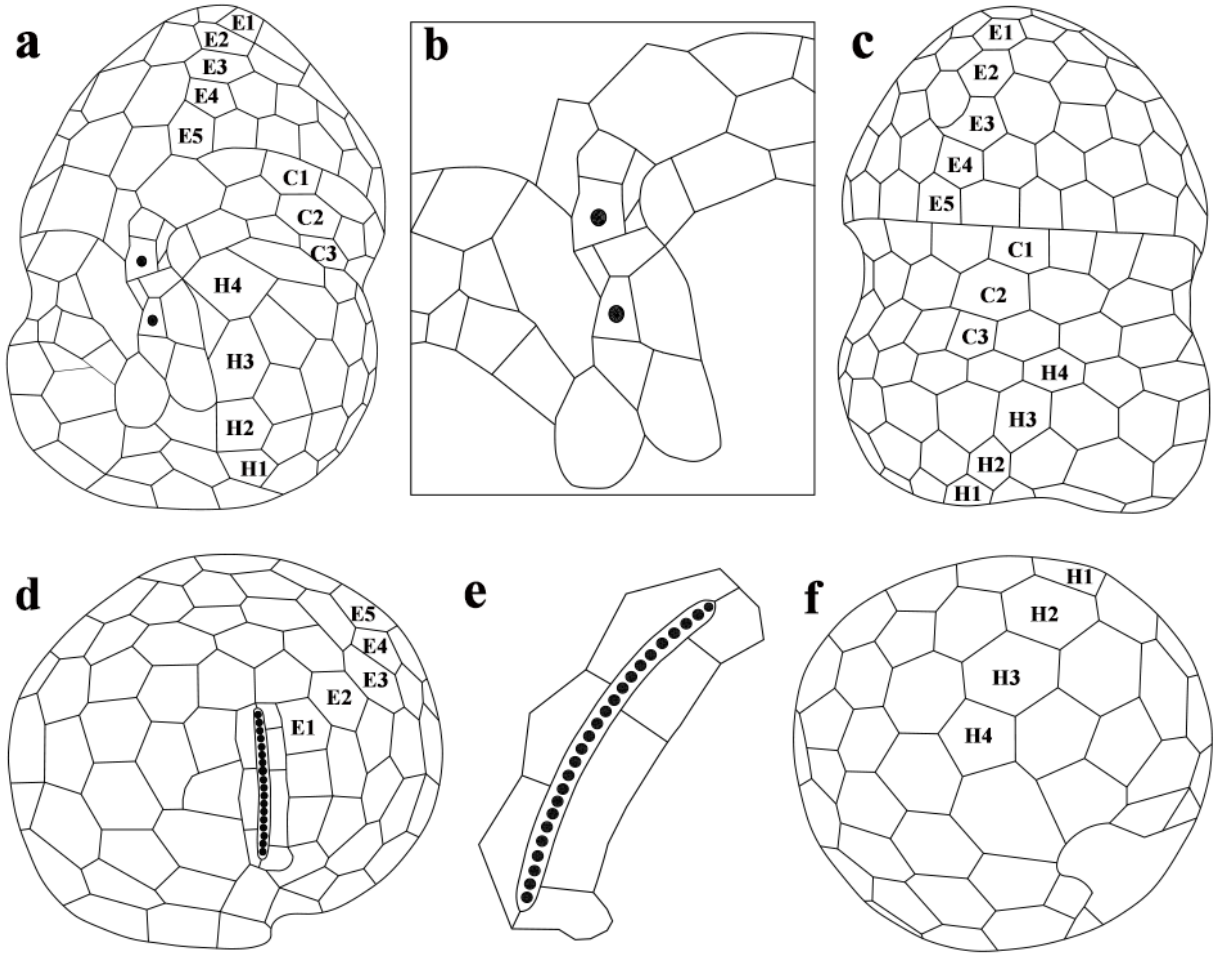

Figure 3. Schematic illustrations of the arrangement of amphiesmal vesicles of *Ansanella natalensis* comb. nov. (not to scale). **(a)** Ventral view. **(b)** Drawing of the sulcus, black circles indicate flagellar pores **(c)** Dorsal view. **(d)** Apical view. **(e)** The EAV, showing the surrounding plate arrangement and knobs. **(f)** Antapical view.

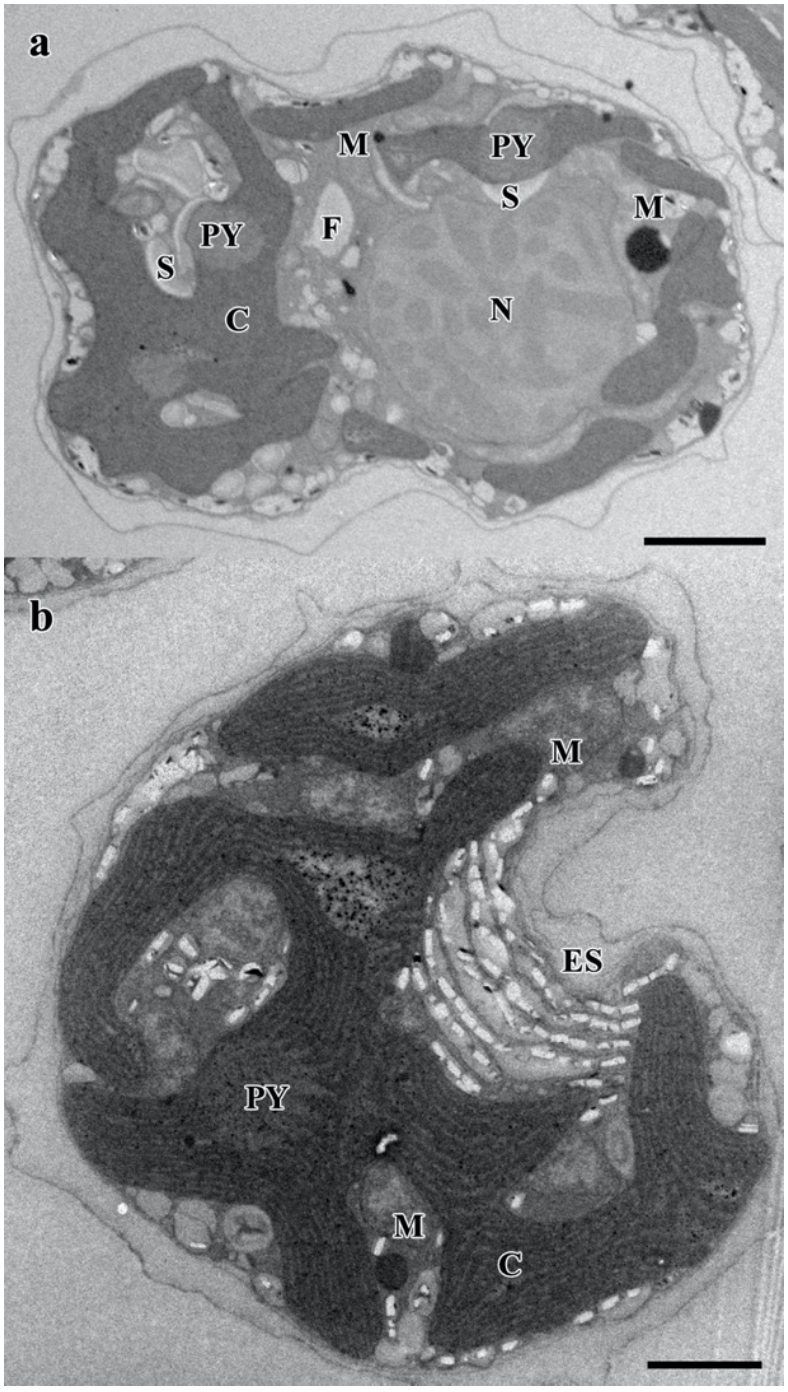

Figure 4. Transmission electron micrographs of a cell of *Ansanella natalensis* comb. nov. CW-19. **(a)** Longitudinal section and **(b)** transverse section, showing the chloroplast lobes (C), nucleus (N), pyrenoid (PY), starch grains (S) eyespot (ES) and mitochondria (M). Scale bars: 2 μm.

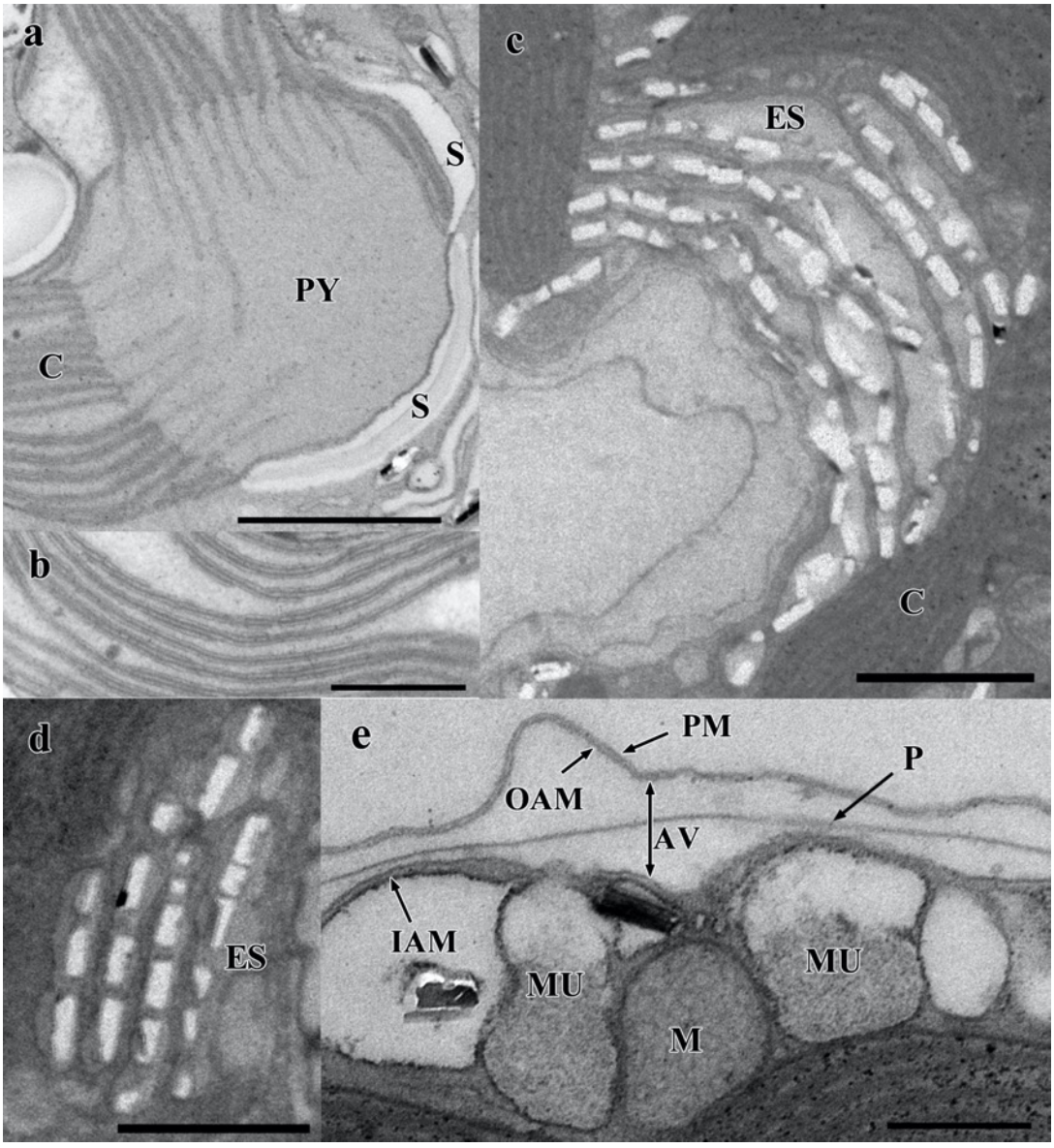

Figure 5. Transmission electron micrographs of *Ansanella natalensis* comb. nov. CW-19. **(a)** Detail of the pyrenoid (PY). The pyrenoid is embedded in the chloroplast matrix and partially surrounded by hemispherical starch grains (S). The pyrenoid matrix is invaded by many terminating sinuous thylakoid bands. **(b)** Detail of a typical section of the chloroplast, showing the arrangement of thylakoids. **(c)** Detail of the conspicuous, c-shaped eyespot (ES), which comprises approximately 7 cisternae containing brick-like material. **(d)** Detail of the eyespot (ES) showing the single membrane enclosing each row of crystalline structures. **(e)** Bottle-shaped mucocysts (MU) and detail of the amphiesma. The amphiesma consists of the plasma membrane (PM), an outer amphiesmal membrane (OAM), the pellicle (P) and the inner amphiesmal membrane (IAM). Scale bars: (a), (c), (d) & (e), 1 µm; (b) 0.5 µm.

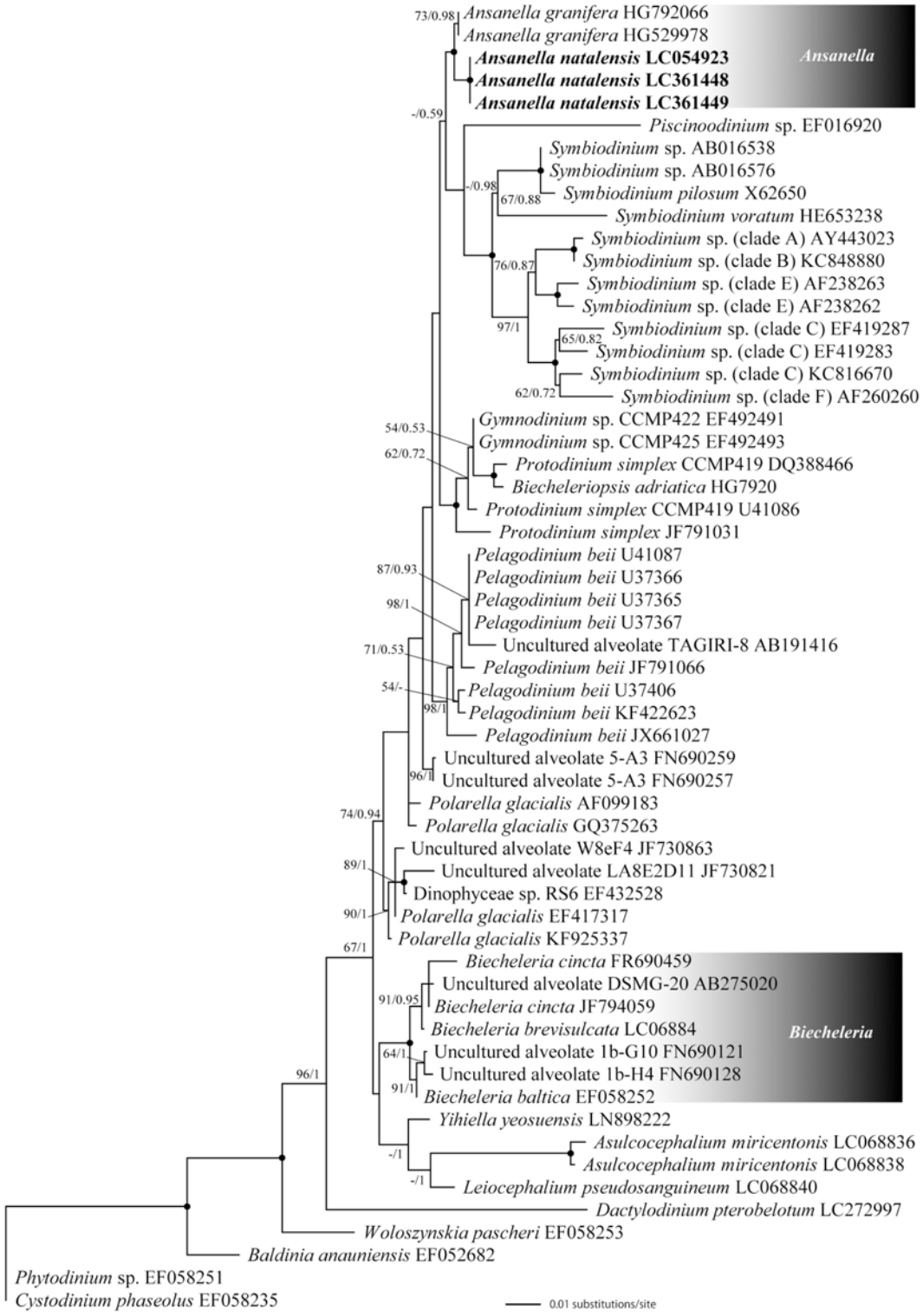

Figure 6. Topology of maximum likelihood (ML) phylogenetic tree inferred from the small-subunit (SSU) ribosomal (r) DNA sequence alignment. ML Bootstrap support (100 pseudoreplicates) ≥50 % and Bayesian posterior probabilities ≥0.8 are also indicated. Nodes marked with filled black circles indicate maximum ML and Bayesian support.

Species	Accession number	LSU rDNA Domain 2 (D2) partial sequences (460-640bp)
		460 470 480 490 500 510 520…630 640
Ag	HG529980	CTCCTGTGATGCCCGGCTGCTTCAGCGCAAGCGTTGTAGTTGGAGTTGAGCGGCTGCGTGT…CTTGCTGA
Ag	HG792066	CTCCTGTGATGCCCGGCTGCTTCAGCGCAAGCGTTGTAGTTGGAGTTGAGCGGCTGCGTGT…CTTGCTGA
An	LC373202	CTCCTGTGATGCCCGGCTGCTTCAGCGCAAGCGTTGTAGTTGGAGTTGAGCGGCTGTGTGT…CTTGCTGA
An	LC373203	CTCCTGTGATGCCCGGCTGCTTCAGCGCAAGCGTTGTAGTTGGAGTTGAGCGGCTGTGTGT…CTTGCTGA
Bp	AF260402	CTCCTGT----------GTGT…TGTG–TGA
Bba	AY628430	CTCCTGT----------GTGT…TGTG–TGA
Bbr	AB858353	CTCCTGT----------GTGT…TGTG–TGA
Bc	KC895465	CTCCTGT----------GTGT…TGTG–TGA
Wsp	FJ024706	CTCCTGT----------GTGT…TGTG–TGA
Gsp	AF318248	CTCCTGT----------GTGT…TGTG–TGA

Figure 7. A comparison of partial sequences of the large subunit (LSU) rDNA Domain 2 (D2) of the species of *Ansanella* and *Biecheleria*. Periods (.) represent nucleotides that are omitted, and dashes (–) denote an alignment gap. The nucleotides are numbered according to the LSU rDNA secondary structure of *Alexandrium tamarense* (Ki & Han, 2007). Ag, *Ansanella granifera*; An, *Ansanella natalensis*; Bp, *Biecheleria pseudopalustris*; Bba, *Biecheleria baltica*; Bbr, *Biecheleria brevisulcata*; Bc, *Biecheleria cincta*; Wsp, *Woloszynskia* sp.; Gsp, *Gymnodinium* sp.

Table 1. Morphological comparison of *Ansanella*, *Biecheleria* and *Biecheleriopsis*.

	A. natalensis[3,13]	*A. granifera*[11]	*B. pseudopalustris*[2,5a]	*B. halophila*[1,5a]	*B. cincta*[6,7,8]	*B. brevisulcata*[10]	*B. baltica*[4,5a]	*Bps. adriatica*[5b,10,12]
Cell size (μm)	L: 9.7-14.2 W: 8.3-12.2	L: 10.0-15.0 W: 8.5-12.4	27.0-30.0	L: 10.0-27.0 W: 13.0-22.0	L: 9.0-15.0 W: 9.0-12.5	L: 10.5-18.0 W: 9.0-16.5	L: 17.0-35.0 W: 12.0-32.0	L: 12.5-23.0 W: 7.5-15.5
Chloroplast(s)	Single yellowish brown	5-8 yellowish brown	Many golden	Many[a]	Many yellow-brown	Many yellow-brown	Many golden-brown	Many yellowish brown & golden
Grana-like thylakoid	Absent	Present	Absent	NA	Absent[a]	Absent[a]	Absent[a]	Absent
Eyespot type	E	E	E	E	E	E	E	E
Total AVs	>50	>50	>50[b]	>50	>50	>50	>50	>50
Latitudinal vesicle series	11-13	10-14	>20[b]	17	10-12	9-10	10-12	11-13
Apical furrow	EVA	EVA	EVA	EVA	EVA	EVA	EVA	EVA
Episome series	5-6	4-6	>10[b]	8	4-5	3-4	5-6	4-5
Cingulum series	3	3-4	3-4	2	3	3	2	3
Lower margin of the cingulum	Zigzag	Zigzag	Zigzag[a]	Zigzag[a]	Zigzag[a]	Zigzag[a]	Zigzag	Straight
Hyposome series	3-4	3-4	>5[b]	7	3-4	3	3-4	4-5
Nuclear fibrous connective	Absent	Absent	Absent	NA	NA	Absent	Absent	Present
Peduncle	Absent	Absent	Present	NA	Present	NA	Present	NA
Resting cyst (-like) cell	No	NA	Yes	Yes	Yes	Yes	Yes	Yes
Habitat	Tidal pool	Estuarine & marine water	Fresh water	Marine	Marine	Marine	Cold brackish	Marine

[a]Not mentioned, but seen from the figures; [b]Not mentioned but measured from the figures; NA, not available;
[1]Biecheler (1952), [2]von Stosch (1973), [3]Horiguchi and Pienaar (1994a, 1994b), [4]Kremp *et al*. (2005), [5]Moestrup *et al*. (2009a, 2009b), [6]Siano *et al*. (2009), [7]Kang *et al*. (2011), [8]Balzano *et al.* (2012), [9]Luo *et al*. (2013), [10]Takahashi *et al*. (2014), [11]Jeong *et al*. (2014), [12]Jang *et al*. (2015), [13]Present study

CHAPTER VI

Expanding species boundary of the newly erected family Peridiniopsidaceae (Peridiniales, Dinophyceae), *Peridiniopsis hexapraecingula* comb. nov. a tidal pool dinoflagellate from subtropical Japan

INTRODUCTION

A new family, Peridiniopsidaceae Gottschling, Kretschmann & Zerdoner, was erected by Gottschling *et al*. (2017) consisting of three genera, *Peridiniopsis*, *Parvodinium* and *Palatinus*, and all members are described to be primarily of freshwater dinophytes. The designated type genus of this family, *Peridiniopsis*, was proposed by Lemmermann (1904) based on the basic description of the theca of the species *P. borgei* Lemmermann. Later on, *P. borgei* was transferred into the genus *Peridinium* by Lemmermann along with a newly described species *P. cunningtonii* (1910), and treated as *Peridinium borgei* for almost six decades until it was re-transferred to its original genus, *Peridiniopsis*, by Bourrelly (1968a). Although *P. borgei* was re-examined by Lindemenn (1923) and Bourrelly (1968b), yet the full description of its external morphology was finalized in the report of the Toriumi & Dodge (1993) on the external structures surrounding the apical pore of *P. borgei* (Entz 1926, 1930, Dodge 1985; Ling et al. 1989). The internal morphology along with the flagellar apparatus were examined by Calado & Moestrup (2002). The plate formula of the *P. borgei* is: Po, x, 3′, 1a, 6″, 6c, 5s, 5‴, 2⁗. Except for one crucial difference in their morphology, the number of intercalary plates (0~1 in *Peridiniopsis*, 2~3 in *Peridinium*), it is, sometimes, not easy to discriminate the species of *Peridiniopsis* and *Peridinium* from each other without the support of the molecular data.

A number of dinoflagellates, *Bysmatrum gregarium* (Lombard & Capon) Horiguchi & Hoppenrath (as *Peridinium gregarium* Lombard & Capon), (Lombard and Capon 1971), *Bysmatrum arenicola* Horiguchi & Pienaar (Horiguchi and Pienaar 1988b), *Scrippsiella hexapraecingula* Horiguchi & Chihara (Horiguchi and Chihara 1983), *Gymnodinium*

pyrenoidosum Horiguchi & Chihara (Horiguchi and Chihara 1988), *Ansanella natalensis* Dawut et al. (Dawut et al. 2018b) (as *Gymnodinium natalense* Horiguchi & Pienaar) (Horiguchi & Pienaar 1994), *Alexandrium hiranoi* Kita & Fukuyo (Kita and Fukuyo 1988) and *Bysmatrum austrafrum* Dawut *et al*. (Dawut *et al*. 2018a) have been reported from tidal pools where they form visible blooms during the low tide and are known to have the characteristic of vertical migratory behavior in accordance with the tidal movement (Horiguchi & Chihara 1988). *S. hexapraecingula* was reported from a tidal pool with its detailed external morphology, and a plate formula, Po, x, 4′, 3a, 6″, 6c, 5s, 5‴, 2⁗, was provided (Horiguchi & Chihara 1983). Because of its similarity in the plate tabulation, based on the traditional convention, *S. hexapraecingula* was classified into the genus *Scrippsiella* (tabulation: Po, x, 4′, 3a, 7″, 6c, 5s, 5‴, 2⁗), as a new member, regardless of the difference in the number of the precingular plate.

In their report, Horiguchi & Chihara (1983) also argued the mistreatment of a strain (UTEX 1948) in its nomenclature. This particular strain, UTEX 1948, also known as the type culture of *Peridinium gregarium,* was isolated from a tidal pool by Loeblich III in 1969 and kept the Culture Collection of Algae at the University of Texas (Start 1978). The re-examination of UTEX 1948 showed that the external morphology of this strain resembled *S. hexapraecingula* the most rather than *P. gregarium* (Horiguchi & Chihara 1983). Later, in order to eliminate the confusion in the nomenclature of these two taxa, *P. gregarium* and UTEX 1948, a second ex-examination of UTEX 1948 and the type materials (permanently fixed slides) of *P. gregarium* was conducted (Horiguchi & Pienaar 1988). The result not only further supported the argument from the first re-examination on the UTEX 1948, but *P. gregarium* was transferred into the genus *Scrippsiella* with a new taxon name *S. caponii* based on the new data collected. And subsequently Faust and Steidinger (1998) transferred the species to their new genus, *Bysmatrum*,

making the combination *B. caponii*. However, the name *S. caponii* was superflous and thus illegitimate and *B. caponii* was also illegitimate. Finally, Horiguchi and Hoppenrath proposed the correct combination, *Bysmatrum gregarium* (Lombard et Capon) Horiguchi et Hoppenrath in Hoppenrath *et al*. (2014).

The application of various molecular sequence data in taxonomic studies significantly improved the accuracy of species classification work. A combination of the molecular and morphological analysis has greatly elucidated the phylogenetic relationships of dinophytes. For example, *P. gregarium* was, once again, moved to a new genus *Bysmatrum*, as *B. gregarium* based on its molecular data and morphological observations (Hoppenrath *et al*. 2014). However, the true identity of other two species, *S. hexapraecingula* and UTEX 1948, which are resembled the *B. gregarium* the most, remained unclear due to the fact that there was no molecular data to confirm their phylogenetic relationships. Although UTEX 1948 has its SSU rDNA sequence data (No. EF492509) in the NCBI database under the name of *Peridinium sociale*, this species was identified as same species as *Scrippsiella hexapraecingula* by Horiguchi and Chihara (1983).

During our sampling trip, we have found a species that morphologically resembles *S. hexapraecingula* from a tidal pool at Heisaura, Chiba prefecture, Japan. Our results showed that the new isolate from this tidal pool was exactly the same as *S. hexapraecingula* based on its morphology with some minor variations, but the molecular data revealed its close relations with the genus *Peridiniopsis* rather than to *Scrippsiella*. Here, we describe this species on the basis of light microscopy, scanning and transmission electron microscopy and infer its phylogenetic placement on the basis of the concatenated (SSU, ITS and LSU rDNA) phylogenetic analysis.

MATERIAL AND METHODS

Sampling and culture establishment

Water samples were collected from a tidal pool at Heisaura (平砂浦), Chiba Prefecture (千葉県), Japan (34˚18.815′S, 18 ˚27.737′E) on 31 August 2015 using a large pipette and were transported to the Laboratory of Phycology in the Faculty of Science, Hokkaido University in small screw cap glass bottles. In the laboratory, water samples were transferred into plastic dishes containing autoclaved seawater supplemented with Daigo`s IMK medium (Nihon Pharmaceutical Co., Tokyo, Japan) for enrichment and were cultured at 25°C at an irradiance of 50 μmol photons $m^{-2}s^{-1}$ with a 16:8 light:dark regime. Swimming cells were isolated using drawn capillary Pasteur pipettes and subsequently a clonal culture (designated as HEI 6-1) was established. This culture strain has been maintained in IMK medium under the same conditions mentioned above.

Light Microscopy

Light microscopic observations of motile cells were made using a Carl Zeiss Axioskop 2 microscope equipped with Nomarski interference optics (Carl Zeiss Japan, Tokyo). An image analysis system was used to measure the length and width of motile cells from micrographs taken using a Leica MC-120HD digital camera (Leica Microsystems, Wetzlar, Germany). The shape and number of chloroplasts were characterised using autofluorescence (Carl Zeiss Axioskop 2 with a filter set No. 15).

Scanning electron microscopy

For scanning electron microscopy, cells were fixed in 5% glutaraldehyde (final concentration) for 40 min. The fixed cells were rinsed first with IMK medium, then with IMK medium diluted 1:1 with distilled water, and finally with distilled water. The samples were dehydrated in an ethanol series (30, 50, 70, 90, 95%) followed by two rinses in 100% ethanol for 30 min and dried in a critical point drier (Hitachi HPC-2, Tokyo, Japan). The dried cells were sputter-coated with gold for 180 s at 12 mA (Hitachi E-1045) and observed with a scanning electron microscope (S-3000N, Hitachi).

Transmission electron microscopy

Cells were concentrated by gentle centrifugation (800 r.p.m for 5 min), fixed with cold 2.5% (v/v) glutaraldehyde for 30 min on ice, rinsed with filtered sea water (FSW), and post-fixed with 1% (v/v) osmium tetroxide for 1h on ice. After one rinse in FSW and one in distilled water, the sample was dehydrated in an ethanol series of 25, 50, 70, 95, 100%, with two subsequent washes in 100% ethanol and three in 100% acetone. Finally, cells were embedded in low viscosity (LV) resin (Agar Scientific, Essex, England). After polymerization at 65°C for 16h, thin sections were cut using a diamond knife on an ultramicrotome (Leica EM UC6, Germany). Sections were picked up on formvar-coated one-slot grids and viewed with a transmission electron microscope (H-7650, Hitachi).

DNA extraction, polymerase chain reaction (PCR) amplification

Approximately 15-20 motile cells were used to extract DNA by applying the Quick Extract™ FFPE DNA extraction kit (Epicentre, Tokyo, Japan) according to the manufacturer's protocol.

The small subunit ribosomal RNA gene (SSU rDNA), the internal transcribed spacer (ITS, including ITS1, 5.8s, ITS2) and the large subunit ribosomal RNA gene (LSU rDNA) were amplified. The amplification of all three genes was conducted in a 25 μL reaction mix with slightly different amplification programme on a PCR machine (Simpli Amp thermal cycler, Applied Biosystems, Foster City). SSU rDNA: initialization (1 cycle, 5 min at 94℃; denaturation (35 cycles, 30 s at 94℃), annealing (30 s at 50℃); extension (90 s at 72℃); and final extension (at 72℃ for 7 min). The PCR reaction of ITS rDNA was done using parameters described by Yamashita and Koike (2013). For LSU rDNA: initialization (1 cycle, 6 min at 94℃; denaturation (35 cycles, 30 s at 94℃), annealing (30 s at 52℃); extension (90 s at 72℃); and final extension (at 72℃ for 6 min). The PCR products were purified and sequenced with ABI PRISM Big Dye Terminator (Perkin-Elmer, Waltham, Massachusetts, USA). The final step of sequencing was achieved using a DNA auto-sequencer ABI PRISM310 Genetic Analyzer (Perkin-Elmer).

Phylogenetic analysis

The DNA sequences determined in the present study were aligned with the sequences of the broadly sampled species of Peridiniopsidaceae, *Scrippsiella* and Peridiniaceae from GenBank/ European Molecular Biology Laboratory (EMBL)/ DNA Data Bank of Japan (DDBJ), of which sequence information in all three regions were available (except for UTEX 1948 for which only SSU rDNA sequence was available), using MAFFT v7.130b (Katoh & Standley 2013). Gblocks (Castresana 2000) was used to edit and eliminate gap positions in the aligned sequences. The aligned sequences were analysed by the maximum likelihood (ML) method using PAUP* version 4.0b10 (Swofford 2001) and the Bayesian method using MrBayes 3.2.1 (Huelsenbeck &

Ronquist 2001; Ronquist & Huelsenbeck 2003). The programme jModel Test version 2.1.4 (Guindon & Gascuel 2003; Darriba *et al*. 2012) was used to calculate the evolutionary model that was the best fit for the ML analysis of the data set.

For the phylogenetic of the concatenated data set, GTR+I+G model was selected. The heuristic search for the ML analysis was performed with the following options: a tree bisection reconnection branch-swapping algorithm and the Kimura 2-parameter neighbour-joining tree as a starting tree. The parameters used for the analysis were as follows: assumed nucleotide frequencies (user-specified) A=0.242423 C=0.198084 G=0.292317 and T=0.267176; substitution rate matrix with A<->C=0.749019, A<- >G=3.06082, A<->T=0.750661, C<->G=0.361753, C<->T=6.1928, G<->T=1; proportion of sites assumed to be invariable=0.376655; rates for variable sites assumed to follow a gamma distribution with shape parameter=1.00348; and the number of rate categories=4. For the Bayesian analysis, GTR+I+G was selected as the best evolutionary model by MrModeltest 2.3 (Nylander et al. 2004). Markov-chain Monte Carlo iterations were carried out until 500,000 generations were attained, when the average standard deviations of split frequencies fell below 0.01, indicating the convergence of the iterations.

RESULTS

Light microscopy

Motile cells of *Peridiniopsis hexapraecingula* comb. nov. were photosynthetic, somewhat egg-shaped from the ventral view, 24–45 µm long and 20–40 µm wide (n = 20) (Figures 1a–c). The epitheca was conical with slightly pointy apex, while the hypotheca was dome-shaped and sometimes pointed (Figure 1a–c). The nucleus was located in the hypocone (Figure 1b, c). A

single, yellowish-brown chloroplast with numerous, irregular to rod-shaped radiating lobes were from the center of the cell; the distal end of each chloroplast lobe was densely distributed along the cell (Figure 1d). A relatively large pyrenoid and several vacuoles can also be seen by the light microscopy (Figure 1a–c). The orange-coloured eyespot was small, rectangular and located near the sulcus (Figure 1b). *P. hexapraecingula* formed a dense bloom within the tidal pool. Motile cells in the bloom were entangled in a gelatinous matrix and formed a cloud-like mass (not shown). In culture, during the dark period, all the motile cells settled and attached to the substratum, becoming non-motile. An apical stalk (AS) consisting of a transparent gelatinous matrix (Figure 1a–c) formed from the apex of motile cells and was used when the cells attached to the substratum. Cell division took place in the non-motile phase and was stimulated by light. Motile cells were released from the non-motile parent cells, leaving numerous empty thecae on the bottom of the culture dish (not shown).

Scanning electron microscopy

The thecal plates of the *Peridiniopsis hexapraecingula* comb. nov. were smooth and perforated by many, different size of pores (Figure 2). The thecal plate arrangement was: Po, x, 4′, 3a, 6″, 6c, 5s, 5‴, 2‴′ (Fig. 2). The schematic illustration of the thecal plates arrangement is shown in Fig .3. Both epitheca (from apical view) and hypotheca (from antapical view) were almost symmetric (Figures 2d, f, 3b, c). The apical pore complex (APC), consisting of the apical pore plate (Po) and the canal plate (x), was elongated and somewhat rounded at the Po end. Due to the thick collar-like margin surrounding the entire apical pore plate, it was impossible to observe the actual size and shape of the Po; the canal plate (x) was four-sided and made contact with Po, 1′, 2′ and 4′ (Figures 2a, d, e, 3a, b). The size of the epitheca was almost the same as that of the

hypotheca in dorsal views (Figure 2c). In the apical view, the epitheca was almost circular, with a slight depression on the ventral side (Figures 2d & 3b).

The first apical plate (1′) was asymmetric, hexagonal, slightly expanded towards the right and made contact with the canal plate (x), plates 2′, 4′, 1″, 6″ and the anterior sulcal plate (Sa). The other three apical plates (2′, 3′, 4′) were also all hexagonal (Figures 2a–e, 3a, b). All three intercalary plates (1a-3a) were pentagonal, connected and one side of each was made contact with 3′ (Figures 2b–d, 3b). Except for 5″ and 6″ were being hexagonal, all four other precingular plates were pentagonal in shape (Figures 2a–d, 3a, b).

The cingulum was well excavated, descended by its own height and consisted of six plates. The entire margins on both sides of the cingulum were lined by narrow cingular lists. A fine line of multiple pores was situated under the lower cingular margin and encircled the entire cell (Figures 2a–d, 3a). The dorso-ventrally slightly depressed sulcus was consisted of five plates; the anterior sulcal plate (Sa) was asymmetric, relatively narrow and slightly elongated into the epitheca; while the posterior sulcal plate (Sp) was gradually widened towards the hypotheca and invaded all the way almost till the end of the antapex. A small platelet and a crack (maybe the location where the flagella were) were always present (Figures 2a & 3a, arrowheads). The first postcingular plate (1‴) was the smallest of the five postcingular plates, and all four postcingular plates (1‴, 2‴, 4‴, 5‴) were quadrangular, except the 3‴, which was pentagonal (Figures 2a–c, f, 3a, c). Those two antapical plates (1⁗, 2⁗) were pentagonal in shape and almost equal in size (Figures 2b, c, f, 3c).

Transmission electron microscopy

The cells of *P. hexapraecingula* comb. nov. showed typical dinoflagellate organization, with a peripherally situated chloroplast network. Thylakoid-free areas were also observed in some chloroplast lobes (Figures 4 & 5, asterisks). A typical dinokaryotic nucleus with chromosomes was present in the hyposome occupying a large portion of it (Figures 4 & 5a). The pyrenoid was single, distinct, stalked and located in the lower part of the episome. It was surrounded by a thick starch sheath and connected to the chloroplast lobs; no thylakoids penetrated the pyrenoid matrix (Figures 4 & 5a, d). Mitochondrial profiles (M) and trichocytes (arrow) were scattered throughout the cell (Figures 4a, 5a, b). A vacuole with fine fibers, which are assumed to be flagellar hairs (F), was commonly observed (Fig. 5a (arrowhead), b). A pusule (Pu) that connected with the sac pusule (Sp), and a vacuole (V) were also present (Figure 5a). A large eyespot (E) consisting of a double layer of globules located between the chloroplast envelope and the outermost thylakoids was located near the cell surface on the ventral side, mostly underneath the sulcus (Figure 5c).

Phylogenetic analysis

Figure 5 elucidates the phylogeny deduced from ML and Bayesian analyses (BA) based on concatenated rDNA sequences, including other 51 Peridiniales sequences and two outgroup taxa (i.e., *Heterocapsa* sp. and *Heterocapsa pygmaea*). The result showed that *P. hexapraecingula* (97/1) along with UTEX 1984 formed a robust sister clade with the type species *P. borgei* indicating their close relationships with the genus *Peridiniopsis* rather than *Scrippsiella*.

DISCUSSION

The species *Scrippsiella hexapraecingula* was described from tidal pools in temperate Japan (Horiguchi & Chihara 1983). Based on the thecal plate arrangement, especially the fact that the number of cingular plates (6 plates) agreed with that of *Scrippsiella*, Horiguchi and Chihara (1983) placed this species in the genus *Scrippsiella*, although the number of precingular plates was 6 instead of 7 as most *Scrippsiella* species have. No molecular data were available for this species until today. In this study, molecular phylogenetic data were obtained for the first time allowing to infer its taxonomic position.

Identity of the strain HEI 6-1

The strain HEI 6-1, used in this study possessed the thecal plate arrangement, Po, x, 4′, 3a, 6″, 6c, 5s, 5‴, 2⁗. This arrangement is exactly the same as that of *S. hexapraecingula* as described in the original description by Horiguchi and Chihara (1983). Other features, including cell size, cell contour and the arrangement of organelles such as the position of the nucleus and the conspicuous pyrenoid, also agree with those of *S. hexapraecingula*. The only one discrepancy is that the peduncle was not able to detected in my culture, although Horiguchi and Chihara (1983) described the presence of a peduncle in their strain. Despite this minor difference, based on the overall morphological similarities and the similar habitat and habits (tidal pool bloom forming species), I have concluded that my strain is indeed *S. hexapraecingula*.

Phylogenetic position and taxonomic placement

My molecular phylogenetic analysis indicated that *S. hexapraecingula* is very closely related to the freshwater dinoflagellate, *Peridiniopsis borgei.* This species is the type species of the genus *Peridiniopsis*. The strain UTEX1948, originally named as *Peridinium sociale*, appears in the sister position of *P. borgei*/*S. hexapraecingula* clade. According to Horiguchi and Chihara (1983), *P. sociale* was regarded to identical with *S. hexapraecingula*, but the result is quite interesting. *P. sociale* is also a tidal pool species (marine) and morphologically similar to *S. hexapraecingula* as described by Horiguchi and Chihara (1983), but phylogenetically, *S. hexapraecingula* is more closely related to the freshwater dinoflagellate *P. borgei* rather than to a similar tidal pool species from California. This result suggests that *P. sociale* is an undescribed new tidal pool dinoflagellate.

Although *P. borgei* and *S. hexapraecingula* are phylogenetically very close to each other. However, their morphologies are quite different from each other. The thecal plate arrangement of *P. borgei* is Po, 3', 1a, 6", 6c, 5s, 5"', 2"" and the arrangement and number of thecal plates in the epitheca is completely different from that of *S. hexapraecingula* (Calado & Moestrup 2002). The former has only 3 apical plates and 1 anterior intercalary plate, the latter possesses 4 apical plates and 3 apical intercalary plates. The ultrastructure of the eyespot is also different. In *P. borgei*, there are multiple rows of osmiophilic globules within the chloroplast, while in *S. hexapraecingula*, only two rows of globules were observed. On the other hand, the type of pyrenoid and structure of apical pore complex are more or less similar to each other (Calado & Moestrup 2002).

My molecular tree indicated that *S. hexapraecingula* has little affinities with members of the genus *Scrippsiella*. And thus, accommodating this species in *Scrippsiella* is not appropriate.

Then, to which genus should this species belong? There are two options, i.e. to accommodate the species in the genus *Peridiniopsis* or to establish a new genus for this species. Because thecal plate arrangement in epitheca is quite different from each other, one might hesitate to place *S. hexapraecingula* in the genus *Peridiniopsis* and thus establish a new genus might be the answer. However, on the other hand, genetically two species are very closely related –almost genetically identical. There are examples that variations of thecal plate arrangement exist within the same genus. In this case, I believe it is appropriate to accommodate *S. hexapraecingula* in the genus *Peridiniopsis* based on genetic affinities.

***Peridiniopsis hexapraecingula* (Horiguchi et Chihara) comb. nov.**

Basionym: *Scrippsiella hexapraecingula* Horiguchi et Chihara, 1983, Bot. Mag., Tokyo 96: p. 357. fig. 1.

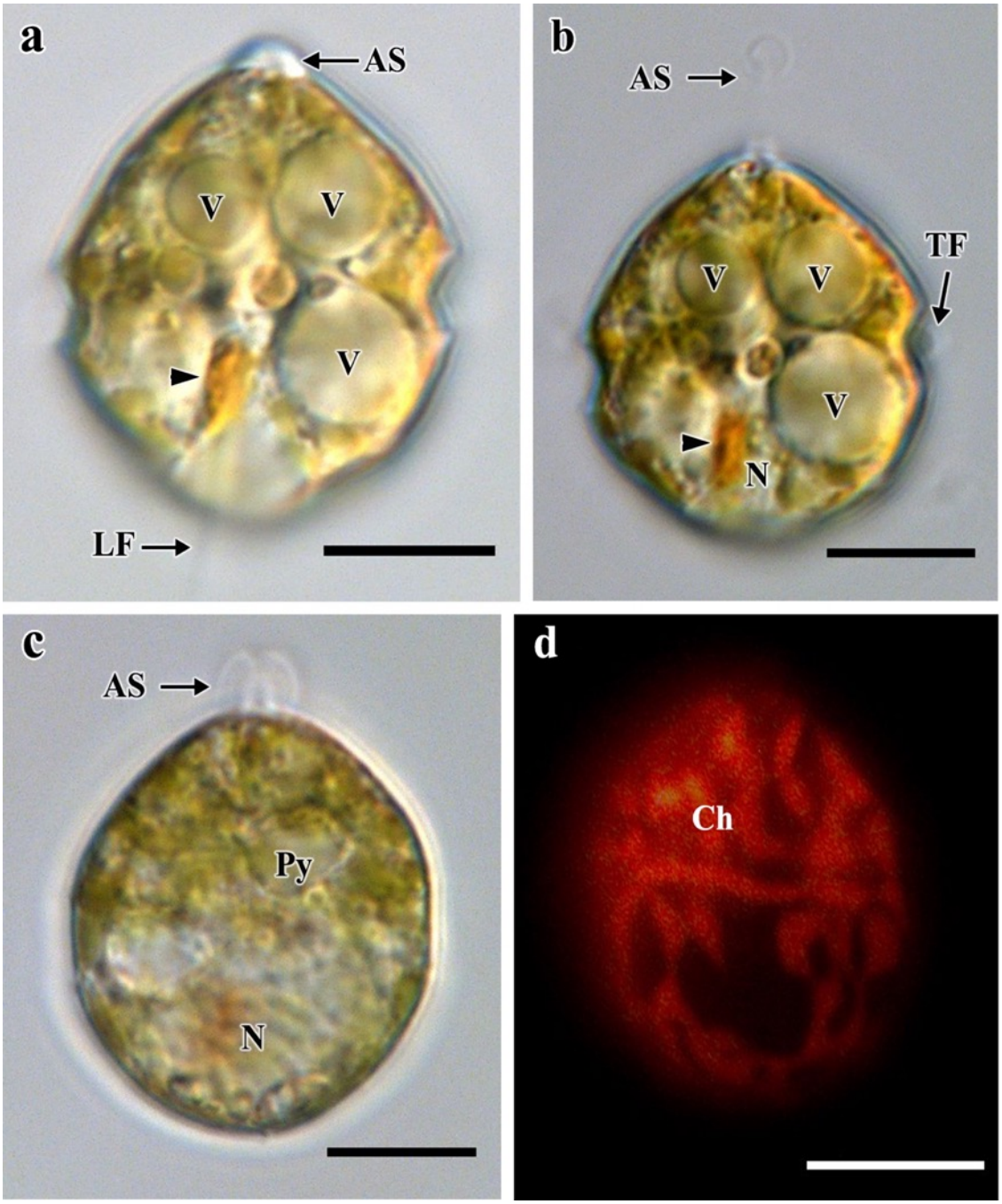

Figure 1. Light micrographs of *Peridiniopsis hexapraecingula* (Horiguchi et Chihara) comb. nov. **(a)** Motile cell showing cell outline. AS: apical stalk, LF: longitudinal flagellum, V: vesicles. Arrowhead indicates eyespot. **(b)** Motile cell, showing transverse flagellum (TF) and apical stalk (AS). N: nucleus, V: vesicle. **(c)** Partly collapsed cell, showing apical stalk (AS), pyrenoid (Py) and dinokaryotic nucleus (N) in the hypotheca. **(d)** Fluorescent microscopic photograph, showing arrangement of chloroplast lobes (Ch). Scale bars = 10 µm.

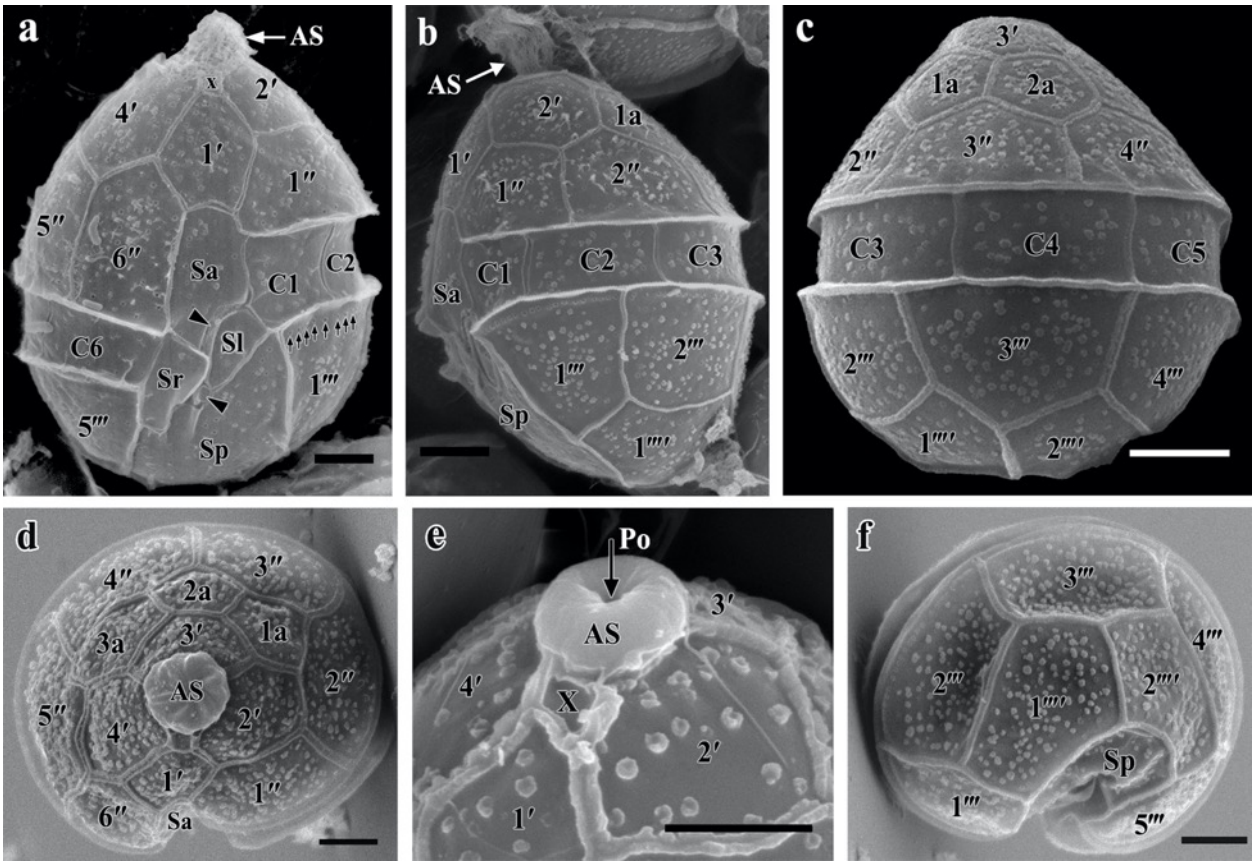

Figure 2. Scanning electron micrographs of *Peridiniopsis hexapraecingula* (Horiguchi et Chihara) comb. nov. **(a)** Ventral view, **(b)** Left lateral view, **(c)** Dorsal view, **(d)** Apical view, showing the arrangement of epithecal plates, **(e)** Close-up of apical pore complex. AS: apical stalk, Po: Pore plate, **(f)** Antapical view, showing thecal arrangement of hypotheca. Scale bar = 3 μm.

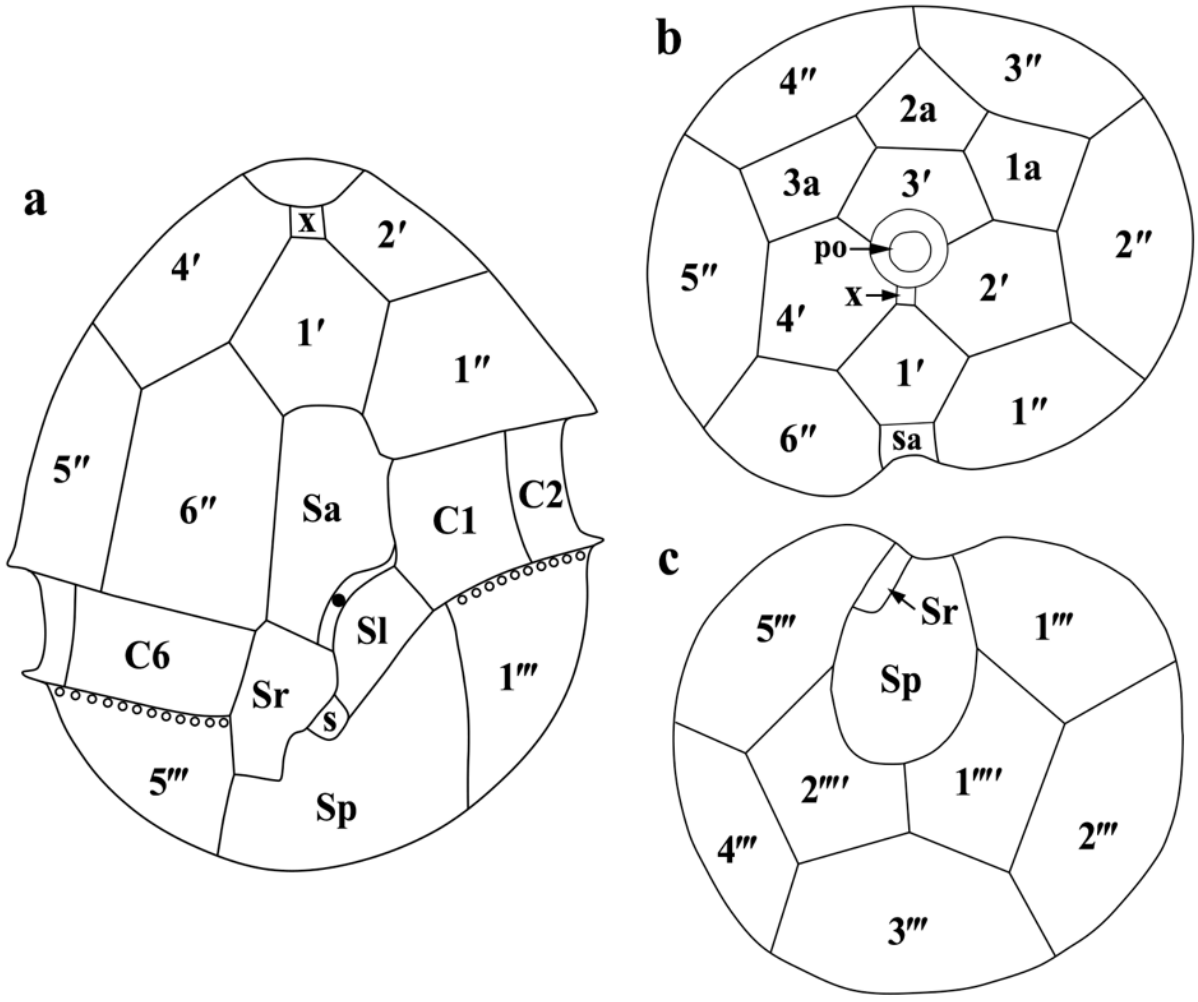

Figure 3. Schematic drawings of thecal plate arrangement of *Peridiniopsis hexapraecingula* (Horiguchi et Chihara) comb. nov. (not to scale)

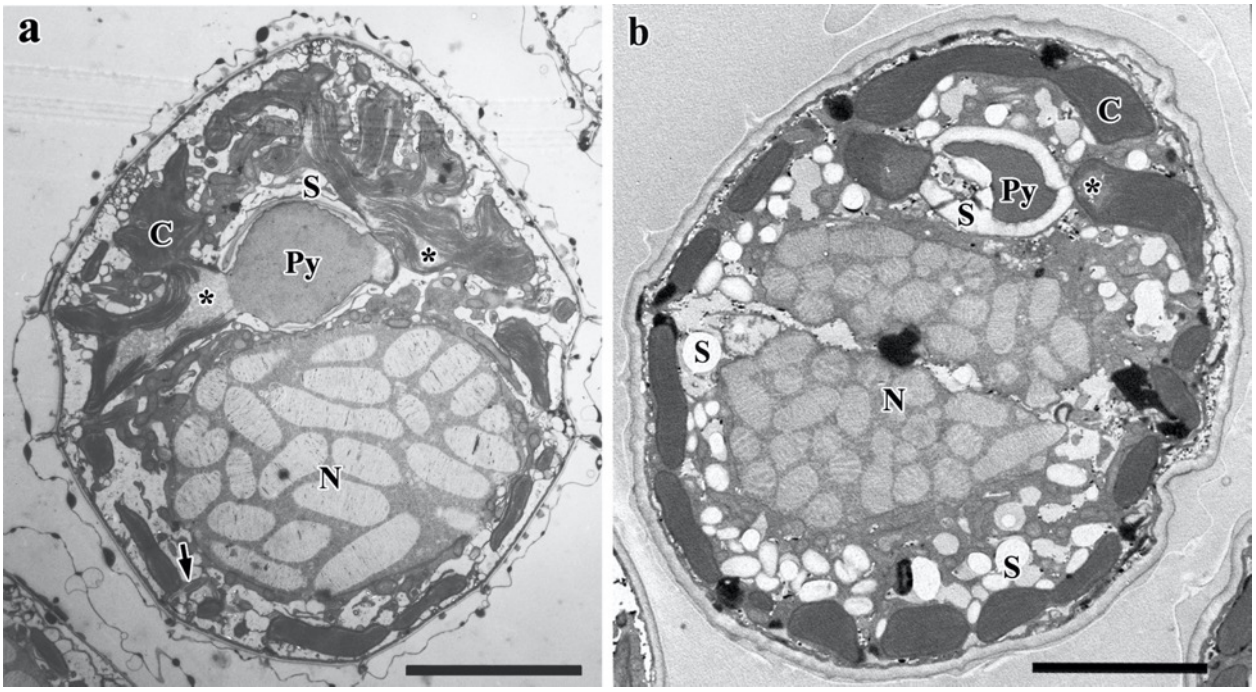

Figure 4. Transmission electron micrographs of *Peridiniopsis hexapraecingula* (Horiguchi et Chihara) comb. nov. **(a)** Longitudinal section of motile cell, showing chloroplast (C), nucleus (N), pyrenoid (Py) with starch sheath (S). **(b)** Longitudinal cell of non-motile cell. Divided nuclei and many starch globules (S) can be seen. C, chloroplast; Py, pyrenoid. Scale bar = 3 µm

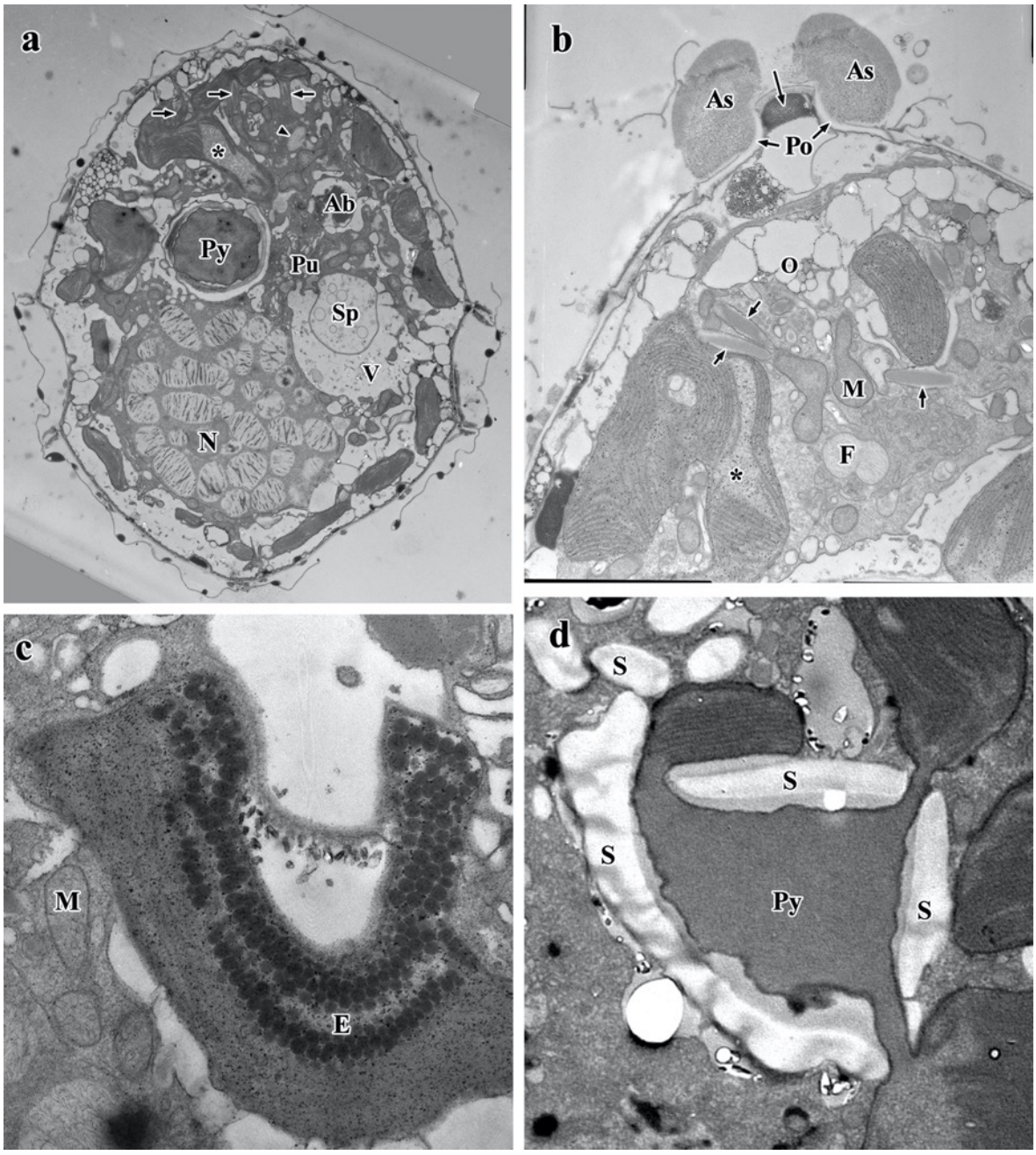

Figure 5. Transmission electron micrographs of *Peridiniopsis hexapraecingula* (Horiguchi et Chihara) comb. nov. **(a)** Longitudinal section of motile cell, showing trichocysts (arrow) and hair-containing vesicle (arrowhead). Pusule (Pu) and accumulation body (Ab) can be seen. **(b)** Close-up of part of motile cell, showing trichocysts (arrow) and mitochondria (M). **(c)** Close-up of eyespot (E) in chloroplast. Mitochondria with tubular cristae can be seen. **(d)** Detail of pyrenoid (Py) which is surrounded by starch sheaths (S). No penetration of thylakoids or cytoplasmic tunnels are observed in pyrenoid matrix.

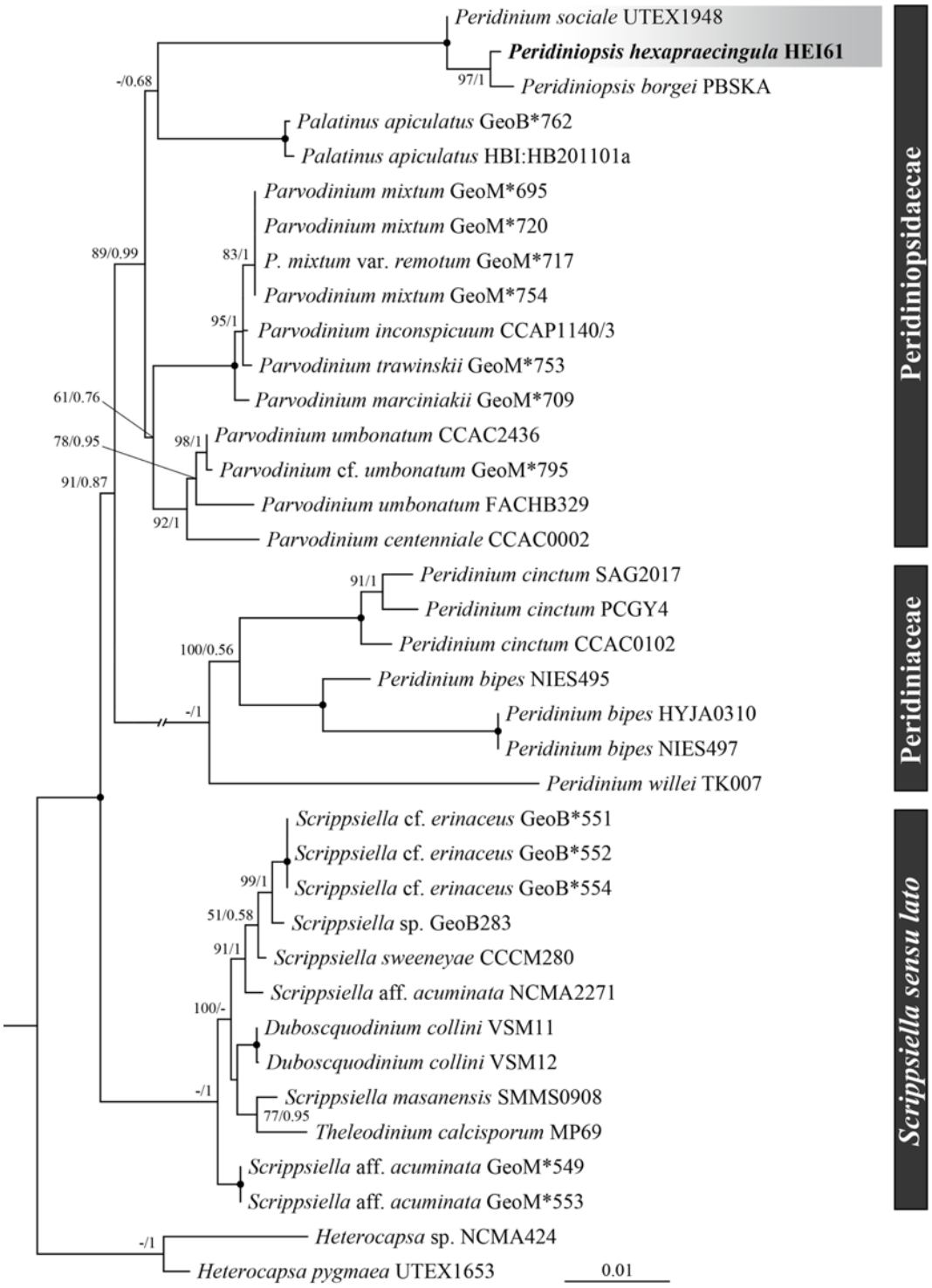

Figure 6. Bayesian tree inferred from concatenated (SSU-ITS-LSU) genes. Bootstrap value and Posterior Probabilities are indicated at each node. Note that *Peridiniopsis borgei*, *S. hexapraecingula* and *Peridinium sociale* (UTEX 1948) form robust clade with high support.

REFERENCES

Adams, L. M., Cumbo, V. R. & Takabayashi, M. 2009. Enhanced primary acquisition of *Symbiodinium* by asymbiotic coral larvae exposed to sediments when compared to the water column. Marine Ecology Progress Series **377:** 149–56.

Aligizaki, K., Nikolaidis, G., Katikou, P., Baxevanis, A. D. & Abatzopoulos, T. J. 2009. Potentially toxic epiphytic *Prorocentrum* (Dinophyceae) species in Greek coastal waters. *Harmful Algae* **8:** 299–311.

Anglès, S., Reñe, A., Garcés, E., Lugliè, A., Sechi, N., Camp J. & Satta, C. T. 2017. Morphological and molecular characterization of *Bysmatrum subsalsum* (Dinophyceae) from the western Medierranean Sea reveals the existence of cryptic species. *Journal of Phycology* **53:** 833-847.

Baker, A. C. 2003. Flexibility and specificity in coral-algal symbiosis: diversity, ecology, and biogeography of Symbiodinium. *Annual Review of Ecology, Evolution, and Systematics* **34:** 661–689.

Balech, E. 1959. Two new genera of dinoflagellates. *The Biological Bulletin* **116:** 195–203.

Balech, E. 1964. Tercera contribucion al conocimiento del genero *Peridinium*. *Museo Argentino de ciencias naturales ('Bernadino Rivadavia' e Instituto nacional de investigacion de las ciencias naturales, Revista, Hydrobiologia* **4:** 179–195.

Balech, E. 1974. EI genero *Protoperidinium* Bergh, 1881 (*Peridinium* Ehrenberg, 1831, partim). *Revista del Museo Argentino de Ciencias Naturales*. *Bernardino Rivadavia, Hidrobiologia* **4:** 1–79.

Balech, E. 1980. On thecal morphology of dinoflagellates with special emphasis on circular (sic) and sulcal plates. *Anales del Centro de Ciencias del Mar y Limnologfa. Universidad Nacional Autonomica de Mexico* **7:** 57–68.

Balzano, S., Gourvil, P., Siano, R., Chanoine, M., Marie, D., Lessard, S., Sarno, D. & Vaulot, D. 2012. Diversity of cultured photosynthetic flagellates in the northeast Pacific and Arctic Oceans in summer. *Biogeosciences* **9**: 4553–71.

Biecheler, B. 1952. Recherches sur les Péridiniens. *Bulletin biologique de la France et de la Belgique* **36** (suppl.): 1–149.

Blackburn, S. I., Hallegraeff, G. M. & Bolch, C. J. 1989. Vegetative reproduction and sexual life cycle of the toxic dinoflagellate *Gymnodinium catenatum* from Tasmania, Australia. *Journal of phycology* **25:** 577–590.

Blackwell, J. R. & Gilmour, D. J. 1991. Stress tolerance of the tidal pool chlorophyte, *Chlorococcum submarinum*. *British Phycological Journal* **26:** 141–147.

Bourrelly P. 1968a. Notes sur les Péridiniens d'eau douce. *Protistologica* **4:** 5–13.

Bourrelly P. 1 968b. Note sur *Peridiniopsis borgei* Lemm. *Phykos* **7:** 1–2.

Calado, A.J. and Moestrup, Ø., 2002. Ultrastructural study of the type species of *Peridiniopsis*, *Peridiniopsis borgei* (Dinophyceae), with special reference to the peduncle and flagellar apparatus. *Phycologia* **41:** 567–584.

Carlos, A.A., Baillie, B.K., Kawachi, M. & Maruyama, T. 1999. Phylogenetic position of *Symbiodinium* (Dinophyceae) isolates from tridacnids (Bivalvia), cardiids (Bivalvia), a sponge (Porifera), a soft coral (Anthozoa), and a free-living strain. *Journal of Phycology* **35:** 1054–1062.

Carty, S. 2008. *Parvodinium* gen. nov. for the Umbonatum Group of *Peridinium* (Dinophyceae). *Ohio Journal of Science* **108:** 103–107.

Castresana, J. 2000. Selection of Conserved Blocks from Multiple Alignments for Their Use in Phylogenetic Analysis. *Molecular Biology and Evolution* **4:** 540–552.

Chang, F.H. 1983. Winter phytoplankton and microzooplankton populations off the coast of Westland, New Zealand. *New Zealand Journal of Marine and Freshwater Research* **17:** 279–304

Coffroth M.A. & Santos S.R. 2005. Genetic diversity of symbiotic dinoflagellates in the genus *Symbiodinium*. *Protist* **156:** 19–34.

Craveiro, S. C., Moestrup Ø, Daugbjerg, N. & Calado, A. J. 2010. Ultrastructure and large subunit rDNA-based phylogeny of *Sphaerodinium cracoviense*, an unusual freshwater dinoflagellate with a novel type of eyespot. *Journal of Eukaryotic Microbiology* **57:** 568–585.

Craveiro, S. C., Daugbjerg, N., Moestrup, Ø. & Calado, A. J. 2015 Fine-structural characterization and phylogeny of *Peridinium polonicum*, type species of the recently described genus *Naiadinium* (Dinophyceae). *European Journal of Protistology* **51:** 259–279.

Darriba, D., Taboada, G. L., Doallo, R. & Posada, D. 2012. jModelTest 2: more models, new heuristics and parallel computing. *Nature Methods* **9:** 772–772.

Dawut, M., Sym, S. D., Suda, S. & Horiguchi, T. 2018a. *Bysmatrum austrafrum* sp. nov. (Dinophyceae), a novel tidal pool dinoflagellate from South Africa. *Phycologia* **57:** 169–178.

Dawut, M., Sym, S.D. & Horiguchi, T. 2018b. Re-investigation of *Gymnodinium natalense* (Dinophyceae), a tidal pool dinoflagellate from South Africa and the proposal of a new combination *Ansanella natalensis*. *Phycological Research* **66:** 300–309.

Dethier, M. N. 1980. Tidepools as refuges: predation and the limits of the harpacticoid copepod Tigriopus californicus (Baker). *Journal of Experimental Marine Biology and Ecology* **42:** 99–111.

Dodge, J. D. & Crawford, R. M. 1971. A fine-structural survey of dinoflagellate pyrenoids and food-reserves. *Botanical Journal of the Linnean Society* **64:** 105–115.

Dodgej, D. 1985. *Atlas of dinoflagellates*. Farrand Press, London. pp 119.

Dyhrman, S. T. 2008. Molecular approaches to diagnosing nutritional physiology in harmful algae: Implications for studying the effects of eutrophication. *Harmful Algae* **8:** 167–174.

Ehrenberg C. G. (1838) Die Infusionsthierchen als volkommene Organismen. Ein Blick in das Tiefere organische Leben der Natur. Leopold Voss, Leipzig, pp 547.

Entz G. 1926. Beiträge zur Kenntnis der Peridineen. 1. Zur Morphologie und Biologie von *Peridinium* Borgei. Archiv für Protistenkunde **56:** 397–446.

Entz G. 1930. Uber Gehemmte Lebens- und Absterbeerscheinungen einiger Dinoflagellaten. *Arbeiten des Ungarischen biologischen Forschungs-Institllles* **3:** 206–243.

Faust, M.A. 1996. Morphology and ecology of the marine dinoflagellate *Scrippsiella subsalsa* (Dinophyceae). *Journal of Phycology* **32:** 669-675.

Faust, M. A. & Steidinger, K. A. 1998. *Bysmastrum* gen. nov. (Dinophyceae) and three new combinations for benthic scrippsielloid species. *Phycologia* **37:** 47–52.

Fay, S. A., Weber, M. X. & Lipps, J. H. 2009. The distribution of *Symbiodinium* diversity within individual host foraminifera. *Coral Reefs* **28:** 717–726.

Fensome, R.A., Taylor, F.J.R., Norris, G., Sarjeant, W.A.S., Wharton, D.I. & Williams, G.L. 1993. A Classification of Living and Fossil Dinoflagellates. Micropaleontology Special Publication no. 7. New York: American Museum of Natural History, 245 pp.

Franklin, E.C., Stat, M., Pochon, X., Putnam, H.M. & Gates, R.D. 2012. GeoSymbio: a hybrid, cloud-based web application of global geospatial bioinformatics and ecoinformatics for *Symbiodinium*- host symbioses. Molecular Ecology Resources **12:** 369–373

Freudenthal, H. D. 1962. *Symbiodinium* gen. nov. and *Symbiodinium microadriaticum* sp. nov., a zooxanthella: taxonomy, life cycle, and morphology. *Journal of Protozoology* **9:** 45–52.

Gavelis, G. S., Keeling, P. J. & Leander, B. S. 2017. How exaptations facilitated photosensory evolution: Seeing the light by accident. *Bioessays* **397:** 1600266.

Gibson, R. N. (1986) Intertidal teleosts: life in a fluctuating environment. In: The behaviour of teleost fishes. pp. 388-408.

Gómez, F. 2005. A list of free-living dinoflagellate species in the world's oceans. *Acta Botanica Croatica* **64:** 129–212.

Gómez, F. 2012. A quantitative review of the lifestyle, habitat and trophic diversity of dinoflagellates (Dinoflagellata, Alveolata). *Systimetics and Biodiversity* **10:** 267–275.

Gornik, S. G., Ford, K. L., Mulhern, T. D., Bacic, A., McFadden, G. I. & Waller, R. F. 2012. Loss of nucleosomal DNA condensation coincides with appearance of a novel nuclear protein in dinoflagellates. *Current Biology* **22:** 2303–2312.

Gottschling, M., Soehner, S., Zinssmeister, C., John U., Plötner, J., Schweikert, M., Aligizaki, K. & Elbrächter, M. 2012. Delimitation of the Thoracosphaeraceae (Dinophyceae), including the calcareous dinoflagellates, based on large amounts of ribosomal RNA sequence data. *Protist* **163:** 15–24.

Gottschling, M., Kretschmann, J. & Alasan, A. Ž. Č. 2017. Description of Peridiniopsidaceae, fam. nov. (Peridiniales, Dinophyceae). *Phytotaxa* **299:** 293–296.

Gou, W., Sun, J., Li, X., Zhen, Y., Xin, Z., Yu, Z. & Li, R. 2003. Phylogenetic analysis of a free-living strain of *Symbiodinium* isolated from Jiaozhou Bay, PR China. *Journal of Experimental Marine Biology and Ecology* **296:** 135-144.

Granados-Cifuentes, C., Neigel, J., Leberg, P. & Rodriguez-Lanetty, M., 2015. Genetic diversity of free-living *Symbiodinium* in the Caribbean: the importance of habitats and seasons. *Coral Reefs* **34:** 927–939.

Guindon, S. & Gascuel, O. 2003. A simple, fast, and accurate algorithm to estimate large phylogenies by maximum-likelihood. *Systematic Biology* **52:** 696–704.

Guiry, M.D. 2012. How many species of algae are there? *Journal of phycology* **48:** 1057–1063.

Guschina, I. A. & Harwood, J. L. 2006. Lipids and lipid metabolism in eukaryotic algae. *Progress in Lipid Research* 45: 160–186.

Hagino, K., Bendif, E.M., Young, J.R., Kogame, K., Probert, I., Takano, Y., Horiguchi, T., de Vargas, C. & Okada, H. 2011. New evidence for morphological and genetic variation in the cosmopolitan coccolithophore *emiliania huxleyi* (prymnesiophyceae) from the COX1b-ATP4 genes 1. *Journal of phycology* 47: 1164–1176.

Hansen, G., Botes, L. & De Salas, M. 2007. Ultrastructure and large subunit rDNA sequences of *Lepidodinium viride* reveal a close relationship to *Lepidodinium chlorophorum* comb. nov. (= *Gymnodinium chlorophorum*). *Phycological Research* **55:** 25–41.

Hansen, G. & Daugbjerg, N. 2009. *Symbiodinium natans* sp. Nov.: a “free-living” dinoflagellate from tenerife (northeast-atlantic ocean) 1. *Journal of Phycology* **45:** 251–263.

Hansen, P.J. 2011. The role of photosynthesis and food uptake for the growth of marine mixotrophic dinoflagellates 1. *Journal of Eukaryotic Microbiology* **58:** 203–214.

Harrison, P.L., 2011. Sexual reproduction of scleractinian corals. In: Coral reefs: an ecosystem in transition pp. 59–85.

Hill, M. S. 1996. Symbiotic zooxanthellae enhance boring and growth rates of the tropical sponge *Anthosigmella varians* forma *varians*. *Marine Biology* **125:** 649–54.

Hill, M., Allenby, A., Ramsby, B., Schönberg, C. & Hill, A. 2011. *Symbiodinium* diversity among host clionaid sponges from Caribbean and Pacific reefs: evidence of heteroplasmy and putative host-specific symbiont lineages. *Molecular Phylogenetics and Evolution* **59:** 81–88.

Hirano, R. 1967. Mechanism of development of red tide in estuarine waters. *Information Bulletin on Planktology in Japan* **42:** 25–29.

Hirose, M., Reimer, J. D., Hidaka, M. & Suda, S. 2008. Phylogenetic analyses of potentially free-living *Symbiodinium* spp. isolated from coral reef sand in Okinawa, Japan. Marine Biology **155:** 105–112.

Hoppenrath, M., Murray, S. A., Chomerat, N. & Horiguchi, T (2014) VII. Toxins of benthic dinoflagellates and benthic harmful algal bloom. In: Marine benthic dinoflagellates - unveiling their worldwide biodiversity. pp. 218–227

Hoppenrath, M. 2016. Dinoflagellate taxonomy – a review and proposal of a revised classification. *Marine Biodiversity* **47:** 381–403.

Horiguchi, T. & Chihara, M. 1983. *Scrippsiella hexapraecingula* sp. nov. (Dinophyceae), a tida pool dinoflagellate from the Northwest Pacific. *The Botanical Magazine* **96:** 351–358.

Horiguchi, T. & Chihara, M. 1988. Life cycle, behavior and morphology of a new tide pool dinoflagellate, *Gymnodinium pyrenoidosum* sp. nov. (Gymnodiniales, Pyrrophyta*). The Botanical Magazine* **101:** 255–265.

Horiguchi, T. & Pienaar, R.N. 1988a. A re-description of the tidal pool dinoflagellate *Peridinium gregarium* based on a re-examination of the type material. *British Phycological Journal* **23:** 33–39.

Horiguchi, T. & Pienaar, R.N. 1988b. Ultrastructure of a new sand-dwelling dinoflagellate, *Scrippsiella arenicola* sp. nov. *Journal of Phycology* **24:** 426–438.

Horiguchi, T. & Pienaar, R. 1994a. *Gymnodinium natalense* sp. nov. (Dinophyceae), a new tide pool dinoflagellate from South Africa. *Japanese Journal of Phycology* **42:** 21-28.

Horiguchi, T. & Pienaar, R. N. 1994b. Ultrastructure and ontogeny of a new type of eyespot in dinoflagellates. *Protoplasma* **179**: 142–50.

Horiguchi, T. & Pienaar, R. 2000. Validation of *Bysmatrum arenicola* Horiguchi *et* Pienaar, sp. nov. (Dinophyceae). *Journal of Phycology* **36:** 237–237.

Horiguchi, T. (2015) Chapter 16. Diversity and phylogeny of marine parasitic dinoflagellates. In Ohtsuka S, Suzaki T, Horiguchi T, Suzuki T & Not, F (2015) Marine Protists - Diversity and Dynamics, pp. 397–419.

Huang, H., Zhou, G., Yang, J., Liu, S., You, F. & Lei, X. 2013. Diversity of free-living and symbiotic *Symbiodinium* in the coral reefs of Sanya, South China Sea. *Marine Biology Research* **9:** 117–128.

Huelsenbeck, J. P. & Ronquist, F. 2001. Bayesian inference of phylogenetic trees. *Bioinformatics* **17:** 754–755.

Hume, B.C., D'Angelo, C., Smith, E.G., Stevens, J.R., Burt, J. & Wiedenmann, J. 2015. *Symbiodinium thermophilum* sp. nov., a thermotolerant symbiotic alga prevalent in corals of the world's hottest sea, the Persian/Arabian Gulf. *Scientific reports* **5:** 8562.

Ishida, K. & Green, B. R. 2002. Second- and third-hand chloroplasts in dinoflagellates: phylogeny of oxygen-evolving enhancer 1 (PsbO) protein reveals replacement of a nuclear-encoded plastid gene by that of a haptophyte tertiary endosymbiont. *Proceedings of the National Academy of Sciences* **99:** 9294-9299.

Iwataki, M., Kawami, H., Mizushima, K., Mikuishi, C. M., Doucette, G. J., Relox, J. R. Jr., Anton, A., Fukuyo, Y. & Matsuoka, K. 2008. Phylogenetic relationships in the harmful dinoflagellate *Cochnlodinium polykrikoides* (Gymnodiniales, Dinophyceae) inferred from LSU rDNA sequences. *Harmful Algae* **7:** 271-277.

Jang, S. H., Jeong, H. J., Moestrup, Ø., Kang, N. S., Lee, S. Y., Lee, K. H., Lee, M. J. & Noh, J. H. 2015. Morphological, molecular and ecophysiological characterization of the phototrophic dinoflagellate *Biecheleriopsis adriatica* from Korean coastal waters. *European Journal of Phycology* **50**: 301–17.

Janouškovec, J., Gavelis, G. S., Burki, F., Dinh, D., Bachvaroff, T. R., Gornik, S. G., Bright, K. J., Imanian, B., Strom, S. L., Delwiche, C. F. & Waller, R. F., 2017. Major transitions in dinoflagellate evolution unveiled by phylotranscriptomics. *Proceedings of the National Academy of Sciences* **114:** 171-180.

Janson, S. 2004. Molecular evidence that plastids in the toxin-producing dinoflagellate genus *Dinophysis* originate from the free-living cryptophyte *Teleaulax amphioxeia*. *Environmental microbiology* **6:** 1102–1106.

Jensen, S. L. & Muller-Parker, G. 1994. Inorganic nutrient fluxes in anemone-dominated tide pools. *Pacific Science* **48:** 32–43.

Jeong, H. J., Yoo, Y. D., Kim, J. S., Seong, K. A., Kang, N. S. & Kim, T. H. 2010. Growth, feeding and ecological roles of the mixotrophic and heterotrophic dinoflagellates in marine planktonic food webs. *Ocean Science Journal* **45:** 65–91.

Jeong, H. J., Jang, S. H., Kang, N. S., Du, Y. Y., Kim, M. J., Lee, K. H., Yoon, E. Y., Potvin, É., Hwang, Y. J., Kim, J. I. & Seong, K. A. 2012. Molecular characterization and morphology of the photosynthetic dinoflagellate *Bysmatrum caponii* from two solar saltons in western Korea. *Ocean Science Journal* **47:** 1–18.

Jeong, H. J., Yoo, Y. D., Lee, K. H., Kim, T. H., Seong, K. A., Kang, N. S., Lee, S. Y., Kim, J. S., Kim, S. & Yih, W. H. 2013. Red tides in Masan Bay, Korea in 2004-2005: I. Daily variations in the abundance of red-tide organisms and environmental factors. *Harmful Algae* **30:** 75-88.

Jeong, H.J., Jang, S.H., Moestrup, Ø., Kang, N.S., Lee, S.Y., Potvin, E. & Noh, J.H. 2014. *Ansanella granifera* gen. et sp. nov. (Dinophyceae), a new dinoflagellate from the coastal waters of Korea. *Algae* **29**: 75–99.

Jeong, H.J., Lee, S.Y., Kang, N.S., Yoo, Y.D., Lim, A.S., Lee, M.J., Kim, H.S., Yih, W., Yamashita, H. and LaJeunesse, T.C. 2014. Genetics and morphology characterize the dinoflagellate *Symbiodinium voratum*, n. sp., (Dinophyceae) as the sole representative of *Symbiodinium* clade E. *Journal of Eukaryotic Microbiology* **61:** 75–94.

Jeong, H.J., Lim, A.S., Yoo, Y.D., Lee, M.J., Lee, K.H., Jang, T.Y. & Lee, K. 2014. Feeding by the heterotrophic dinoflagellate and ciliates on the free-living dinoflagellate *Symbiodinium* sp. (Clade E). *Journal of Eukaryotic Microbiology* **61:** 27–41.

John, U., Fensome, R.A. & Medlin, L.K., 2003. The application of a molecular clock based on molecular sequences and the fossil record to explain biogeographic distributions within the *Alexandrium tamarense* "species complex" (Dinophyceae). *Molecular biology and evolution* 20: 1015–1027.

Jonsson, P. R. 1994. Tidal rhythm of cyst formation in the rock pool ciliate *Strombidium oculatum* Gruber (Ciliophora, Oligotrichida): a description of the functional biology and an analysis of the tidal synchronization of encystment. *Journal of experimental marine biology and ecology* **175:** 77–103.

Kang, N.S., Jeong, H.J., Yoo, Y.D., Yoon, E.Y., Lee, K.H., Lee, K. & Kim, G. 2011. Mixotrophy in the newly described phototrophic dinoflagellate *Woloszynskia cincta* from western Korean waters: feeding mechanism, prey species, and effect of prey concentration. *Journal of Eukaryotic Microbiology* **58**: 152–70.

Katoh, K. & Standley, D.M. 2013. MAFFT Multiple Sequence Alignment Software Version 7: Improvements in Performance and Usability. *Molecular Biology and Evolution* **30:** 772–780.

Ki, J.S. & Han, M.S. 2007. Informative characteristics of 12 divergent domains in complete large subunit rDNA sequences from the harmful dinoflagellate genus, *Alexandrium* (Dinophyceae). *Journal of Eukaryotic Microbiology* **54**: 210–9.

Kirst, G. O., Thiel, C., Wolff, H., Nothnagel, J., Wanzek, M. & Ulmke, R. 1991. Dimethylsulfoniopropionate (DMSP) in icealgae and its possible biological role. *Marine Chemistry* **35:** 381–388.

Kita, T. & Fukuyo, Y. 1988. Description of the gonyaulacoid dinoflagellate *Alexandrium hiranoi* sp. nov. inhabiting tide pools on Japanese Pacific coast. *Bulletin of Plankton Society of Japan* **35:** 1–7.

Knowlton, N. 1993. Sibling species in the sea. *Annual Reviews of Ecology and Systematics* **24:** 189–216.

Kofoid, C. A. & Swezy, O. 1917. On the orientation of *Erythropsis*. *Zool* **18:** 89–101.

Koike, K., Yamashita, H., Oh-Uchi, A., Tamaki, M. & Hayashibara, T. 2007. A quantitative real-time PCR method for monitoring *Symbiodinium* in the water column. *Galaxea* **9:** 1–12.

Kremp, A., Elbrächter, M., Schweikert, M., Wolny, J.L. & Gottschling, M. 2005. *Woloszynskia halophila* (Biecheler) comb. nov.: a bloom-forming cold-water dinoflagellate co-occurring with *Scrippsiella hangoei* (Dinophyceae) in the Baltic Sea. *Journal of Phycology* **41**: 629–42.

Kumar, S., Stecher, G. & Tamura, K. 2016. MEGA7: Molecular evolutionary genetics analysis version 7.0 for bigger datasets. *Molecular Biology and Evolution* **33**: 1870–4.

LaJeunesse, T. C. 2002. Diversity and community structure of symbiotic dinoflagellates from Caribbean coral reefs. *Marine Biology* **141:** 387–400.

Lajeunesse T.C. 2005. Species radiations of symbiotic dinoflagellates in the Atlantic and Indo-Pacific since the Miocene–Pliocene transition. *Molecular Biology and Evolution* **22:** 570–581.

LaJeunesse, T.C., Parkinson, J.E. and Reimer, J.D. 2012. A genetics-based description of *Symbiodinium minutum* sp. nov. and *S. psygmophilum* sp. nov. (Dinophyceae), two dinoflagellates symbiotic with cnidaria. *Journal of Phycology* **48:** 1380–1391.

LaJeunesse, T.C., Wham, D.C., Pettay, D.T., Parkinson, J.E., Keshavmurthy, S. and Chen, C.A. 2014. Ecologically differentiated stress-tolerant endosymbionts in the dinoflagellate genus *Symbiodinium* (Dinophyceae) Clade D are different species. *Phycologia* **53:** 305–319.

LaJeunesse, T.C., Lee, S.Y., Gil-Agudelo, D.L., Knowlton, N. & Jeong, H.J. 2015. *Symbiodinium necroappetens* sp. nov. (Dinophyceae): an opportunist 'zooxanthella' found in bleached and diseased tissues of Caribbean reef corals. *European journal of phycology* 50: 223–238.

LaJeunesse, T.C. 2017. Validation and description of *Symbiodinium microadriaticum*, the type species of *Symbiodinium* (Dinophyta). *Journal of Phycology* **53:** 1109–1114.

LaJeunesse, T. C., Parkinson, J. E., Gabrielson, P. W., Jeong, H. J., Reimer, J. D., Voolstra, C. R. & Santos, S. R. 2018. Systematic Revision of Symbiodiniaceae Highlights the Antiquity and Diversity of Coral Endosymbionts. *Current Biology* **28:** 2570–2580.

Lee, M. J., Jeong, H. J., Jang, S. H., Lee, S. Y., Kang, N. S., Lee, K. H., Kim, H. S., Wham, D. C., LaJeunesse, T. C. 2016. Most Low-Abundance "Background" *Symbiodinium* spp. Are Transitory and Have Minimal Functional Significance for Symbiotic Corals. *Microbial Ecology* **71:** 771–783.

Lee, S. K., Jeong, H. J., Jang, S. H., Lee, K. H., Kang, N. S., Lee, M. J. & Potvin, É. 2014. Mixotrophy in the newly described dinoflagellate *Ansanella granifera*: Feeding mechanism, prey species, and effect of prey concentration. *Algae* **29:** 137–152.

Lee, S.Y., Jeong, H. J., Kang, N. S., Jang, T. Y., Jang, S. H. & Lajeunesse, T.C. 2015. *Symbiodinium tridacnidorum* sp. nov., a dinoflagellate common to Indo-Pacific giant clams, and a revised morphological description of *Symbiodinium microadriaticum* Freudenthal, emended Trench & Blank. *European Journal of Phycology* **50:** 155–172.

Lemmermann E. 1904. Das Plankton schwedischer Gewässer. *Arkiv för Botanik* **2:** 1–209.

Lemmermann, E. 1910. *Kryptogamenflora der Mark Brandenburg*. *Bd. 3. Algen 1 (Schizophyceen, Flagellaten, Peridineen)*. Gebrüder Borntraeger, Leipzig. 712 pp.

Lewis, C. L. & Coffroth, M. A. 2004. The acquisition of exogenous algal symbionts by an octocoral after bleaching. *Science* **304:** 1490–1492.

Lin, S. 2011. Genomic understanding of dinoflagellates. *Research in Microbiology* **162:** 551–569.

Lin, S., Zhang, Y., Zhang, H., Ji, Z., Cai, M. & Zhuang, Y. 2015. The *Symbiodinium kawagutii* genome illuminates dinoflagellate gene expression and coral symbiosis. *Science* **350:** 691–694.

Limoges, A., Mertens, K. N., Ruíz-fernández, A. C. & Vernal, D. E. A. 2015. First report of fossilized cysts produced by the benthic *Bysmatrum subsalsum* (Dinophyceae) from a shallow Mexican lagoon in the Gulf of Mexico. *Journal of Phycology* **51:** 211–215.

Lindemann E. 1 923. Eine EntwickJungshemmung bei *Peridinium* borgei und ihre Folgen. *Archiv für Protistenkunde* **46:** 378–382.

Ling, H.U., Croome, R.L. & Tyler, P.A. 1989. Freshwater dinoflagellates of Tasmania, a survey of taxonomy and distribution. *British Phycological Journal* **24:** 111–129.

Littman, R. A., van Oppen, M. J. H. & Willis, B. L. 2008. Methods for sampling free-living *Symbiodinium* (zooxanthellae) and their distribution and abundance at Lizard Island (Great Barrier Reef). *Journal of Experimental Marine Biology and Ecology* **364:** 48–53.

Loeblich, A.R. III. 1968. A new marine dinoflagellate genus, *Cachonina*, in axenic culture from the Salton Sea, California with remarks on the genus *Peridinium*. *Proceedings of the Biological Society of Washington* **81:** 91–96.

Loeblich Jr, A. R. 1970. Morphology, ultrastructure and distribution of Paleozoic acritarchs. In: Proceedings of the North American Paleontological Convention, Chicago. part G, Vol. 2, pp. 705–788.

Loeblich, A.R. & Sherley, J.L. 1979. Observations on the theca of the mobile phase of free-living and symbiotic isolates of *Zooxanthella microadriaticum* (Freudenthal) comb. nov. *Journal of the Marine Biological Association of the United Kingdom* **59:** 195–205.

Lombard, E. H. & Capon, B. 1971. Observation on the tide pool ecology and behavior of *Peridinium gregarium*. *Journal of Phycology* **7:** 188–194.

Luo, Z., Yang, W., Xu, B. & Gu, H. 2013. First record of *Biecheleria cincta* (Dinophyceae) from Chinese coasts, with morphological and molecular characterization of the strains. *Chinese Journal of Oceanology and Limnology* **31**: 835–45.

Luo, Z., Lim, Z.F., Mertens, K.N., Gurdebeke, P., Bogus, K., Carbonell-Moore, M.C., Vrielinck, H., Leaw, C.P., Lim, P.T., Chomérat, N. & Li, X. 2018. Morpho-molecular diversity and phylogeny of *Bysmatrum* (Dinophyceae) from the South China Sea and France. *European Journal of Phycology* **53:** 318-335.

Manning, M. & Gates, R. D. 2008. Diversity in populations of free-living *Symbiodinium* from a Caribbean and Pacific reef. *Limnology and Oceanography* **53:** 1853–61.

Medlin, L.K., Metfies, K., John, U. & Olsen, J. L. 2007. Algal molecular systematics: a review of the past and prospects for the future. In Brodie, J. & Lewis, J. [Eds.] Unravelling the Algae: The Past, Present, and Future of Algal Systematics. Taylor and Francis, Boca Raton, Florida, pp. 341–53.

Metaxas, A. & Scheibling, R. E. 1993. Community structure and organization of tidepools. *Marine Ecology Progress Series* **98:** 187–198.

Moestrup, Ø. & Daugbjerg, N. (2007) On dinoflagellate phylogeny and classification. In: Brodie, J. & Lewis, J. (Eds) Unravelling the algae, the past, present, and future of algal systematics. pp. 215–230.

Moestrup Ø., Lindberg, K. & Daugbjerg, N. 2009a. Studies on Woloszynskioid dinoflagellates IV: The genus *Biecheleria* gen. nov. *Phycological Research* **57:** 203–220.

Moestrup, Ø., Lindberg, K. and Daugbjerg, N. 2009b. Studies on woloszynskioid dinoflagellates. V. Ultrastructure of *Biecheleriopsis* gen. nov., with description of *Biecheleriopsis adriatica* sp. nov. *Phycological Research* **57**: 221–37.

Mohammad-noor, N., Daugbjerg, N., Moestrup Ø. & Anton, A. 2007. Marine epibenthic dinoflagellates from Malaysia – a study of five cultures and preserved samples based on light and scanning electron microscopy. *Nordic Journal of Botany* **24:** 629-690.

Morton, S. L., Faust, M. A., Fairey, E. A. & Moeller, P. D. R. 2002. Morphology and toxicology of *Prorocentrum arabianum* sp. nov., (Dinophyceae) a toxic planktonic dinoflagellate from the Gulf of Oman, Arabian Sea. *Harmful Algae* **1:** 393–400.

Murray, S., Hoppenrath, M., Larsen, J. & Patterson, D. J. 2006. *Bysmatrum teres* sp. nov., a new sand-dwelling dinoflagellate from north-western Australia. *Phycologia* **45:**161–167.

Murray, S. A., Suggett, D. J., Doblin, M. A., Kohli, G. S., Seymour, J. R., Fabris, M. & Ralph, P. J. 2016. Unravelling the functional genetics of dinoflagellates: a review of approaches and opportunities. *Perspectives in Phycology* **3:** 37–52.

Nagahama, Y., Murray, S., Tomaru, A. & Fukuyo, Y. 2011. Species boundaries in the toxic dinoflagellate *prorocentrum lima* (Dinophyceae, Prorocentrales), based on morphological and phylogenetic characters. *Journal of Phycology* **47:** 178–189.

Nitschke, M. R., Davy, S. K. & Ward, S. 2016. Horizontal transmission of *Symbiodinium* cells between adult and juvenile corals is aided by benthic sediment. *Coral Reefs* **35:** 335–344.

Nosenko, T., Lidie, K. L., Van Dolah, F. M., Lindquist, E., Cheng, J. F. & Bhattacharya, D. 2006. Chimeric plastid proteome in the Florida "red tide" dinoflagellate *Karenia brevis*. *Molecular Biology and Evolution* **23:** 2026–2038.

Nylander, J. A. A., Ronquist, F., Huelsenbeck, J. P. & Nieves-aldrey, J. 2004. Bayesian phylogenetic analysis of combined data. *Systematic Biology* **53:** 47-67.

Orr, R. J. S., Murray, S. A., Stüken, A., Rhodes, L. & Jakobsen, K. S. 2012. When Naked Became Armored: An Eight-Gene Phylogeny Reveals Monophyletic Origin of Theca in Dinoflagellates. *PLoS ONE* **7:** 1–15.

Ostenfeld, C.H. 1908. The phytoplankton of the Aral Sea and its effluents. *Wissenschaftliche Ergebnisse der Aralsee-Expedition. St. Petersburg* **8:** 123–225.

Parkinson, J. E., Baumgarten, S., Michell, C. T., Baums, I. B., LaJeunesse, T. C. & Voolstra, C. R. 2016. Gene Expression Variation Resolves Species and Individual Strains among Coral-Associated Dinoflagellates within the Genus *Symbiodinium*. *Genome biology and evolution* **8:** 665–680.

Parkinson, J.E., Coffroth, M.A. and LaJeunesse, T.C. 2015. New species of Clade B *Symbiodinium* (Dinophyceae) from the greater Caribbean belong to different functional guilds: *S. aenigmaticum* sp. nov., *S. antillogorgium* sp. nov., *S. endomadracis* sp. nov., and *S. pseudominutum* sp. nov. *Journal of phycology* **51:** 850–858.

Pawlowski, J., Holzmann, M., Fahrni, J.F., Pochon, X. & Lee, J.J. 2001. Molecular identification of algal endosymbionts in large miliolid foraminifera: 2. Dinoflagellates. *Journal of Eukaryotic Microbiology* **48:** 368–373.

Pochon, X. & Gates, R. D. 2010. A new *Symbiodinium* clade (Dinophyceae) from soritid foraminifera in Hawai′i. Molecular Phylogenetics and Evolution **56:** 492–497.

Pochon, X., LaJeunesse, T.C., & Pawlowski, J. 2004. Biogeographic partitioning and host specialization among foraminiferan dinoflagellate symbionts (*Symbiodinium*; Dinophyta). Marine Biology **146:** 17–27.

Pochon, X., Montoya-Burgos, J.I., Stadelmann, B. & Pawlowski, J. 2006. Molecular phylogeny, evolutionary rates, and divergence timing of the symbiotic dinoflagellate genus *Symbiodinium*. Molecular Phylogenetics Evolution **38:** 20–30.

Pochon, X., Putnam, H. M., Burki, F. & Gates, R. D. 2012. Identifying and characterizing alternative molecular markers for the symbiotic and free-living dinoflagellate genus *Symbiodinium*. *PLoS One* **7:** 29816.

Pochon, X., Putnam, H. M. & Gates, R. D. 2014. Multi-gene analysis of *Symbiodinium* dinoflagellates: a perspective on rarity, symbiosis, and evolution. *PeerJ* **2:** e394.

Pochon, X., Stat, M., Takabayashi, M.T., Chasqui, L., Logan, D.D. & Gates, R.D. 2010. Comparison of endosymbiotic and free-living *Symbiodinium* (Dinophyceae) diversity in a Hawaiian reef environment. *Journal of Phycology* **46:** 53–65.

Porto, I., Granados, C., Restrepo, J. C., Sánchez, J. A. & Humphries, S. 2008. Macroalgal associated dinoflagellates belonging to the genus *Symbiodinium* in Caribbean reefs. *PLoS ONE* **3:** e2160.

Ramsby, B.D., Hill, M.S., Thornhill, D.J., Steenhuizen, S.F., Achlatis, M., Lewis, A.M. and LaJeunesse, T.C. 2017. Sibling species of mutualistic *Symbiodinium* clade G from bioeroding sponges in the western Pacific and western Atlantic oceans. *Journal of phycology* **53:** 951–960.

Ratledge, C. 2004. Fatty acid biosynthesis in microorganisms being used for Single Cell Oil production. *Biochimie* **86:** 807–815.

Reimer, J.D., Shah, M.M.R., Sinniger, F., Yanagi, K. & Suda, S. 2010 Preliminary analyses of cultured *Symbiodinium* isolated from sand in the oceanic Ogasawara Islands, Japan. *Marine Biodiversity* **40:** 237–247.

Rizzo, P. J. 1991. The Enigma of the Dinoflagellate Chromosome. *The Journal of Protozoology* **38:** 246–252.

Rodriguez-Lanetty, M. 2003. Evolving lineages of *Symbiodinium*-like dinoflagellates based on ITS1 rDNA. *Molecular Phylogenetics and Evolution* **28:** 152–168.

Ronquist, F. & Huelsenbeck, J. P. 2003. MrBayes 3: Bayesian phylogenetic inference under mixed models. *Bioinformatics* **19:** 1572–1574.

Rowan R. & Powers D.A. 1992. Ribosomal-RNA sequences and the diversity of symbiotic dinoflagellates (zooxanthellae). *Proceedings of the National Academy of Sciences of the United States of America* **89:** 3639–3643.

Saldarriaga, J. F. & Taylor, F. J. R. (2017) Dinoflagellates. In: Archibald, J.M., Simpson, A.G.B. & Slamovits, C.H. Handbook of the Protist (2nd ed). pp. 625–678.

Sampayo, E. M., Dove, S. & Lajeunesse, T. C. 2009. Cohesive molecular genetic data delineate species diversity in the dinoflagellate genus *Symbiodinium*. *Molecular Ecology* **18:** 500–519.

Santos, S.R., Taylor, D.J., Kinzie, R.A.III., Hidaka, M., Sakai, K. & CoVroth, M.A. 2002. Molecular phylogeny of symbiotic dinoXagellates inferred from partial chloroplast large subunit (23S)-rDNA sequences. *The Molecular Phylogenetics and Evolution* **23:** 97–111.

Sarno, D., Kooistra, W.C.H.F., Medlin, L.K., Percopo, I., Zingone, A. 2005. Diversity in the genus *Skeletonema* (Bacillariophyceae). II. An assessment of the taxonomy of *S. costatum*-like species, with the description of four new species. *Journal of Phycology* **41:** 151–176.

Siano, R., Kooistra, W.H.C.F., Montresor, M. & Zingone, A. 2009. Unarmoured and thin-walled dinoflagellates from the Gulf of Naples, with the description of *Woloszynskia cincta* sp. nov. (Dinophyceae, Suessiales). *Phycologia* **48**: 44–65.

Schnepf, E. & Elbrächter, M. 1988. Cryptophycean-like double membrane-bound chloroplast in the dinoflagellate, Dinophysis Ehrenb.: evolutionary, phylogenetic and toxicological implications. *Plant Biology* **101:** 196–203.

Schnepf, E. & Elbrächter, M. 1992. Nutritional strategies in dinoflagellates: A review with emphasis on cell biological aspects. *European Journal of Protistology* **28:** 3–24.

Schoenberg, D.A. & Trench, R.K. 1980. Genetic variation in *Symbiodinium* (=*Gymnodinium*) *microadriaticum* Freudenthal, and specificity in its symbiosis with marine invertebrates. 1. Isoenzyme and soluble-protein patterns of axenic cultures of *Symbiodinium microadriaticum*. Proceedings. *Biological sciences Royal Society* **207:** 405–427.

Schnepf, E. & ElbräChter, M. 1999. Dinophyte chloroplasts and phylogeny-A review. *Grana* **38:** 81–97.

Sekida, S., Horiguchi, T. & Okuda, K. 2001. Development of the cell covering in the dinoflagellate *Scrippsiella hexapraecingula* (Peridiniales, Dinophyceae). *Phycological Research* **49:** 163–176.

Selander, E., Thor, P., Toth, G. & Pavia, H. 2006. Copepods induce paralytic shellfish toxin production in marine dinoflagellates. *Proceedings of the Royal Society B: Biological Sciences* **273:** 1673–1680.

Shah, M.M.R., Reimer, J.D., Horiguchi, T. & Suda, S. 2010. Diversity of dinoflagellate blooms in reef flat tide pools at Okinawa, Japan. *Galaxea, Journal of Coral Reef Studies* **12:** 49.

Sherr, E. B. & Sherr, B. F. 2007. Heterotrophic dinoflagellates: A significant component of microzooplankton biomass and major grazers of diatoms in the sea. *Marine Ecology Progress Series* **352:** 187–197.

Spector, D. L., Vasconcelos, A. C. & Triemer, R. E. 1981. DNA duplication and chromosome structure in the Dinoflagellates. *Protoplasma* **105:** 185–194.

Steidinger, K. A. & Balech, E. 1977. *Scrippsiella subsalsa* (Ostenfeld) comb. nov. (Dinophyceae) with a discussion on *Scrippsiella*. *Phycologia* **16:** 69–73.

Steidinger, K. A. & Tangen, K. 1996. Dinoflagellates. In: Identifying marine diatoms and dinoflagellates (Ed. by C.R. Thomas). Academic Press, San Diego. pp 387–598.

von Stosch, H. A 1964. Zum Problem der sexuellen Fortpflanzung in der Peridineengattund Ceratium. *Helgolander Wissenschaftliche Meeresuntersuchungen* **10:** 140–152.

von Stosch, H. A. 1973. Observations on vegetative reproduction and sexual life cycles of two freshwater dinoflagellates, *Gymnodinium pseudopalustre* schiller and woloszynskia apiculata sp. nov. *British Phycological Journal* **8:** 105–134.

von Stein, F. R. (1883) Der Organismus der Infusionsthiere nach eigenen Forschungen in systematischer Reihenfolge bearbeitet. III. Abteilung, II. Hälfte. Die Naturgeschichte der arthrodelen Flagellaten. Wilhelm Engelmann, Leipzig, 30 pp.

Stoecker, D.K. 1999. Mixotrophy among dinoflagellates. *Journal of Eukaryotic Microbiology* **46:** 397–401.

Swofford, D. L. 2001. PAUP*. Phylogenetic analysis using parsimony (*and other methods). Version 4.0b10. Sinauer Associates, Sunderland, Massachusetts.

Takabayashi, M., Adams, L.M., Pochon, X. & Gates, R.D. 2012. Genetic diversity of free-living *Symbiodinium* in surface water and sediment of Hawai'i and Florida. *Coral Reefs* **31:** 157–167.

Takahashi, K., Sarai, C. & Iwataki, M. 2014. Morphology of two marine woloszynskioid dinoflagellates, *Biecheleria brevisulcata* sp. nov. and *Biecheleriopsis adriatica* (Suessiaceae, Dinophyceae), from Japanese coasts. *Phycologia* **53**: 52–65.

Takano, Y. and Horiguchi, T. 2006. Acquiring scanning electron microscopical, light microscopical and multiple gene sequence data from a single dinoflagellate cell 1. *Journal of Phycology* **42:** 251–256.

Takano, Y., Yamaguchi, H., Inouye, I., Moestrup Ø, Horiguchi, T. 2014. Phylogeny of five species of *Nusuttodinium* gen. nov. (Dinophyceae), a genus of unarmoured kleptoplastidic dinoflagellates. *Protist* **165:** 759–778.

Tamura, M., Takano, Y. & Horiguchi, T. 2009. Discovery of a novel type of body scale in the marine dinoflagellate, *Amphidinium cuplatisquama* sp. nov. (Dinophyceae). *Phycological Research* **57:** 304-312.

Taylor, F. J. R. 1980. On dinoflagellate evolution. *BioSystems* **13:** 65–108.

Taylor, F.J.R. (1987b) General group characteristics, special features of interest; and a short history of dinoflagellate study. In: Taylor FJR (ed) The biology of dinoflagellates. pp. 1–23.

Taylor, F.J.R. (1987c) Dinoflagellate morphology. In: Taylor FJR (ed) The biology of dinoflagellates. pp. 24–91.

Taylor, F. J. R. 1999. Charles Atwood Kofoid and his dinoflagellate tabulation system: an appraisal and evaluation of the phylogenetic value of tabulation. *Protist* **150:** 213–220.

Taylor, F.J.R. (2004) Harmful dinoflagellate species in space and time and the value of morphospecies. In: Steidinger, K.A., Landsberg, J.H., Tomas, C.R. et al (eds) Harmful algae 2002. Fla Fish Wildl. Cons Comm, Fla Inst Ocean, IOC UNESCO, St. Petersburg, Fla, pp. 555–559.

Taylor, F. J. R., Hoppenrath, M. & Saldarriaga, J. F. 2008. Dinoflagellate diversity and distribution. *Biodiversity and Conservation* **17:** 407–418.

Ten-Hage, L., Turquet, J., Quod, J. P., Puiseux-Dao, S. & Coute, A. 2000. *Prorocentrum borbonicum* sp. nov. (Dinophyceae), a new toxic benthic dinoflagellate from the southwestern Indian Ocean. *Phycologia* **39:** 296–301.

Ten-Hage, L., Quod, J-P., Turquet, J. & Couté, A. 2001. *Bysmatrum granulosum* sp. nov., a new benthic dinoflagellate from the southwestern Indian Ocean. *European Journal of Phycology* **36:** 129–135.

Thornhill, D.J., Daniel, M.W., LaJeunesse, T.C., Schmidt, G.W. & Fitt, W.K. 2006. Natural infections of aposymbiotic *Cassiopea xamachana* scyphistomae from environmental pools of *Symbiodinium*. *Journal of Experimental Marine Biology and Ecology* **338:** 50–56.

Tillmann, U., Alpermann, T., John, U. & Cembella, A. 2008. Allelochemical interactions and short-term effects of the dinoflagellate Alexandrium on selected photoautotrophic and heterotrophic protists. *Harmful Algae* **7:** 52–64.

Toriumi S. & Dodge J. D. 1993. Thecal apex structure in the Peridiniaceae (Dinophyceae). *European Journal of Phycology* **28:** 39–45.

Trench, R.K. & Blank, R.J. 1987. *Symbiodinium microadriaticum* Freudenthal, *S. goreauii* sp. nov., *S. kawagutii* sp. nov. and *S. pilosum* sp. nov.: gymnodinioid dinoflagellate symbionts of marine invertebrates. Journal Phycology **23:** 469–481.

Trench, R.K. & Thinh, L.V. 1995. *Gymnodinium linucheae* sp. nov.: the dinoflagellate symbiont of the jellyfish *Linuche unguiculata*. *European Journal of Phycology* **30:** 149–154.

Underwood, A. J. & Skilleter, G. A. 1996. Effects of patch-size on the structure of assemblages in rock pools. *Journal of Experimental Marine Biology and Ecology* **197:** 63–90.

Venera-Ponton, D.E., Diaz-Pulido, G., Rodriguez-Lanetty, M. & Hoegh-Guldberg, O, 2010. Presence of *Symbiodinium* spp. in macroalgal microhabitats from the southern Great Barrier Reef. *Coral Reefs* **29:** 1049–1060.

Walker, L. M. & Steidinger, K. A. 1979. Sexual reproduction in the toxic dinoflagellate *Gonyaulax monilata*. *Journal of Phycology* **15:** 312–315.

Weisz, J. B., Massoro, A. J., Ramsby, B. D. & Hill, M. S. 2010. Zooxanthellar symbionts shape host sponge trophic status through translocation of carbon. The Biological Bulletin **219:** 189–97.

Westfall, J. A., Bradbury, P. C. & Townsend, J. W. 1983. Ultrastructure of the dinoflagellate Polykrikos. I. Development of the nematocyst-taeniocyst complex and morphology of the site for extrusion. *Journal of cell science* **631:** 245–261.

Wham, D.C., Ning, G. and LaJeunesse, T.C. 2017. *Symbiodinium glynnii* sp. nov., a species of stress-tolerant symbiotic dinoflagellates from pocilloporid and montiporid corals in the Pacific Ocean. *Phycologia* **56:** 396–409.

Yamada, N., Terada, R., Tanaka, A. and Horiguchi, T. 2013. *Bispinodinium angelaceum* gen. et sp. nov. (Dinophyceae), a new san-dwelling dinoflagellate from the seafloor off Mageshima Island, Japan. *Journal of phycology* **49:** 555–569.

Yamada, N., Tanaka, A. & Horiguchi, T. 2015. Pigment compositions are linked to the habitat types in dinoflagellates. *Journal of Plant Research* **128**: 923–32.

Yamashita, H. & Koike, K. 2013. The genetic identity of free-living *Symbiodinium* obtained over a broad latitudinal range in the Japanese coast. *Phycological Research* **61:** 68–80.

Zhang, Z., Green, B. R. & Cavalier-Smith, T. 1999. Single gene circles in dinoflagellate chlroplast genomes. *Nature* **400:** 155–159.

Zhou, G., Huang, H., Yu, Z., Dong, Z. & Li, Y. 2012. Genetic diversity of potentially free-living *Symbiodinium* in the Xisha Islands, South China Sea: Implications for the resilience of coral reefs. *Aquatic Ecosystem Health & Management* **15:** 152–160.